Sara Sofia Barreiro Correia

Licenciada em Bioquímica

Fucose-containing exopolysaccharide 3D constructs for oral drug delivery

Dissertação para obtenção do Grau de Mestre em Biotecnologia

Orientador: Prof. Doutora Ana Aguiar-Ricardo, FCT-UNL

Co-orientador: Prof. Doutor João Paulo Borges, FCT-UNL

FACULDADE DE CIÊNCIAS E TECNOLOGIA
UNIVERSIDADE NOVA DE LISBOA

Sara Sofia Barreiro Correia

Licenciada em Bioquímica

Fucose-containing exopolysaccharide 3D constructs for oral drug delivery

Exopolysaccharide-based orodispersible film production for drug delivery

Acknowlegments

First of all, I would like to thank my supervisors, Ana Aguiar-Ricardo and João Paulo Borges for giving me the opportunity to develop my MSc dissertation while providing the support and orientation throughout this last year. I would also like to acknowledge LabRMN at FCT/UNL and Rede Nacional de RMN, supported with funds from Fundação para a Ciência e a Tecnologia (FC&T, Lisbon), Projecto de Re-equipamento Científico, Portugal for access to the facilities. This work was also supported by the Associate Laboratory Research Unit for Green Chemistry - Technologies and Processes Clean – LAQV and CENIMAT/I3N. LAQV is financed by national funds from FC&T (UID/QUI/50006/2013) and co-financed by the ERDF under the PT2020 Partnership Agreement (POCI-01-0145-FEDER - 007265), CENIMAT/I3N is supported by FEDER funds through the COMPETE 2020 Program and National Funds through FCT - Portuguese Foundation for Science and Technology under the project number POCI-01-0145-FEDER-007688 Reference UID/CTM/50025.

Since it took a village, a lot of support and guidance for this work to succeed, I would like to thank Professor Jorge Silva for allowing me to perform cytotoxic studies, Ana Rego for her help with XPS analysis, Madalena Dionísio for helping me with DSC studies and analysis, Teresa Casimiro for taking the time to steer me in the right direction, Isabel Nogueira for the SEM images, João Canejo for all his help in electrospinning and mechanical testing, Coro Zabala for the rheometric measures, Ana Rita Ferreira for providing the Teflon disc required to for solvent casting procedures and Nuno Costa for the HPLC assay, making the impossible possible.

To all my colleagues and ex-colleagues from the 510/512 group: Vanesa Almeida, Patrícia Morgado, Gosia Zakrzewska, Raquel Viveiros, Telma Barroso, Vasco Bonifácio, Carmen Montoya, Inês Paninho and Pedro Lisboa, thank you for the support and good vibes. A special thanks to Rita Pires for never losing her patience and always finding the time to help me (or everyone else for that matter), even when I would nag her with thousands of questions at the same time. A special thanks to Marta Silva for helping me think when I couldn't, allowing me to blow off some steam when I was angry, dancing with me when I was happy or listening when I just wanted to talk, always listening to my crazy shenanigans and ramblings. To Fabiana: if it weren't for you, this work would not be done. You scraped me of the pavement and brought sunshine to my life in the darkest of days, always by my side throughout the long hours of the night (and weekends!), being capable of turning around my pessimistic mood into a laugh. Thank you, from the bottom of my heart, for the brainstorming and all the help and wisdom provided, not only in the workplace, but by pointing me out my own strengths and weaknesses when I wasn't able to see them.

For Sérgio, I have no words to describe how thankful and blessed I am for having a person like you in my life. Thank you, from the bottom of my heart for the incredible amount of support and strength that you provided.

To my big sister, Diana, for her constant support and for inspiring the work performed in this dissertation; I cannot thank you enough.

To my parents Ricardo and Isabel, for their unwavering support, making it possible for me to progress in my academical studies.

Abstract

Although the oral route of administration tends to be the most common and feasible way to orally deliver drugs, there are some pediatric and geriatric patients that experiences discomfort when ingesting drugs, a problem often associated with physical and / or mental restraints, or even the size of the drug in itself. Now-a-days, there has been an increase in the development of fast drug delivery systems that have an appealing and convenient design, without compromising its effectiveness and pharmaceutical dosage. Thus, the goal was the creation of two oral formulations: an orodispersible film containing an antiemetic (e.g. metoclopramide) for the fast relief of emesis or vomiting, and a scaffold containing a saliva-inducing agent (e.g. xylitol) for symptomatic relief of xerostomia. Hence, electrospinning – a fiber forming technique that uses an applied electrical field in order to obtain fibers from electrically conductive polymeric solutions – was used in the manufacture of orodispersible films, and cryogelation coupled with supercritical carbon dioxide extraction or drying – a technique that induces pore formation through ice crystal growth at subzero temperatures, with subsequent solvent extraction by carbon dioxide in supercritical conditions – was used to produce scaffolds. FucoPol was the main component in both formulations – a hydrophilic, biocompatible and biodegradable bacterial exopolysaccharide. The fiber-rich planar orodispersible films dissolved in 6 to 10 seconds, releasing 80% of its metoclopramide content. The films had an overall thickness of (10±2) x 10 μm and an average fiber diameter of (1.6 ± 0.08) x 10 μm and (2.9 ± 0.03) x 10 μm. Cytotoxic studies revealed that the films had cytotoxic behavior when higher amounts of metoclopramide (> 1mg/mL) were present. Scaffolds, non-toxic cylindrical porous structures, presented 500 to 800 mm in height, having an average pore diameter of 154 μm. Additionally, scaffolds presented a maximum water uptake of 30% before mass-loss due to disintegration, a process that occurred between 5 to 15 minutes. Both structures (i.e. orodispersible films and scaffolds) showed that the drug delivery was controlled by anomalous diffusion (Korshmeyer-Peppas model) and although there is still room for improvement, both techniques proven to be suitable for the production of orodispersible films and scaffolds.

Resumo

Apesar de a via oral ser um dos métodos mais práticos e comuns no que toca à toma de medicamentos, certas populações pediátricas e geriátricas apresentam maior dificuldade na ingestão de medicamentos muitas vezes associado a constrangimentos físicos e/ou psicológicos, ou à própria dimensão do fármaco. Nos últimos anos, têm-se desenvolvido medicamentos de acção rápida que possuam um design mais apelativo e conveniente, sem comprometer a sua eficácia e dosagem farmacêutica. Assim, neste trabalho, teve-se por objectivo a criação de duas formulações orais: um filme orodispersível para o alívio rápido da emése ou vómito, contendo um antiemético (e.g. metoclopramida) e um *scaffold* para alívio sintomático provocado pela xerostomia, contendo um indutor de saliva (e.g. xilitol). Para tal, recorreu-se à electrofiação – técnica electroestática que induz a formação de fibras a partir de soluções poliméricas electricamente condutoras – para a produção de filmes orodispersíveis, e à criogelação com recurso a extração ou secagem por dióxido de carbono supercrítico – cristalização de uma solução aquosa a temperaturas negativas com posterior extracção em condições supercríticas – para produção de *scaffolds*. Ambas as formulações tiveram como base o FucoPol – exopolissacárido bacteriano que apresenta elevada hidrofilicidade, biocompatibilidade e biodegradabilidade. Os filmes orodispersíveis, estruturas planares ricas em fibras, dissolveram-se entre 6 a 10 segundos, libertando 80% do seu conteúdo em metoclopramida por difusão anómala (Korshmeyer-Peppas). Apresentam, em média, (10±2) x 10 μm de espessura e um diâmetro médio de fibra entre (1.6±0.08) x 10 μm e (2.9±0.03) x 10 μm. Demonstram ainda um comportamento citotóxico quando o fármaco se encontra presente em concentrações >1mg.mL^{-1}. Os *scaffolds*, estruturas tridimensionais cilíndricas e porosas, sem efeito citotóxico, apresentaram 500 a 800 μm de espessura, possuindo um diâmetro médio de poro de 154 μm. Com uma capacidade de absorção de água de 30% e um tempo de dissolução entre 5 a 15 minutos. Ambas as estruturas (os filmes orodispersíveis e os *scaffolds*) apresentam libertação do fármaco controlada por uma difusão anómala através das suas matrizes (modelo Korshmeyer-Peppas) e, embora ainda haja espaço para melhorar, os resultados obtidos mostram que ambas as técnicas provaram ser adequadas para a produção de filmes orodispersíveis e scaffolds de misturas poliméricas contendo Fucopol.

Table of Contents

List of Figures

List of Tables

List of Abbreviations

3D	Tridimensional
A	Cross-sectional area
AA	Acetic acid
AFM	Atomic-force Microscopy
ANS	Autonomic Nervous System
API	Active Pharmaceutical Ingredient
ATR	Attenuated Ressonance
BE	Binding energy
CINV	Chemotherapy induced nausea and vomiting
CO_2	Carbon dioxide
DMEM	Dulbecco's Modified Eagle Medium
DMSO	Dimethyl sulfoxide
DSC	Differencial Scanning Calorimetry
EPS	Exopolysaccharide
ES	Electrospinning
ESEM	Environmental Scanning Electron Microscope
FA	Formic acid
FAT	Fourrier Attenuated Transmission mode
FCT	Faculdade de Ciências e Tecnologia
FDA	Food and Drug Administration
FID	Flame Ionization Detector
FP	FucoPol
FP/PEO	Physical blend blend between FucoPol (2wt.%) and poly (ethylene oxide) (1 wt.%)
FTIR	Fourier Transform Infrared Spectroscopy
HPC	Hydroxylpropil cellulose

HPLC	High pressure liquid chromatography
HPMC	Hydroxylpropil methylcellulose
IST	Instituto superior técnico
IgG	Immunoglobulin G
MET	Metoclopramide hydrochloride
M_t	Mass of drug release at a time
M_∞	Mass of drug release as time approaches infinit
MWCO	Molecular weight cut-off
N&V	Nausea and Vomiting
NS	Non-soluble
ODF	Orodispersible film
ODT	Orodispersible tablet
PEO	Poly (ethylene oxide)
PGSS	Particle generation with supercritical carbon dioxide
OS	Partially soluble
PVP	Polyvinilpirrolidone
PVA	Poly (vynil alcohol)
REQUIMTE	Rede de química e tecnologia
RESS	Rapid expansion of supercritical solutions
S	Soluble
SC	Solvent casting
$scCO_2$	Supercritical carbon dioxide
SCA	Scaffold
SCF	Supercritical fluid
SEM	Scanning Electron Microscopy
SFE	Supercrirital fluid extration
STMP	Sodium trimetaphosphate

$T_{boiling}$	Boiling temperature
T_c	Cristalization temperature
T_g	Glass-transition temperature
TEM	Transmission Electron Microscope
T_m	Melting temperature
UCIBIO	Research Unit on Applied Molecular Biosciences
UNL	Universidade NOVA Lisboa
UV	Ultraviolet
WHO	World Health Organization
XPS	X-Ray Photoelectron Spectroscopy

List of symbols

1s	K atomic orbital (low energy)
a	Cylinder radius
C	Carbon
D	Constant drug diffusion coeficient
E	Young's modulus
F	Applied force
H	Hidrogen
h	Planck constant
k	Constant
L_0	Distance between clamps
Mg	Magnesium
n	Diffusional exponent
O	Oxigen
N	Nitrogen
NaOH	Sodium hydroxide
t	Time
γ	Shear rate
Δl	Displacement
ε	Strain
η_0	Viscosity at Newtonian-plateau
η	Viscosity
υ	Frequency
π	Pi
σ	Stress
τ	Shear stress

General Introduction

In this chapter we start by motivating our work, giving an overview of the context in which our work is based on and a brief description of other techniques that aim to tackle some of the challenges that we have identified. Later, we provide a description of our proposed solution to these challenges and concluding with the outline of this document.

1.1 Motivation

Exploring new biomaterials and techniques will enable process optimization and the design of newer products with enhanced properties, capable of improving the efficiency of a given therapy and promoting overall well being. Bio-based materials (e.g. polysaccharides) have been gaining interest as a viable alternative for pharma excipients in drug delivery systems. Their unique chemical characteristics as stabilizing, thickening or film formation agents makes them versatile as emerging new polymers in tissue engineering and in pharma applications.

Plus, current fuel fossil depletion has led the industry to the investment in sustainable greener bulk materials and technologies that can provide equal, or higher performance as the ones available on the market, at lower production costs (e.g. bacterial polysaccharides).

With that in mind, the work presented in this dissertation proposes to combine medical therapy efficiency with the needs of the industry, using a bacterial synthetized fucose-containing exopolysaccharide in order to develop two new drug delivery systems – an orodispersible film (ODF) and a cryogel – using electrospinning for orodispersible film (ODF) production and cryogelation

followed by supercritical carbon dioxide drying (supercritical CO_2-assisted drying) for scaffold (SCA) production.

1.2 Context

1.2.1 Oral drug administration

Drug intake can be mainly performed through the skin (i.e. transdermal), blood (i.e. parenteral) or gastrointestinal tract (i.e. enteral). In enteral administration the drug is swallowed by the mouth, digested in the stomach and absorbed in the intestines. In general, enteral oral dosage forms show considerably higher drug loadings due to gastric of liver absorption, promoting a decrease in the drugs bioavailability upon reaching the systemic circulation. This process is known as first-pass metabolism (Hearnden et al., 2012; Rowland, 1972). In order to bypass first-pass effect, new drug releasing systems have been developed in order to allow drugs to diffuse into the systemic circulation through, pulmonary alveoli (e.g. inhalations devices) or epithelial tissue (e.g. sublingual dosage forms). Through these systems, the drug can diffuse through the mucous membrane directly into the blood stream without experiencing first-pass effect. (Allen and Cullis, 2004; Prausnitz and Langer, 2008)

The human mouth has non-keratinized and keratinized tissues that comprise the masticatory, lining and specialized mucosa (e.g. tongue). Masticatory mucosa, responsible for processes like mastication and speech, includes the dorsal side of the tongue, gingiva and hard palate. The lining comprises the inner cheeks, soft palate, sublingual and ventral tongue areas, being responsible for secretion and selective adsorption; it also provides mechanical strength and avoids stress-induced chemical abrasion. (Marieb and Hoehn, 2007)

The oral cavity is filled with saliva, an exocrine solution made from 99% water and 1% electrolytes, proteins, hormones and vitamins. Due to masticatory function, enzymes like α-amylase are present to initiate starch breakdown, while lipase disintegrates dietary triglycerides and lysozyme acts as an antibacterial agent by hydrolysis of the peptidoglycan present in bacterias' cell wall. As seen in Figure 1.**1**, approximately 90% of saliva is produced by three major salivary glands: the submandibular (65%), the parotid (20%) and the sublingual (5-7%). Minor glands like labial, lingual, buccal and palatine produce the remaining 10%. In normal conditions (i.e. unstimulated secretion) salivary flow is about 0.1 to 0.3 mL/minute in healthy subjects, reaching a maximum of 3 to 7 mL/min when artificially stmulated. (Dodds et al., 2005). Saliva production is controlled by the autonomic nervous system (ANS) and its production can vary depending on several conditions, including stress, thirst or sweet/sour food. (Dodds et al., 2015; Soares Nunes et al., 2015; Wang et al., 2015)

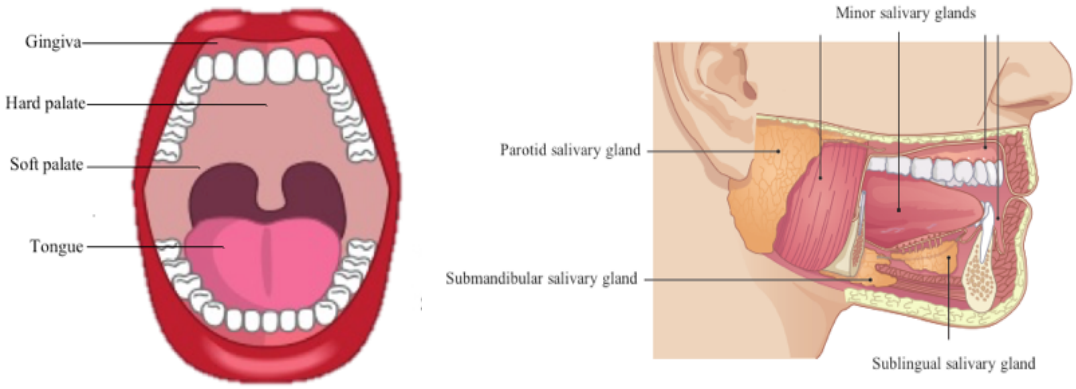

Figure 1.1 - Oral cavity and its main components; adapted from http://www.hibbettpatientcare.com, assessed 24th October 2015 and Dodds et al., 2015.

Oral complications can arise from a number of causes. Usually, there is a breakdown in cellular growth and a disruption of healthy bacteria in the mouth. These changes may lead to bleeding gums, mouth sores, infections and tooth decay. Other common side effects are the loss of normal salivary flow, nausea and vomiting (Epstein et al., 2012).

Tablets are the most common oral drug delivery devices used in the treatment or the relieve of a number of ailments. Among others, there are several key factors that are taken into account when projecting and designing a pharmaceutical formulation, namely the drug's bioavailability and loading, as well the drug's absorption process and its therapeutic window. (Slavkova and Breitkreutz, 2015) A description of different compounds (e.g. excipients) and techniques applied in the production of pills, or oral dosage forms, is provided ahead.

1.2.2 Oral excipients manufacturing

Excipients, synthetic or natural matrix developed alongside an active pharmaceutical ingredient (API); the most common are shown in Figure 1.2. Excipients are evolving from their traditional role as providers of stable physicochemical support in weight, volume and consistency, having a great input as release, solubility and delivery performance enhancers. Plus, they are able to incorporate different types of molecules; for instance, dendrimers can enhance the solubility of poor water-soluble drugs (e.g. ibuprofen), providing a controlled drug release in a wide range of pH. (Restani et al., 2014)

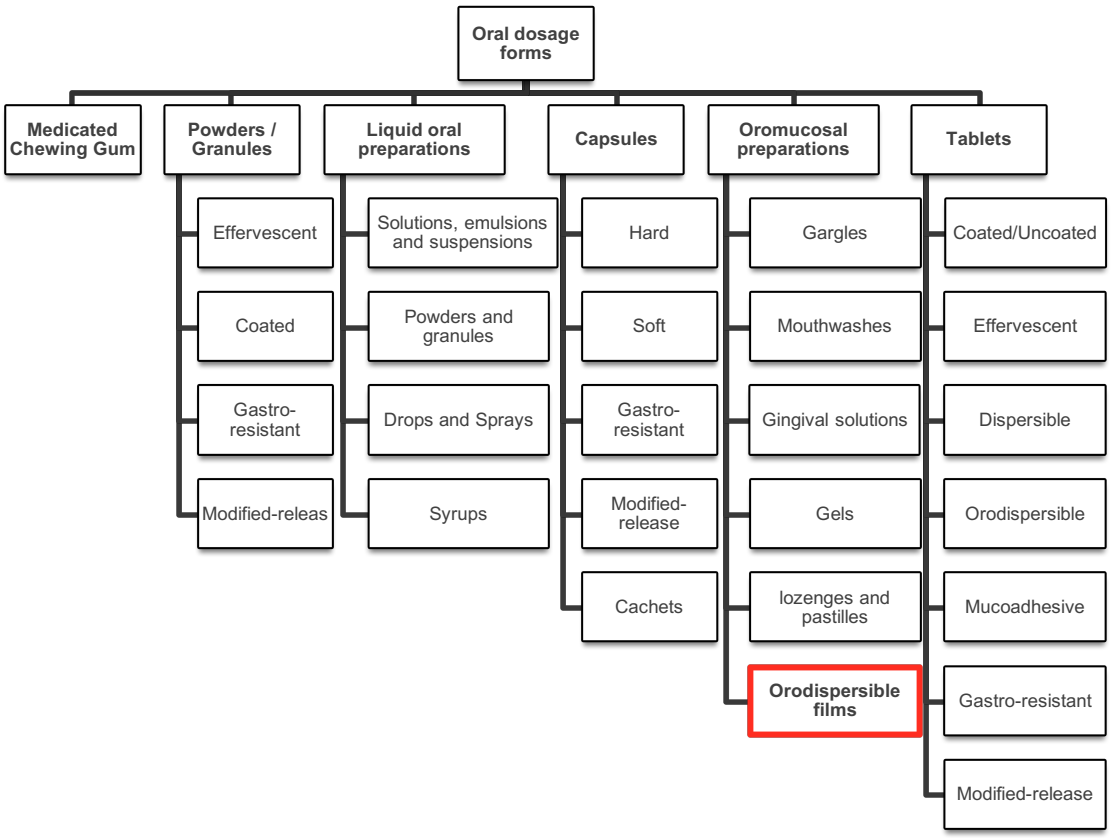

Figure 1.2 - Outline of oral dosage forms (Ph. Eur. 5th, 2000); orodispersible films where recently added in (Ph. Eur. 8th Edition, 2015)

In the last few years, the pharma sector has been researching new drug delivery systems that promote higher drug bioavailability. In order to obtain these two oral formulations, different excipients and manufacturing techniques can be applied (Kadajji and Betageri, 2011; Leuner and Dressman, 2000; Rathbone et al., 2008). Table 1.1 provides a simplified recap of most common procedures used to produce oral dosage forms.

Table 1.1 – Short recap of most common production methods for oral dosage forms. *(Kailash et al., 2014; Ph. Eur. 5th, 2000)*

	Compression	Solvent Casting	Freeze-drying	Injection molding	Hot-melt extrusion	Printing	Spray-drying	Other
Medicated Chewing-gum	✓							✓
Powders / Granules							✓	✓
Liquid preparations								✓
Capsules		✓		✓	✓			
Oromucosal preparations	✓	✓	✓		✓	✓		✓
Tablets	✓	✓	✓		✓	✓		✓
References	(Garg and Goyal, 2014; Jiang et al., 2004; Kailash et al., 2014; Kolakovic et al., 2013; Saigal et al., 2008)							

Bio-based materials can be used as solid matrices for drug delivery in different forms, such as orodispersible films, gels, scaffolds, beads and micro or nanoparticles. Oral thin films and scaffolds can be built from polymeric matrices made from natural or semi-synthetic polymers, which are naturally occurring polymers that suffered chemical treatment in order to obtain certain specific characteristics that did not occur without chemical modification (e.g. cellulose). Cellulose or chitin derivatives like hydroxypropil (HPC) (Qiu and Hu, 2013), hydroxypropil methylcellulose (HPMC) and chitosan (Takeuchi et al., 2013) are often found in many marketed oromucosal formulations (e.g. buccal films), due to their characteristic adhesive properties and their natural ability to swell and retain water. Polyvinyl alcohol (PVA) (Alipour et al., 2015), polyvinylpyrrolidone (PVP) (Illangakoon et al., 2014) and poly(ethylene oxide) (PEO) (Kojima et al., 2008) are some of the most common synthetic polymers used in oral thin films since they exhibit enhanced stability and hydrophilicity, ideal for fast dissolving dosage forms (Borges et al., 2015). Hydrocolloids – dispersion of hydrophilic polymers in in a two-phase aqueous system – can also be found in many oral formulations, being already well established in the food industry as thickeners and starch substitutes, in order to avoid unpleasant mouthfeel. Many hydrocolloids are polysaccharides derived from natural sources, like plants (e.g. cellulose, pectin) or algi (e.g. agar-agar), while others arise as a byproduct of bacterial growth.

1.2.3 Polysaccharides

In 2008, the extraction of natural polysaccharides from plants and algae represented a market value of over $4 million (Freitas et al., 2011). Polysaccharides present high molecular weights (10^4-10^6), and can be classified as intracellular, structural or extracellular according to their function and biosynthesis. Intracellular polysaccharides provide energy as an intrinsic carbon source while structural polysaccharides act as main components of the cell wall; extracellular polysaccharides - exopolysaccharides (EPS) - are discharged into the environment as capsules or as slime, a loose matrix made from a combination of water and extracellular polymer in order to protect the cell from desiccation and/or predation (Venugopal, 2011). Slimes or biofilms are very simple to extract when microbial fermentation occurs in a controlled environment, such as in an aseptic closed bioreactor. Exopolysaccharides can be linear or branched, made by several types of monosaccharides linked together by glycosidic bonds. Homopolysaccharides, like dextran or levan, present the same monomeric unit repeatedly, while heteropolysaccharides (e.g. xanthan, gellan) are built from different types of sugar monomers. (Stephen et al., 2006)

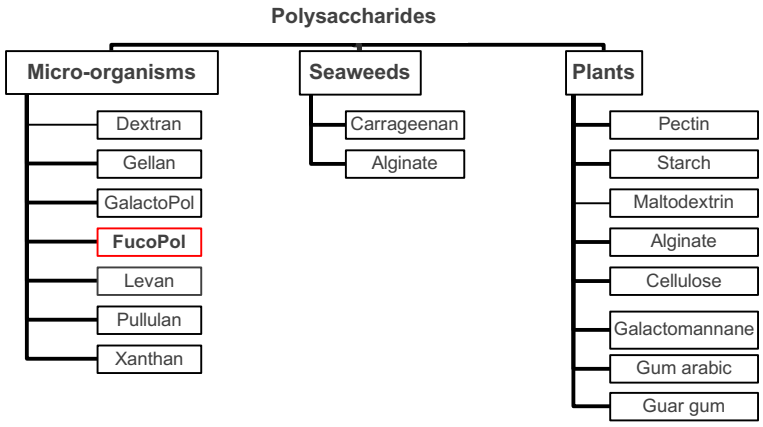

Figure 1.3 – Outline of polysaccharides and their bio-based sources. *(Freitas et al., 2011; Venugopal, 2011)*

Although there are a number of polysaccharide sources available (Figure 1.3), microorganisms can, unlike plants, be exponentially grown in days instead of months or years. In this controlled process, they are safeguarded against climate or environmental change, allowing for less product variability and higher product purity that sometimes cannot be achieved in plants or algae (e.g. bacterial cellulose). Plus, microbial strains are not exposed to seasonal changes, meaning that under controlled conditions a consistent product can be achieved, with low production costs at high production rates (e.g. days instead of months). The use of industrial waste is another a way to obtain

different product outcomes while process optimization (e.g. glycerol, CO_2 or cheese whey). (Antunes et al., 2015; Freitas et al., 2009)

Polysaccharides' physicochemical versatility is applied industrially as thickening, emulsifying, stabilizing and flocculating agents. Table 1.2 shows dextran, the first microbial polysaccharide to be commercialized and approved for food applications by FDA, followed by xanthan gum, used in pharma as stabilizer or thickening agent able to retard drug release in tablets. (Benny et al., 2014)

Table 1.2 – Water-soluble microbial EPS produced by eukaryotic and prokaryotic microorganisms.

Microorganism	Strain	EPS	Composition	Properties	Applications	
Yeast and fungi	*Aureobasidium pullulans*	Pullulan*	Glucose	Adhesive Fiber and film forming	Food Tissue engeneering	(Agarwal and Chakraborty, 2015)
Bacteria	*Acetobacter xylinum*	Cellulose	Glucose	High tensile strength and moldability High cristalinity	Tissue engeneering	(RömLing and Galperin, 2015)
	Leuconostoc mesenteroides	Dextran	Glucose	Stable Fiber and film forming	Food Pharma Tissue engineering	(Casettari et al., 2015)
	Sphingomonas paucimobilis	Gellan	Glucose Glucoronic acid Rhamnose Acetate Glycerate	Stable in a wide range of pH Gelling capacity	Food Pharma	(Mahdi et al., 2015)
	Zymomonas mobilis	Levan	Fructose	Adhesive Film-forming Low viscosity	Food Cosmetics Pharma	(Srikanth et al., 2015)
	Xanthomas campestris	Xanthan*	Glucose Glucoronic acid Mannose Pyruvate Acetate	Viscous at low concentrarios Stable in a wide range of pH and temperature	Food Pharma Cosmetics	(de Mônaco Lopes et al., 2015)

*Generally Recognized As Safe polymers for human consumption by FDA, available for consultation under GRAS 170.30

The pharmaceutical industry continues to strive for innovation and efficiency in their products. EPS intrinsic properties can be extremely desirable, available to be exploited by different technologies in order to expand the scope of biopolymer application.

1.2.3.1 FucoPol

A conscious effort has been made to decrease most common toxic procedures and increase the use of greener technologies that aim to reduce or eliminate the use of hazardous substances in the design, manufacture and application of chemical products. The use of renewable feedstock from industrial waste (e.g. glycerol) has added value to industrial waste, maximizing the reuse of otherwise forgotten substrates. Biodiesel industry is predicted to produce 140 billion liters by 2016, in which 17.700 tons correspond to the production of glycerin each year (Yang et al., 2012).

FucoPol (W.O. Patent No. 011073874 A3, 2010) is a recent EPS of high molecular weight (10^6), a fucose-containing heteropolysaccharide produced by gram-negative bacteria *Enterobacter* A47 DSM 23139 (Freitas et al., 2010). Bacterial fermentation occurred under nitrogen and oxygen depletion, using an industrial waste – glycerol – as the energy source, insuring the bacteria's survival and growth (Freitas et al., 2010, Reis et al., 2016).

Torres, 2012 produced FucoPol in a stirred bioreactor where in the first 24 hours there was an exponential bacterial growth, under nitrogen exhaustion (batch mode); the following 72 hours, a sustained carbon source and nutrient fed was provided to the bioreactor (fed-batch mode). Freitas et al., 2010 were the first to synthesize this new exopolysaccharide, measuring its sugar content, molecular weight, intrinsic viscosity and rheological properties. Torres, 2012 and Freitas et al., 2014 obtained different amounts of FucoPol with different chemical compositions by changing the fermentative parameters; standard production parameters FucoPol contains a mixture of neutral sugars that involve fucose (35 mol.%), glucose (29% mol.%) and galactose (21 mol.%) as main components, along with glucoronic acid (12 mol.%), and mannose (3 mol.%) or rhamnose (3 mol.%), common in shorter FucoPol biosynthesis. Pyruvate, succinate and acetate are branched acyl groups responsible for the polymers' anionic character, with concentration varying from batch-to-batch (Cândido, 2015). The presence of high molecular weight residual proteins can also be found, since proceeding purifications steps are unable to remove them upon dialysis without washing away part of the polymer (Freitas et al., 2014).

Lourenço, 2015 performed DSC analysis in order to determine the amount of heat required to observe fusion and crystallization phenomena when FucoPol was exposed to 25 ºC to 550 ºC, with heating rates of 5 ºC.min^{-1} in air. Lourenço states that FucoPol does not present a glass transition or melting temperature (Tg) due to its amorphous character, possessing a degradation temperature around 220 ºC to 250 ºC. Although the polymer's molecular structure is still unknown, FucoPol has already shown great versatility, revealing promising emulsifying and flocculating activities, as well as

emulsion and stabilizing properties for food (Antunes et al., 2015) and packaging applications (Ferreira et al., 2014).

FucoPol was also used to produce ethanol dehydration membranes by pervaporation, using trichloroacetic acid and polyethersulfone as crosslinking agents (Meireles et al., 2013). In biotechnological applications FucoPol was used as a nanoparticle coating agent for antibody capture (Dhadge et al., 2014) and a main component in the production of novel polymeric structures by dissolution in biocompatible ionic liquids (Cândido, 2015). Its fiber forming abilities, as well as its interaction with supercritical carbon dioxide, will be analyzed in Chapter 2 and Chapter 3 of this dissertation.

When using FucoPol as a platform for biological applications, product design must be carefully evaluated; its ability to absorb water (i.e. hygroscopy) can be advantageous as an oral excipient for film or hydrogel production. Orodispersible formulations require fast dissolution rates, even when in contact with low salivary flow. Hydrogels, despite experiencing a slower dissolution due to hydroscopic behavior, are, generally, long-lasting matrices that can have higher drug loadings and sustained drug release profiles. The manufacturing techniques to be used in the production of an orodispersible film and a hydrogel require careful evaluation, since each design differs in application, drug loading and morphology.

1.3 Proposed solution

Since occasionally tablets reveal themselves as non-compliant for patients that somehow exhibit physical or mental restrains like Alzheimer's disease, the creation of two new oral drug delivery platforms with higher patient compliance is proposed, since they display biodegradable properties that can be developed to increase the drugs bioavailability while promoting faster drug release rates.(García-González et al., 2011)

To achieve this goal, the use of electrospinning for orodispersible film (ODF) production and cryogelation coupled with supercritical drying for scaffold (SCA) production is proposed. Below is a schematic representation that summarises the work performed in this dissertation (
Figure 1.**4**).

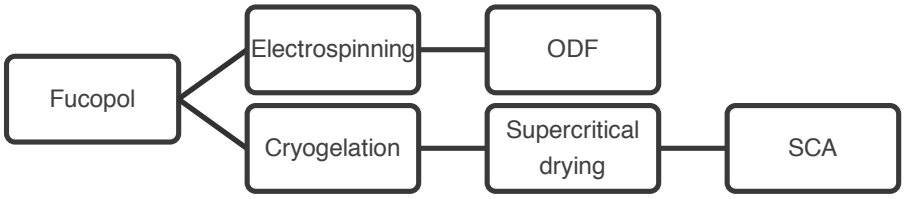

Figure 1.4 – Schematic representation of the work performed in this dissertation in order to produce and ODF and a SCA.

1.4 Outline

In Chapter 1 context is brought to the reader through the gathering of previous work, along with some fundamentals required for understanding our experimental development throughout this dissertation. An initial example of the proposed solution is provided while concluding with the main contributions of the work performed.

Chapter 2 will be devoted to the production process of FucoPol-based orodispersible film, providing an overview of fiber forming technologies, focusing on electrospinning and its fundamentals, related work and current marketed products. A description of the experimental procedure will be detailed, concluding with a discussion of the obtained results, while providing some concluding remarks and future work.

In Chapter 3 a scaffold will be produced using cryogelation and supercritical extraction techniques. A brief survey of most common scaffold production techniques will be mentioned, converging to cryogelation and supercritical fluid technology, describing the fundamentals and related work. Experimental description of the performed process will be provided in detail, as well as a discussion of the obtained results, previous to concluding remarks and future work.

Finally, in Chapter 4 some concluding remarks about the work that was done in this dissertation will be provided, discussing some possibilities of future work.

Production of a FucoPol orodispersible film by electrospinning

In this chapter, the production of the first of the two platforms intended for oral drug delivery will be presented. A FucoPol-containing fast-dissolving platform will be obtained by electrospinning, a green fiber forming technique that will be described in detail throughout this chapter. An overview of orodispersible systems regarding their advantages, formulations and currently marketed products will be described, with emphasis on chemotherapy induced nausea and vomiting (CINV). A description of the experimental procedure, performed in order to obtain a FucoPol-based orodispersible film, will be detailed. Additionally, a brief description of each technique used to physically, chemically and morphologically characterize FucoPol-based orodispersible film will be provided and further discussed upon analysis of the experimental data.

2.1 Fiber formation technology

Much like spider's silk spun webs, most fibers are created by forcing a viscous solution through the holes of a device called spinneret. Man-made spinnerets are similar to shower heads and, through different configurations, can spin several hundreds of fibers at the same time. Fibers can be manufactured by four conventional solution spinning processes: wet spinning, dry spinning, dry-wet spinning and melt spinning. In wet spinning (Jalili and Shepherd, 2013) a fiber forming solution is forced through a spinneret that is submerged in a chemical bath with a precipitating/anti-solvent agent, while in dry spinning (Zhang and Ogale, 2013) the solvent evaporates due to a stream of air or inert gas. Dry-wet spinning (Tasselli et al., 2013) combines the two processes mentioned above, being applied to gels; the gel-like solution travels by an air cooled path into a cooled liquid bath where fiber precipitation occurs. Melt spinning (Tkatch et al., 2002) is the most common process and is used industrially to produce nylon and polystyrene fibers, among

others. The substance is melted upon extrusion through the spinneret and, once it passes through it, is directly solidified by cooling.

Electrospray is a technique in which high voltage is applied in order to induce aerosolization of a liquid, through a glass or metallic capillary. It is commonly applied in inkjet printing, mass spectrometry (Loo, 1997), FID detectors (Rigort et al., 2012) and in the production of drug carriers and particles of different shapes and formulations. When a concentrated fiber forming solution is ejected from an electrospray device, a solid fiber is formed in a process known as electrospinning, exemplified in Figure 2.1. (Li and Wang, 2013)

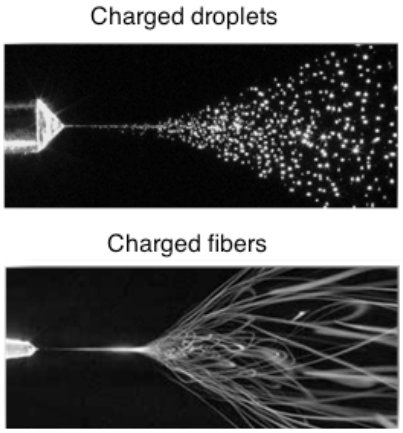

Figure 2.1 – Electrospray versus electrospinning: droplet and fiber production, respectively; (adapted from www.bioinicia.com, acessed 28th February 2016).

In the beginning of the 20th century Cooley, 1900 and Morton, 1902 made electrospinning noteworthy by filing for four different spinneret patents. Since then, the process gained attention (Norton, 1936) and, in the 60's, Sir Geoffrey Taylor mathematically modeled the shape of a liquid droplet when exposed to an electrical field, commonly known as the Taylor's cone (Taylor, 1964). In the mid-1990's Doshi and Reneker, 1995 became interested in the production of nanofibers due to their high surface to volume ratio, a potential advantage in scaffold production and nano-filtration devices. In short, electrospinning can be considered a variation of electrospray and melt-spinning, since instead of droplets a fiber is produced, and instead of direct cooling of the extruded solution, a jet is stretched due to applied electrostatic forces. Electrospinning apparatus can be adapted into melt electrospinning (Nagy et al., 2013), coaxial electrospinning (Ye et al., 2015), emulsion electrospinning (Yazgan et al., 2015), wire electrospinning (Chiu and Chen, 2015), high speed electrospinning (Nagy et al., 2015) and others (Hernández-Navarro et al., 2016).

Over the last century, natural polymers produced by animals, plants, algae or microbial sources have gained relevance due to an ongoing investment in renewable energy. In a report filed by Preis et al., 2014, marketed ODF are mostly made by a mixture of sweeteners (e.g. sucralose), plasticizers (e.g. glycerol),

cross-linkers (e.g. citric acid) and natural polysaccharides like maltodextrin, carrageenan, starch, bacterial cellulose, pullulan and xantham gum. (Hoffmann et al., 2011) Orodispersible films made by fiber forming technologies can possess certain heightened characteristics that other oral dosage forms do not; electrospinning produced matrices are made by micro or nanofibers that concede the membrane a high area to volume ratio, even in a small area. Plus, electrospinning is able to produce solvent-free ready-to-use thin films. Thickness of the film can be fine-tuned by extending or decreasing the solutions deposition time. (Pham et al., 2006)

2.2 Electrospinning

Electrospinning is an electrostatically driven process used for non-woven fiber production by solvent loss, yielding fibers whose diameters can range from nano to few microns. It usually involves a syringe pump, a static or rotating collector and a high voltage power supply. In this process, an electrically conductive polymeric solution is subjected to an applied electrical field, while being forced out from a syringe at a constant rate. The fiber is formed when the electrostatic forces overcome the surface tension threshold of the droplet accelerating and stretching the jet. The deformation of the droplet increases with the applied voltage leading to solution ejection and droplet disintegration when the voltage is excessive. Fibers will dry due to gradual solvent evaporation during jet flight towards the collector. (Pham et al., 2006)' (Liang et al., 2007)

Electrospinning has a number of working parameters that need to be controlled and adjusted according to the system under study. These can be divided in solution, processing and environmental parameters. All are essential but each one contributes differently in order to obtain a desired fiber design. Solution parameters involve concentration, viscosity, surface tension, molecular weight and conductivity. Fiber spinning strongly depends upon surface tension, a parameter that will determine the upper and lower boundaries of the electrospinning process. Different solvents can maintain or increase the surface tension of a given solution (Deitzel et al., 2001). Although surface tension can influence fiber morphology and diameter, concentration is the key parameter since electrospinning at low concentrations leads to the production of nano or sub-micron drops in a process known as electrospray (Yang et al., 2004)'(Costa, 2010). While an optimal concentration leads to smoother fibers, higher polymer concentrations favor the production of bead-defected fibers that can hamper the mechanical properties of the polymeric matrix. G Eda and JP Canejo et al. report that electrospun fibers of polystyrene and cellulose at very high concentrations produce helix-shaped ribbons (Canejo et al., 2008)'(Goki Eda, 2007).

Concentration is closely related to the polymer molecular weight and the solutions' viscosity. In general, polymers of higher molecular weight require less mass in order to achieve optimal viscosities and at lower concentrations since the amount of intermolecular interactions is higher, but the minimal amount of polymer

required to obtain fibers differs from system to system (polymer/solvent) and each case must be evaluated. The viscosity of a given solution can also be influenced by mechanical stress and temperature. Viscous solutions can behave as Newtonian or non-Newtonian fluids, depending on how the viscosity changes in the presence of stress (Figure 2.2). Newtonian fluids have linearly proportional to the strain rate (e.g. deformation over time), maintaining a constant viscosity (e.g. water). Non-Newtonian fluids are, however, a lot more common, experiencing shear-thickening (not represented) and/or shear-thinning behavior in the presence of increasing shear rates, leading to a decrease in apparent viscosity with increased deformation. The rearrangement of broken molecular bonds is equally matched by the formation of new ones causing a constant apparent viscosity (Torres et al., 2015). This is rapidly proceeded by a pseudo-plastic behavior resulting from an increase in shear-rate that causes a decrease in viscosity, meaning that the formation of new molecular bonds is overcome by loss of others, disrupting the polymers' internal structure. This is common for some food grade products, silicone coating and some polymeric solutions (da Silva and Rao, 2007).

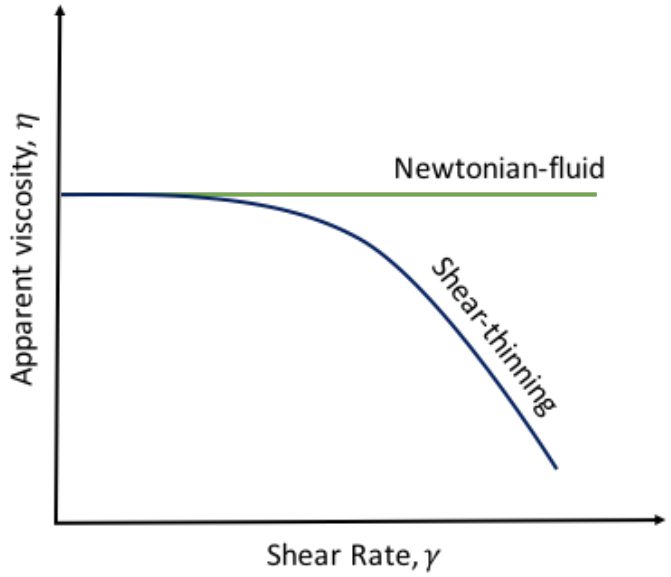

Figure 2.2 – Flow behavior: Newtonian and Non-Newtonian fluids; emphasis on shear-thinning behavior.

Because electrospinning involves an external electrical field, the intrinsic conductivity of the polymer or the solvent has to be carefully evaluated. The ability to conduct electricity increases with the polyelectrolytic nature of the polymer. Higher conductivity induces the formation of thinner fibers since the voltage applied to the charge carrying polymeric jet further stretches the polymeric chains. Subjecting the jet to very high voltage can induce overcharging resulting in jet breaking, solution ejection and overall poor fiber formation.

The charge carrying capacity of the polymer is related to the amount of voltage that is needed to promote the ejection of fiber forming polymer jet from the Taylor's cone, meaning that a lower voltage would be required to induce fiber formation in polymers having a great amount of polyelectrolytes. Everything beyond

that would induce further fiber stretching promoting thinner fibers. On the other hand, Reneker and Chun reported that electrical field and fiber diameter are not related while Zhang et al. and T. Reis et al. (Reis et al., 2013) reported that higher voltages induce higher fiber diameter.

In terms of flow rate and distance between the collector and the tip of the syringe, if the rate is too high, a large portion of the solution will be ejected leading to fibers with larger diameter. If the distance between needle and collector is too short, the solvent will dry slowly, potentially leading to fiber fusion. Larger distances and lower rates are recommended in order to obtain a suitable fiber. Collector should be conductive, but depending on the polymer and the application, the collector can be adjusted. On top of an aluminum foil sheet parchment paper, glass, paper, Teflon, grids, rotating rods or wheels can be placed (Ganesh et al., 2012; Neves et al., 2007; Panda and Ramakrishna, 2007; Thieme et al., 2009).

Last but not least, environmental conditions are the primary factor that can destabilize the electrospinning process because it is very hard to completely monitor and control them. Mit-uppatham et al.(Mit-uppatham et al., 2004) report that an increase in temperature leads to thinner fibers with smaller diameters, while an increase in humidity leads to thicker fibers due to the neutralization of the superficial negative charges of the jet and consequent decrease in stretching forces. Furthermore, Casper et al.(Casper et al., 2004) proved that fiber surface porosity increases with humidity. For some polymers, a low humidity is required since at these conditions the solvent evaporation increases leading to a dried fiber mat. (Li and Wang, 2013)

One of many advantages of electrospinning films is the high surface area to volume ratio. They also present tunable porosity and one can manipulate nanofiber composition in order to get desired properties, function and malleability, over a wide variety of sizes and shapes. (Liang et al., 2007)

2.3 Orodispersible systems

Orodispersible films are a good alternative to administer low dosage forms since the drug can have a faster systemic onset, not requiring chewing or swallowing. With dissolution times usually less than 1 minute, sublingual dosage forms are patient compliant and an easy, painless and efficient alternative in drug release. Due to their fast dissolving purpose, ODFs must be designed with hydrophilic compounds that can quickly disintegrate when in contact with the mouth's salivary flow. (Hoffmann et al., 2011; Shen et al., 2013) Table 2.1 provides a number of ODFs presently available on the market.

Table 2.1 – Over-the-counter orodispersible thin films by market sector (Slavkova and Breitkreutz, 2015) **.**

Area	Active ingredient	Commercial name	Manufacturer
Migraine	Zolmitriptan	Zolmitriptan Renantos	Renantos
Anemia	Ferric oxide	Hemoramin	C.L. Pharm
Erectile disfuntion	Sildenafil citrate	Sildenafil Sandoz	Sandoz
Anti flatulence	Silicone oil	Gas-X Tongue twisters	Gas-X
Mouth refreshner	Mint oil	Listerine pocket packs	Pfizer
Nicotine withdrawal	Nicotine	NiQuitine Strips	GSK
Alzheimer's disease	Donezepil hydrochloride	Donezepil-HCL	Hexal/Sandoz
Schizophrenia	Risperidone	Risperidone HEXAL	Hexal/Sandoz

Pharmaceutical companies try to achieve optimal drug delivery systems that will add value to the product (e.g. enhanced disintegration time) and be convenient for patients. Catalent produce orodispersible tablets (ODT) like Zydis®, Lyoc® and Quicksolv® by freeze-drying/lyophilization, Orasolv®/Durasolv® and Flashtab® by compression and WOWtab® by molding (McLaughlin et al., 2009). These technologies may successfully produce orodispersible sublingual films for protein or peptide delivery (Zydis® Bio). Orodispersible films can incorporate binders (e.g. PEO, xylitol), disintegrants (e.g. PVP, starch), coatings (e.g. gelatin, HPMC) and preservatives (e.g. antioxidants) as well as sweeteners (e.g. sucrose), flavors (e.g. mint) or colors (Stijnman et al., 2011). Excipients can have very complex formulations in order to enhance bioavailability and therapeutic profiles, increasing patient convenience, adherence and compliance while at the same time preventing unwanting behavior like crumbling, sticking, poor handling mechanical strength and product degradation due to environmental water uptake.

There are many different definitions for orodispersible films (ODF) among the literature, with broad terms like thin-film, oral film, oral strip, oral thin film, buccal film and oral mats, as some of the many examples found. These are sometimes mixed together misleading the reader to think that they have the same meaning when in reality they do not, creating misunderstanding and confusion. There is an urgent need to have proper regulation for oral films and their different production methods. Nevertheless, in the latest edition of the European Pharmacopoeia (Ph. Eur. 8th Edition, 2015) an "Orodispersible films" subchapter was added, contained within "Oromucosal preparations". The latter is defined in Ph. Eur. 5th as "solid, semi-solid or liquid preparations containing one or more active substances intended for administration to the oral cavity to obtain a local or systemic effect (...) that are to be absorbed primarily at one or more sites on the oral mucosa.".(Ph. Eur. 5th, 2000) Not to be misinterpreted with buccal films – "oromucosal praparations intended to be attached to oromucosal sites" - or sublingual tablets – "solid preparations each containing a single dose of one or more active substances (..) being usually obtained by compressing uniform volumes of particles." It is also mentioned that "tablets are intended for oral administration, (...) swallowed whole, (...) chewed, (...) dissolved or dispersed in water before being administered and some are retained in the

mouth where the active substance is liberated." (Ph. Eur. 5th, 2000)

FDA defines a drug delivery system as "Modern technology, distributed with or as a part of a drug product that allows for the uniform release or targeting of drugs to the body" (U.S. Food and Drug Administration, 2009) and a soluble film as "A thin layer or coating which is susceptible to being dissolved when in contact with a liquid".(U.S. Food and Drug Administration, 2009) An orodispersible film is a soluble film with drug delivery properties. Plus, has the ability to rapidly disintegrate or disperse in situ when in contact with a liquid, fast releasing its drug content into the oral cavity. (Borges et al., 2015)

With these kind of products, a higher bioavailability maybe obtained related to the fast availability of the drug, even if some part of the drug is swallowed.

2.4 Nausea and vomiting

Cancer therapy is one of the fastest growing sectors in the pharmaceutical industry, expected to reach a market value of $225 billion until 2017 (Global Industry Analysts, 2011). World Health Organization (WHO) reports 14.1 million new cases of cancer occurred worldwide by 2012, 560 thousand of which related to head and neck cancer in the UK only. Nausea and vomiting (N&V), or emesis, are common side effects that can occur during or post chemo or radiotherapy treatments. The global market for antiemetics' was worth $2.4 billion in 2009, being expected to reach 3.6 billion by 2015. With an expected increase of 70% in new cancer cases, and with above 100 cancer types, the need to find alternative solutions that can enhance therapeutic profiling and drug bioavailability is of major importance. (Global Data, 2012).

Nausea and vomiting (N&V) can arise from a number of situations that can be related to the administration of certain opioids or if constipation or infection is developed. Chemotherapy-induced nausea and vomiting (CINV) can be classified as acute (i.e. first 24 hours), delayed (i.e. more than 24 hours), anticipatory (ANV), breakthrough (i.e. after 5 days) and chronic (Niederhuber et al., 2013).

CINV treatments mostly involve the ingestion of pills, which can be hard to swallow and susceptible to first-pass effect. Plus, the ingestion of tablets upon nausea symptoms can many times induce vomiting, or emesis.

In order to avoid it, excipients that are quickly dissolved and absorbed in the oral mucosa (e.g. orodispersible films) are able to bypass gastroentesinal drug absorption, guaranteeing faster drug releases and drug bioavailability in the systemic circulation. A number of orodispersible film that contain antiemetic drugs are already available on the market but none were found with metoclopramide as the active ingredient (Table 2.2).

Table 2.2 – Antiemetic ODF available on the market. (Slavkova and Breitkreutz, 2015)

Commercial name	Active ingredient	Manufacturer
Zuplenz	Odansetron	Galena Biopharma
Setofilm		Norgine
Ondissolve		Takeda Pharmaceuticals
Motilum	Domperidone	Zentiva, Sanofi
Vogalib	Metopimazine	Schwarz Pharma
Naus-ease	Meclizine hydrocloride	Sunascen Therapeutics LLC
Zentrip		Sato Pharmaceutical Co., Ltd
Rizamelt	Rizatriptan benzoate	Mylan

2.4.1 Metoclopramide hydrochloride

Metoclopramide hydrochloride (Figure 2.3) is a low molecular weight, water soluble salt, that acts as an acetylcholine release promoter with central anti-emetic action, used to stimulate the gastrointestinal motility. Metoclopramide can be use to relieve the symptoms of nausea and vomiting during migraine or cancer therapy. (Ph. Eur. 5th, 2000)

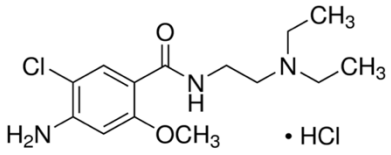

Figure 2.3 –Metoclopramide hydrochloride molecule (adapted from Sigma).

It can be used to relive acute nausea and delayed nausea; for acute nausea it is recommended that metoclopramide is taken before antioneoplastic agent administration, an agent used to prevent, inhibit or halt the development of a neoplasm (e.g. tumor). (Niederhuber et al., 2013)

Metoclopramide hydrochloride is marketed by Salix and IPCA Labs Ltd. as a tablet/orally disintegrating tablet with brand name Metozolv ODT (5 to 10 mg) and/or Perinorm (5 to 10 mg). Ani Pharmaceuticals markets metoclopramide hydrochloride as an oral solution (5mg) and tablet (5 to 10 mg) under the brand name Reglan. Hospira (Pfizer) also provides metoclopramide hydrochloride as an injectable under a generic name (FDA Drug database, FDA, accessed 24th March 2016).

In order to prevent emesis, an oral dosage form that allows for faster drug absorption and prevents emesis due to drug administration is in order. Hence, **the goal in this chapter is to combine FucoPols' hydrophilic properties with its possible fiber forming abilities in order to produce an orodispersible film, using metoclopramide hydrochloride as the antiemetic chosen for the relieve of nausea and emesis symptoms.**

2.5 Experimental section

2.5.1 FucoPol downstream processing

FucoPol purification steps were performed according to (Freitas et al., 2010). 400 mL samples of culture broth were diluted using deionized water 1:2 (v/v) for viscosity reduction. Approximately 200 mL samples of diluted culture broth were transferred to 250 mL centrifugation bottles (Nalgene) where cell debris and denatured proteins were removed by two separate centrifugation cycles of 45min at 8.000 rpm and 4 ºC (Avanti J-25, Beckman), using a JA-14 rotor (Beckman). These cycles were interweaved with a thermal treatment of 1 hour at 70 ºC (Conterm oven, JP Selecta), in order to ensure bacterial enzyme inactivation and preventing polymer degradation. The broth was then dialyzed for 48h with a 12.000 MWCO dialysis membrane (NaloMembran SO farblos, Nalo) against deionized water and freeze-dried for 48 hours (Lyo Quest-55 8 port manifold, Telstar).

2.5.2 Orodispersible film production by electrospinning

In order to produce orodispersible films, three solutions were prepared (e.g. S1, S2 and S3), containing an average of 120 mg of FucoPol, 60 mg of poly (ethylene oxide) and 10 mg of metoclopramide in 6 mL of deionized water (Table 2.3). The resulting orodispersible film contained 94.7 wt.% of polymers and 5.26 wt.% of drug content. Solutions S1, S2 and S3 were also used in the production of orodispersible films by solvent casting, for comparison purposes. Solutions S1, S2 and S3 were transferred into a 100 mm teflon disc (Bola, Germany) provided by Ana Rita Ferreira, and dried overnight in a 30ºC thermostated room.

Table 2.3 – Sample formulations used in the production and characterization of electrospun and solvent casting orodispersible films: Sample S1 - 2 wt.% of FucoPol (FP) **(**bacterial exopolysaccharide produced and provided by Pure Cultures Group from UCIBIO-REQUIMTE/FCT/UNL, Mw ~10^6); Sample S2 – 3 wt. % of a physical blend between FP and poly(ethylene oxide) (PEO) (Sigma-Aldrich, Mw 2x10^6), using the proportion 2:1 (w/w); Sample S3 – Sample S2 and 0.17 wt. % of metoclopramide (MET) (Sigma-Aldrich).

		FucoPol (FP) (mg)	Poly(ethylene oxide) (PEO) (mg)	Metoclopramide (MET) (mg)
Samples	**S1**	120	-	-
	S2	120	60	-
	S3	120	60	10

Solvent: Deionized water

All samples were prepared overnight and pumped the following day through a syringe with 12.04 mm of internal diameter (Inject, Braun) at a rate of 0.5 mL.h^{-1} (KDS100 Syringe Pump, kd Scientific) using a 21-

gauge needle (Sterican 100, Braun). Fiber formation was induced by a high voltage regulated power supply (Glassman High voltage regulated DC Power Supplies, EL Series) at 13.5 kV and collected in computer controlled parchment paper plate (Papstar baking paper). A rotating collector (Figure 2.4) was chosen instead of a static one in order to avoid a heterogeneous fiber density distribution upon electrospinning process. The collector was placed approximately 23 cm from the tip of the needle.

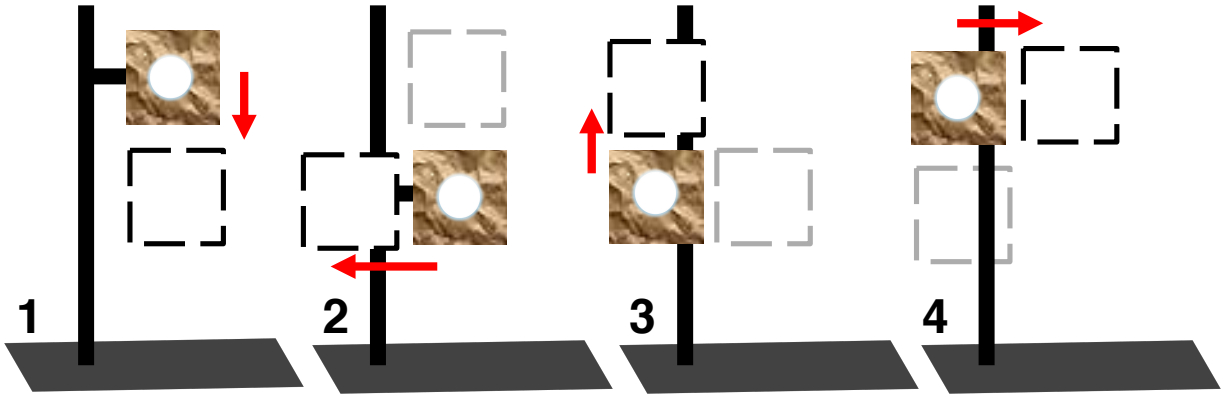

Figure 2.4 – Schematic representation of the computer controlled electrospinning process (A), with special attention to fiber collection. A set of spatial coordinates (defined by the user) are introduced into a graphical interface, establishing a connection between the user and the Arduino microcontroller, used to control the mechanical structure were the collector is placed (Lopes, 2012). The spatial Cartesian coordinates (x,y,z) used were (111,182,31); (114,182,61); (114,165,61) and (114,165,31).

Electrospinning was performed under controlled humidity (20-35%, Tasciugo Ariadry Light DNC 65, DeLonghi) and temperature, at (20-27ºC, Haice). Prior to electrospun orodispersible film characterization, all samples were dried overnight at ambient temperature, and stored in a vacuum desiccator.

2.5.3 Analysis of electrospinning working parameters

2.5.3.1 Apparent viscosity

The use of highly viscous solutions in electrospinning can clog the needle, or promote solution accumulation in the tip of the needle that can lead to the formation of beads in the electrospun fibers. Highly viscous solutions cannot be electrospun since the electrostatic repulsion is unable to surpass the superficial tension that allows the formation of the Taylor's cone and the ejection of fibers. In order to assess the viscosity of a given polymeric blend rheometric studies were performed.

A rheometer is a device that measures the deformation of a solid, liquid or gas under rotational or extensional forces. When measuring the flow between two parallel flat plates (i.e., one plate is mobile, the other is stationary) the fluid is subjected to laminar flow and the resistance of fluid against irreversible positional changes in its volume is called viscosity, expressed by the Equation 2.1 as shear stress (τ) (e.g.

the tangencial force applied to a specific area) multiplied by shear rate (γ) (e.g. a gradient of velocity at which shearing deformation occurs). (Schramm, 1994)

$$\eta = \frac{\gamma\ (s^{-1})}{\tau\ (Pa)} \qquad \text{Equation 2.1}$$

Rheological measurements were performed by Post Doc Reseacher Coro Zabala at CENIMAT, FCT/UNL. The values were the apparent viscosity seems constant (i.e. newtonian viscosity) were obtained from flow curves of all samples used in electrospinning, using a stress-controlled rheometer Bohlin Gemini HR nano, with cone-plate geometries 40mm and 20mm diameters.

2.5.3.2 Differential Scanning Calorimetry (DSC)

Differential Scanning Calorimetry (DSC) is a thermoanalytical technique that uses temperature to measure the amount of heat required to induce physical transformations on a given sample, by registering the different amount of heat absorbed, melting at temperature T_m or crystallizating at a given temperature. DSC analysis also registers mass loss and is able to measure the temperature at which sample degradation occurs. (Höhne et al., 2013)

Since FucoPol is known to be amourphous from previous work (Lourenço, 2015), the behaviour of FucoPol in the presence of a physical crosslinker and/or a drug was assessed by differential scanning calorimetry (DSC), performed by Prof.ª Madalena Dionísio at FCT/UNL. Calorimetric experiences of samples S2 and S3 were carried out using DSC Q2000 from TA Instruments Inc. (Tzero™ DSC technology). Analysis was performed under anhydrous high purity nitrogen at flow rate of 50 $mL.min^{-1}$. Approximately 3 mg of both samples were sealed in aluminium hermetic pans (TA Tzero Pan and lid) and submitted to temperatures ranging from -90 to $+180^0C$, at a rate of $5^0C.min^{-1}$. The lid of the pan was breached in order to allow water evaporation.

2.5.4 Orodispersible film morphological analysis

2.5.4.1 Scanning Electron Microscopy (SEM)

Scanning electron microscopy (SEM) is a type of electron microscopy that uses high voltage to produce a beam of accelerated electrons that probes a given sample in a square pattern (raster scan). The loss of energy that arise from the interaction between the sample and the electron beam is converted into low-energy secondary electron emisson, detected by a secondary and backscattered electron detector and converted, acording to a speficic position, to produce an image. Other type of electron microscopes include transmition electron microscope (TEM) and environmental scanning electron microscope (ESEM). (Goldstein et al., 2012)

In order to measure the average fiber diameter of the electrospun fibers, as well as overall visual imaging of its morphological appearance, SEM imaging was performed at Instituto Superior Técnico (IST) by Isabel Nogueira. Film morphology was obtained by Hitachi S-2400 Scanning Electron Microscope at an accelerating voltage of 15kV and a magnification of 5 and 10K. Samples 2 and 3 were frozen and fractured in liquid nitrogen for cross-section analysis and attached to an aluminum stub using carbon tape. Previous to SEM analysis, samples S2 and S3 were gold coated in order to avoid charge effects.

2.5.4.2 Atomic-Force Microscopy (AFM)

AFM is a type of scanning probe microscopy that uses a piezoelectrical element to oscillate a cantilever in order for it to probe the surface of a given sample. As the cantilever oscillates, a detector records its motion and displacement, converting the positional differential into an electrical signal with proportional intensity to the displacement of the cantilever.

Atomic-Force microscopy was performed within a collaboration (Ana Rego, IST). Samples S2 and S3 were imaged by Bruker Innova Microscope using tapping mode and TESP cantilevers (Bruker AFM probes), at ambient temperature and pressure. The resulting images were software analyzed by NanoScope Analysis 1.5.

2.5.5 Orodispersible film chemical composition

2.5.5.1 X-Ray Photoelectron Spectroscopy (XPS)

How two surfaces interact depends on the physical properties of the layers in contact, which in turn are defined by the elements that are present in the sample and in which way they are connected to each other. X-Ray photoelectron spectroscopy (XPS) is an elemental analysis that can detect which elements are present in the sample in the first 10 nm of its outer surface. In order to do that, an X-Ray beam, produced by the incidence of an electron beam in a aluminum surface, is used to promote electron ejection through photon-electron interaction. This interaction will annihilate the photon and release energy that will induce electron emission from the atom. The kinetic energy is a function of electron binding energy (BE) and can be quantified by an electron energy analyser (van der Heide, 2011).

X-ray photoelectron spectroscopy (XPS) analyses were performed within a collaboration (Ana Rego, IST). Samples S2 and S3 were analyzed using XSAM800 X-ray spectrometer operated in transmission mode (FAT) with a pass energy of 20 eV, a power of 120 W and an incidence of Mg anode non-monochromatic radiation of $h\nu$=1253.6 eV. Spectral data was obtained using Vision 2 with a step of 0.1 eV, while charge shift was corrected using C 1s and carbon singly bound to oxygen binding energy as reference (285 eV and 286.5 eV, respectively). 0.318 (C 1s), 0.736 (O 1s) and 0.505 (N 1s) were the sensitivity factors used during the procedure.

2.5.5.2 Fourier Transform Infrared Spectroscopy (FTIR)

FTIR is a technique that uses the Michelson interferometer to alter the distribution of infrared light that is absorved or emitted by a sample, in order to record the samples' infrared spectrum. The Fourier transform allows the conversion of raw data into light output as a funtion of infrared wavenumber. FTIR spectroscopy was performed since infrared spectroscopy is often used to identify specific groups of atoms or bonds that have known frequency (i.e. functional groups), allowing the confirmation of a given compound in a complex mixture. (Smith, 2011)

Post Doc Researcher Rita Branquinho at CENIMAT, FCT/UNL analyzed samples S2 and S3 using an Attenuated Total Reflectance (ATR) sampling assessory (Smart iTR) equipped with a single bounce diamond crystal on a Thermo Nicolet 6700 Spectrometer. The spectra were acquired with a 45° incident angle in the range of 4000–525 cm^{-1} and with a 4 cm^{-1} resolution.

2.5.6 Orodispersible film characterization

2.5.6.1 Weight, thickness and pH

As a way to assess electrospinning reproducibility and to guarantee that the electrospun orodispersible films were within the requirements (Hoffmann et al., 2011) samples S2 and S3 were measured and weighed with digital display micrometer (0-25 mm, Mitutoyo) and KERN 770 analytical balance (Ph. Eur. 5th, 2000). The number of samples, n, was ten for either S2 and S3 (n=10).

pH was measured in order to assess orodispersible film neutrality, since alkaline or acidic pH may cause irritation of the oral mucosa. The ODFs pH was measured by bringing the electrode in direct contact with all the samples involved in the production of orodispersible films by electrospinning. The final pH resulted was the average between 4 consecutive measures (Shamma and Elkasabgy, 2014)

2.5.6.2 Mechanical properties

Film resistance to manual handling was assessed by stress-strain tests, performed in dry films of 2 cm^2, using Rheometric Scientific (Minimat Firmware 3.1) at room temperature. Samples S2 and S3, of 2cm^2, were cut and stretched uniaxially at a speed of 1 $mm.min^{-1}$ at room temperature, with a maximum load of 20 N and a maximum displacement of 90 mm. Distance between clamps was set to 10 mm. Load extension data was obtained and converted to stress/strain curves by applying Equation 2.2 and Equation 2.3:

$$\sigma(MPa) = \frac{F\ (N)}{A\ (mm^2)} \qquad \textbf{Equation 2.2}$$

$$\varepsilon = \frac{\Delta l\ (mm)}{L_0\ (mm)}$$ **Equation 2.3**

where σ is the stress, ε is the strain, F is the applied force, A is the cross-sectional area in contact with the clamps, Δl is the displacement of the sample under uniaxial elongation and L_0 is the distance between the clamps.

2.5.6.3 *In vitro* disintegration time[1]

Orodispersible systems must disintegrate under 3 minutes, ideally 30 seconds to 1 minute (Hoffmann et al., 2011). Disintegration time was registered according to Vuddanda et al., 2016; samples S2 and S3 (n=3) were applied on the surface of a sponge (Scotch-Brite) measuring 2 cm wide, 5.4 cm long and 0.6 mm in height. The sponge was wetted in 250 mL of simulated saliva (Marques et al., 2011) at pH 6.8. The time required for total disintegration was registered. The same procedure was applied to solvent casting membranes, for comparison purposes.

2.5.6.4 Uniformity and drug content[1]

In order to assess the drug's distribution and its amount in the ODF, peripheral and central segments of samples S2 and S3 (n=3) were transferred to 5 mL glass flask containing 2 mL of simulated saliva (Marques et al., 2011) at pH 6.8 and left for approximately 1 hour at 37ºC and 100 rpm (Orbital shaker Rotaterm, JP Selecta). The samples were diluted 1:15 (v/v) and released metoclopramide was quantified at 272 nm by UV analysis using a Lambda 25, Perkin Elmer UV/Vis spectrometer and two 1 mL QS Quartz suprasil high precision cells, with 10 mm optical path (Hellma Analytics).

2.5.6.5 *In vitro* drug release kinetic profile[1]

The amount of metoclopramide released from the ODF, as a function of time, was possible to be obtained by drug release kinetic profiling. Samples S2 and S3 (n=3) were transferred to glass flasks containing 10 mL of simulated saliva (Marques et al., 2011) at pH 6.8, 37ºC and 100 rpm (Orbital shaker Rotaterm, JP Selecta). Several aliquots were retrieved after 5, 10 and 30 seconds, as well as 5, 10, 15 and 30 minutes, in the course of 4 hours. Due to their hygroscopic character, the samples were placed inside a membrane with a mesh of 1 µm to avoid collecting part of the film during the assay. Metoclopramide was quantified by UV/Visible spectrophotometry (PerkinLambda) using two QS High Precision Cells with 1 cm optical path

[1] Simulated saliva was prepared according to Marques et al., 2011, by weighing 8 $g.L^{-1}$ of sodium chloride (Panreac), 2.38 $g.L^{-1}$ of sodium phosphate dibasic (Sigma-Aldrich), 0.19 $g.L^{-1}$ of potassium phosphate monobasic (Sigma-Aldrich) and 0.05 mg/L^{-1} of Lysozyme (Sigma-Aldrich). Phosforic acid (Sigma-Aldrich) was used to adjust pH 6.8.

(Helma Analytics), at 272 nm. The total mass of drug released is equal to the sum of all aliquots retrieved throughout the 4 hours of drug release. Transport mechanism that induces drug release was determined by the Korsmeyer-Peppas equation. Through Equation 2.4 it is possible to predict which diffusional mechanism are involved in the drug release profile of metoclopramide (e.g. Fickian and non-Fickian mechanisms). The model considers the first 60% of drug release, assuming perfect sink-conditions.

$$\frac{M_t}{M_\infty} = kt^n \qquad \textbf{Equation 2.4}$$

Here, *k* is a constant that reflects the macromolecular network comprising the drug loaded system, *n* is the diffusional exponent, indicative of the transport mechanism and *t* is the time. Fickian diffusion is defined by n=0.5 and non-Fickian diffusion by n>0.5, for slabs. The same procedure was applied to solvent casting membranes, for comparison purposes.

2.5.6.6 Cytotoxicity

All the components used to produce the orodispersible films were assessed in terms of cytotoxicity, since through their combination, a toxic product could be obtained. Due to being an oral application, epithelial VERO cells from monkey kidney (*Cercopithecus aethiops*) were grown in Dulbecco's modified Eagle's medium (DMEM 5030, Sigma) supplemented with 1 % (v/v) of GlutaMAX (Life Technologies), 1% (v/v) of sodium pyruvate (Life Technologies), 1 % (v/v) penicillin/streptomycin (penicillin-streptomycin 10000 units/mL, Invitrogen) and 10 % (v/v) fetal bovine serum (FBS) (Invitrogen). Cells were maintained in 25 cm^2 culture flasks in a CO_2 incubator at 37 °C in a 99 % humidified atmosphere of 5 % (v/v) CO_2.

Cell culture medium was removed and 2 mL trypsin (TrypLE Express, ThermoFisher Scientific) was added to remove cell adhesion from the culture flask; incubation was set for 5 minutes at 37 °C in a 99 % humidified atmosphere of 5 % (v/v) CO_2. Loss of cell adhesion was confirmed using an inverted microscope and 5 mL of DMEM were added to the culture flask to neutralize the trypsin. The solution was transfered to a 15 mL falcon where it remained until cell counting. The number of viable VERO epitelial cells was assessed by the trypan blue assay, a dye that can trespass the plasma membrane of non-viable cells (Strober, 2001). 10 µL of trypan blue was added to a 1 mL cell suspension sample and a 20 µL sample was retrieved and transferred on to a hemocytometer (Figure 2.5), were the number of viable cells was determined using an inverted microscope. The resulting cell density was determined by Equation 2.5.

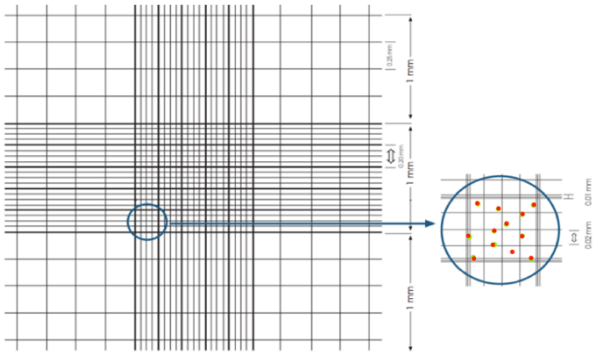

Figure 2.5 – Schematic representation of the hemocytometer used to count the number of viable VERO cells.

$$\#viable\ cells.ml^{-1} = \frac{\Sigma \text{cells per quadrant}}{6\ (number\ of\ quadrants\ counted)} \times 10^4 (chamber\ volume) \times dilution\ factor$$

Equation 2.5

Afterwards, VERO cells were seeded with a density of 1.2 x 10^4 cells/well in a 96-well plate (Figure 2.6) with 200 µl of DMEM media each, supplemented with 1%(v/v) of gentamicin (Life Technologies) and 1% (v/v) of streptomycin (Gibco). Cells were maintained at 37 °C in a 99 % humidified atmosphere of 5 % (v/v) CO_2 for 24 hours prior subtracts incubation. After 24 hours of cell growth, where each well presented a cell monolayer, medium was removed and replaced by 200 µL of fresh media containing 10 mg of each substrat. Cell viability assay was determined using resazurin (20% (v/v), Alfa Aesar), an oxidation-reduction pH indicator.

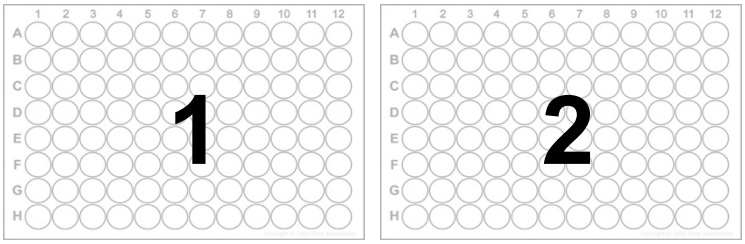

Figure 2.6 – Cytotoxic assays; schematic representation of the two 96-well plates used to test of initial subtracts cytotoxicity used to produce samples S1, S2 and s3: Plate (1) – 1 % (w/v) FP (1 to 5); 1 % (w/v) PEO (6 to 10);positive control (C+): DMEM media with 10 µl of Dimethylsulfoxide (DMSO) (11); negative control (C-): cells grown in DMEM media (12); Plate (2) – 1.5 % (w/v) MET (1 to 5); 2.6 % (w/v) sample S3 (6-10); positive control (C+): DMEM media with 10 µl of DMSO (Merck) (11); negative control (C-): cells grown in DMEM media (12). Successive dilutions of each component were performed in each plate: ½, ¼, 1/8, 1/8, 1/16, 1/32 (w/v) from A to F, with respective media control H (1 to 4). Adapted from http://www.cellsignet.com, assessed in 1st March 2016

2.6 Results and discussion

Part of the goal of this dissertation was to assess the never-before-tested fiber forming abilities of FucoPol, in order to produce an orodispersible film by electrospinning. Several FucoPol concentrations were tested using different solvents. Standalone FucoPol fibers were unable to be obtained, even at high EPS concentrations; instead the formation of droplets of different shapes and sizes was observed, in a process called electrospray (Annex 1). The use of electrospray as an appointed method to produce FucoPol nano or micro spheres/capsules is viable, although capsule production by electrospray is out of the scope of this dissertation. In order to produce an orodispersible film containing FucoPol, several crosslinking, fiber forming, biocompatible polymers were tested. Poly(ethylene oxide) was chosen since it was the one that could produce fibers at the lowest concentration (Annex 2). From this moment on, the results shown are related to the characterization of an orodispersible film produced by electrospinning, using the formulations displayed in Table 2.3, subsection 2.5.2., recollecting that S1, S2 and S3 represent the experimental formulations prepared in order to obtain electrospun ODFs, while all the compounds present in those formulations will be mentioned as FP (i.e. FucoPol), PEO (i.e. poly (ethylene oxide)), MET (i.e. metoclopramide hydrochloride).

2.6.1 Analysis of electrospinning working parameters

2.6.1.1 Apparent viscosity

The viscosity of a given solution, in electrospinning, is a good assessment of the polymers capacity to produce fibers, since viscosity is very commonly related to the solution's concentration. Highly viscous solutions usually have higher polymer content than lower viscosity ones, enabling fiber production (electrospinning), that usually end up producing spheres (electrospray) or extremely beaded fibers. EPS have, in general, high molecular weights, but not all have demonstrated to have fiber forming abilities (Stijnman et al., 2011). They can act as thickeners due to their high stability at lower polymer concentrations. Low molecular weight polymers, like poly (ethylene glycol) (PEG) and polyvinylpyrrolidone (PVP) are many times used in orodispersible film formulations; however, the amount of low molecular weight PEG required to produce fibers exceeds the amount of high molecular weight polymer required to obtain fibers. The minimum amount of poly (ethylene oxide) tested that could induce fiber formation upon electrospinning was 0.5 wt.% (Annex 2). The solution presented low viscosity at ambient temperatures and fiber production during electrospinning was sometimes unstable, with occasional dripping and beaded fibers production. Adding FP increased the solutions' viscosity, helping to stabilize the Taylor's cone and overall electrospinning process. The study of the effect of temperature on the rheological properties of FP is already known from previous work, exhibiting good thermal stability under a wide range of temperatures (Cruz et al., 2011; Torres et al., 2015). Viscosity is closely related to high polymer concentrations, but in complex mixtures, the addition of cross-linkers and plasticizers can increase the viscosity of a given solution.

Apparent viscosities of S1, S2 and S3 were assessed using $1s^{-1}$ to 700 s^{-1} shear forces, at 25 ºC (average temperature encountered in performing electrospinning assays). Flow curves presented in Figure 2.7 :

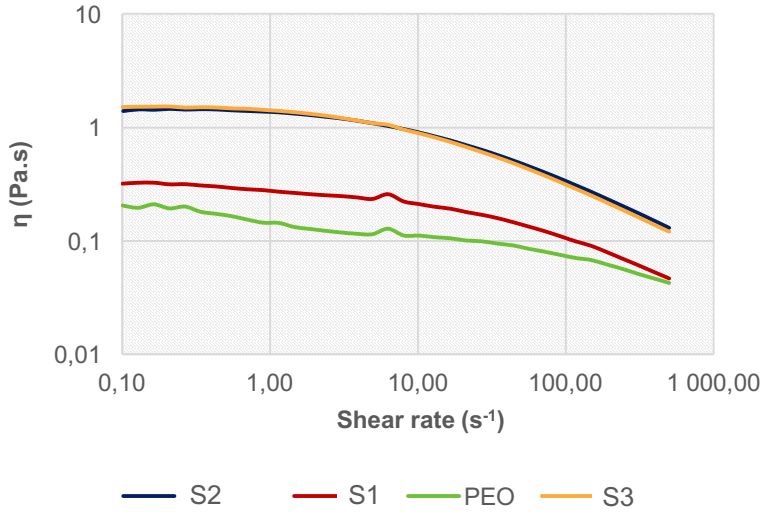

Figure 2.7 – Viscosity (η) of different compounds used to produce the electrospun ODF. All the control samples were prepared according to the individual concentrations found in each ODF sample (Table 2.3). Flow curves were obtained at 25ºC.

All individual chemical components were assessed in order to analyze the influence that different formulations would impose upon the ODFs' viscosity. S1 exhibits similar behavior to FP 0.81% reported by Cruz et al., 2011, an FP sample subjected to consecutive temperature fluctuations (15 ºC to 80 ºC). The sample revealed enhanced stability, maintaining its rheological properties in a wide range temperatures, validated by coincidence of flow curves. The polymers' intrinsic mechanical properties are easily overcome by shear forces that disrupt the polymers internal structure, since the Newtonian plateau is rapidly overthrown by pseudo-plastic behavior (Cruz et al., 2011). Nonetheless, all tested solutions present a Newtonian plateau (η_0) at low shear rates, where the viscosity is higher. This is known as shear-thinning behavior, present in all formulations over 100 s^{-1}.

Apparent viscosity was directly extrapolated from the diagram presented in Figure 2.7, where the flow curves and the *y* axis (η (Pa.s)) cross. FP and PEO have a stand-alone viscosity of 0.32 and 0.206 Pa.s, at at 25ºC, respectively. As expected, S2 shows an increase in viscosity with values around 1.52 Pa.s, at 25ºC. S3 maintained the apparent viscosity of S2 since the amount of metoclopramide present in the solution is residual when in comparison to the polymeric components of the film. For electrospinning, solutions viscosities ranging from 1 to 10 Pas.s are still viable to be electrospun without hampering the procedure, admitting that every system requires previous optimization.

2.6.1.2 Differential Scanning Calorimetry (DSC)

Differential scanning calorimetry was performed in order to evaluate the ODFs phase transformations as melting (transition from crystal to liquid) that occurs at a definite temperature, T_m, crystallization (transition from melt to a crystalline solid) occurring at T_c, and the glass transition taking place over a temperature range, for which a glass transition temperature is defined (e.g. in the mean point of the transition), T_g. The latter transformation is briefly explained: when a material does not crystallize it enters in a supercooled regime. Upon further cooling, the viscosity dramatically increases and the material vitrifies in a disordered solid (amorphous material) when crossing the temperature range of the glass transition. The materials that experience this phase transformation are designated glass formers, becoming hard and fragile (e.g. silicate glass). The glass structure is still solid, but the intermolecular arrangements are looser due to an increase in Gibbs free energy. In particular, for polymers, as the temperature is raised on crossing the glass transition, they start to exhibit a rubber-like behavior, and at even higher temperatures they eventually become free-flowing materials allowing to be molded. Semi-crystalline polymers melt, upon further heating at a given temperature, $T_{m.}$ (Shawe et al., 2000)

A previous sample of FP, from the same batch, was analyzed by DSC in order to assess the ideal processing temperature of FP, without melting the samples. When analyzing FP it was not possible to detect neither a glass transition or a melting temperature, detecting only a degradation temperature around 268 ºC. This means that although FP is essentially made by an intricate heterogeneous proportion of sugars, it lacks the internal three-dimensional structural order found in crystalline materials. FP is reported as an amorphous polymer due to having a random structural arrangement, also found in liquids material (Cândido, 2015). However, the chains' arrangement seems to be too rigid to allow a significant change between the heat capacity of the glass and the one of the rubber-like material, since no heat flux step was observed in the thermal response that can be attributed to a glass transition.

ODF excipient combines FP, PEO and MET. Figure 2.8 provides the DSC data for formulation S1, S2 and S3:

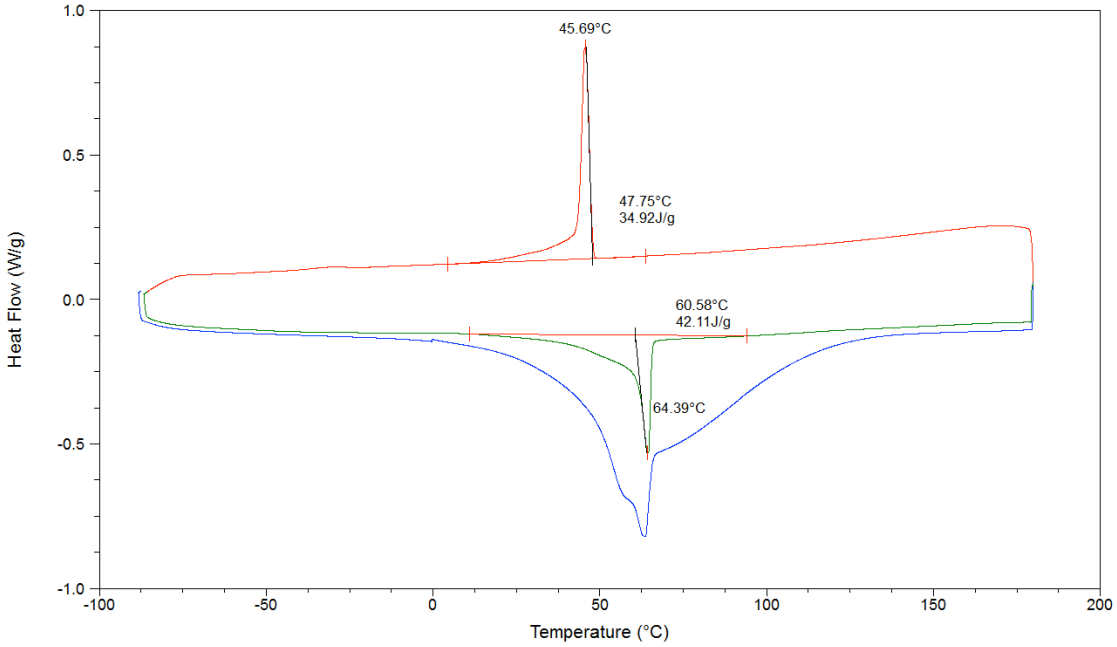

Figure 2.8 – Thermal analysis (DSC) of S3 at a temperature range of -90 ºC to 180 ºC at 5 ºC.min^{-1}. Sample S3 was inserted into an aluminum hermetic pans in order to allow water evaporation. DSC analysis for over 4 hours, using two heating cycles for water evaporation (blue) and sample melting (green) and two cooling cycle for sample recrystallization (red).

PEO and MET present a stand-alone melting temperature of 66.23 ºC and 98ºC, respectively, with PEO having a glass transition temperature around 52ºC; MET do not present recrystallization temperature (Annex 3). Water evaporation temperature is visible in the first heating cycle (blue) where the temperature reaches 180 ºC. Afterwards, the system is cooled down (red) and recrystallization occurs around 45.69 ºC. A third heating cycle (green) is performed in order to assess the melting temperature that is detected around 64.39 ºC. Since FP is amorphous, the T_m and T_c temperatures displayed in Figure 2.8 are probably originated by the presence of PEO in sample S3; moreover, the detected melting and crystallization phenomena occur close to the temperatures found in pure PEO (Tm: 66.23ºC, Tc: 48.61 ºC), whereas MET only melts at 100 ºC. (Annex 3). The low amount of MET present in sample S3 could explain why DSC analysis is not greatly influenced by it.

The combination of the melting temperatures of PEO, MET and ODF is equal or higher than 60 ºC, so it is safe to say that working electrospinning temperatures (20 to 30 ºC) will not promote or induce cristalization or melting upon fiber production, phenomenon many times encountered in electrospinning processes, if the materials have low melting temperatures or are subjected to high temperatures. (Zhou et al., 2006)

2.6.2 Orodispersible film morphological analysis

2.6.2.1 Scanning Electron Microscopy (SEM)

In the beginning of section 2.6 we stated that in the experimental conditions tested (Annex 1), FP seemed to not possess the ability to produce fibers, only droplets or beads. Morphological imaging of electrospun samples S2 and S3 was assessed by SEM; results are shown in Figure 2.9 and Figure 2.10. The fibers observed are defectless, without bead formation and are likely derived from the amount of PEO present in the solution. Some fibers appear to be fused together, a behavior that can be explained by a possible fiber aggregation due to the creation of interconnected honeycomb-like structures, characteristic of high molecular weight PEO (Deitzel et al., 2001). Average fiber diameter, measured by ImageJ, was 0.294±0.034 µm for sample S2 (Figure 2.9), having a maximum and minimum diameter of 0.420 µm and 0.253 µm, respectively. Plus, the fiber cannot be melted together since from previous DSC analysis it was perceived that melting only started to occur at temperatures close to 60 ºC far from the ones used in electrospinning (20 to 30 ºC).

Sample S2

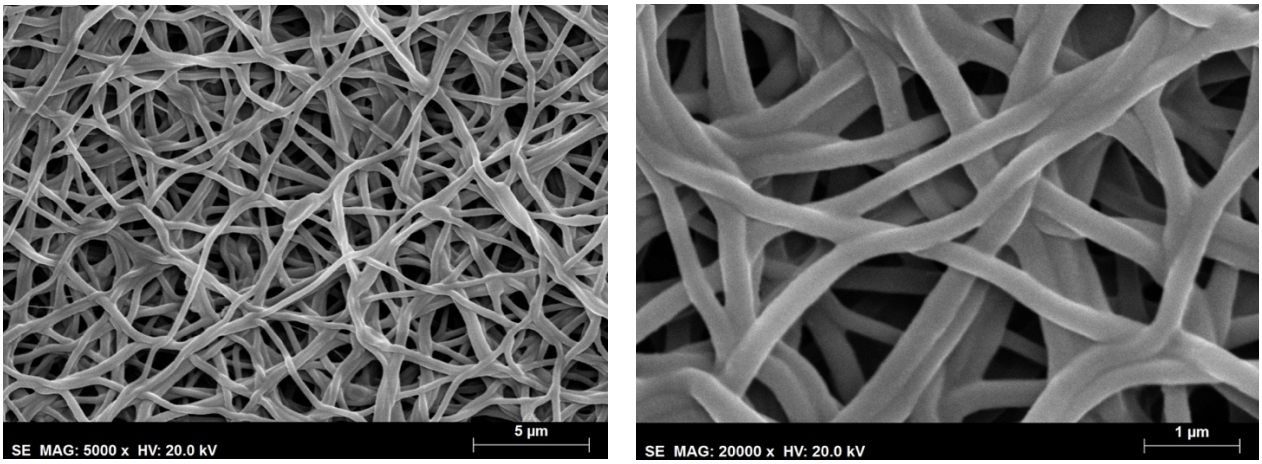

Figure 2.9 – SEM imaging of sample S2 under 5K (left) and 20K (right) amplifications. Electrospinning conditions were set to 0,5mL.h^{-1}, 13.5 kV, 23cm, 20-30% and 25-30ºC. Average fiber diameter and standard deviation – 0.294±0.034 µm – were measured from n=25 different fibers, using ImageJ software.

Sample S3

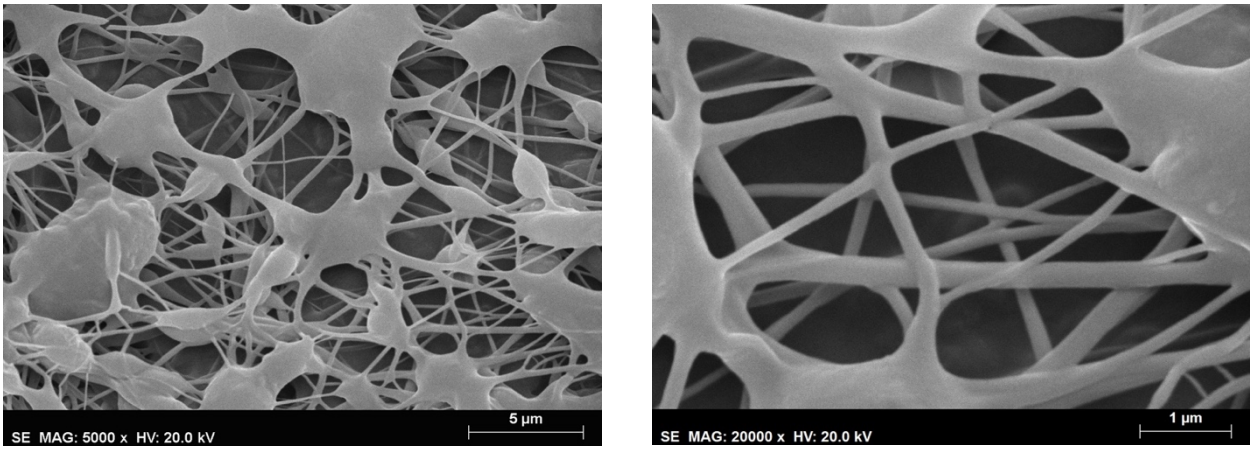

Figure 2.10 - SEM imaging of sample S3 under 5K (left) and 20K (right) amplifications. Electrospinning conditions were set to 0,5mL.h^{-1}, 13.5 kV, 23cm, 20-30% and 25-30ºC. Average fiber diameter and standard deviation – 0.163±0.082 µm – were measured from n=25 different fibers, using ImageJ software.

Metoclopramide hydrochloride is considered as ‘’very soluble’’ drug, in water. However, its solubility parameters are not clear throughout the literature: Meurant, 1987 reports a water solubility of 0.2 mg/mL while Kasim et al., 2004 report a water solubility of 1g/mL. Stosik et al., 2008 measured the solubility of a tablet containing 10 mg of metoclopramide hydrochloride and found that it was only soluble in 265 mL of water. Bhimba, 2013, also performed solubility measurement and found that 1,415 g of the drug was soluble in 1mL of phosphate buffer at pH 7.4. From Figure 2.10 it is perceivable that the addition of metoclopramide affects the fiber morphology, since the drug was not able to solubilize in the experimental conditions (i.e., 10 mg of metoclopramide in 6 mL of water). Average fiber diameter in sample S3 decreased, when compared to sample S2, due to fiber heterogeneity, reaching 0.163±0.082 µm, presenting a maximum and minimum diameter of 0.405 µm and 0.045 µm, respectively.

Generally, as fiber diameter gets close to the nanoscale (i.e., 1 to 100 nm) a greater amount of substance comes in contact with the surrounding material. Although the morphology of sample S3 presents heterogeneous fiber diameters that will probably hamper the mechanical stability of the film, increasing the ODFs superficial area of contact with the oral mucosa through smaller fiber diameters can result in faster film dissolution, enabling faster drug release and absorption. Furthermore, since the goal of the orodispersible film is to disperse in the shortest amount of time possible, its mechanical strength is not that relevant and the occurrence of defected fibers does not have a great impact in its performance. Analyzing SEM images, it is possible to conclude that for our formulation and purpose, electrospinning is able to create a thin fibrous film that displays high area to volume ratio that cannot be found in any other common manufacturing procedure. Plus, film requirements are easy to model since electrospinning has at least 5 degrees of freedom that aid in fiber/film design and modulation (i.e. rate, voltage, needle/collector distance,

process time, humidity and temperature). In order to obtain thicker ODFs one must only increase the amount of time in which a viscous solution is electrospun (i.e. deposition time), meaning that a higher solution volume will have to be electrospun.
Nonetheless, in order to achieve reproducible results and homogeneous fibers, other drugs should be tested and their water solubility should be measured, avoiding erroneous results.

2.6.2.2 Atomic-Force Microscopy (AFM)

AFM analysis (Figure 2.11) was originally intended to act as a substitute to SEM analysis since in the beginning, samples S2 and S3 were melting upon SEM analysis. We believed at the time that FP was not withstanding the energy generated by the SEM electron beam, due to FP being essentially made by a mixture of sugars. That suspicion was not confirmed since SEM was eventually performed without the presence of melting.

AFM is performed using ambient temperature and pressure, being a suitable alternative for an approximate fiber diameter measurement, without chemical modification. AFM was also performed as a complement to X-Ray Photoelectron Spectroscopy (XPS), in order to assess if the X-Ray radiation would influence fiber morphology. XPS analysis of sample S2 is reported ahead. AFM analysis reported an average fiber diameter equal to 0.826 μm and 0.481 μm previous to and after XPS analysis, in sample S2. Given the absence of damage signs in the fiber, the discrepancy in fiber diameter can be explained by the lack of assurance that the same sample region is being analyzed twice.

Before XPS Analysis	After XPS analysis

Sample S2

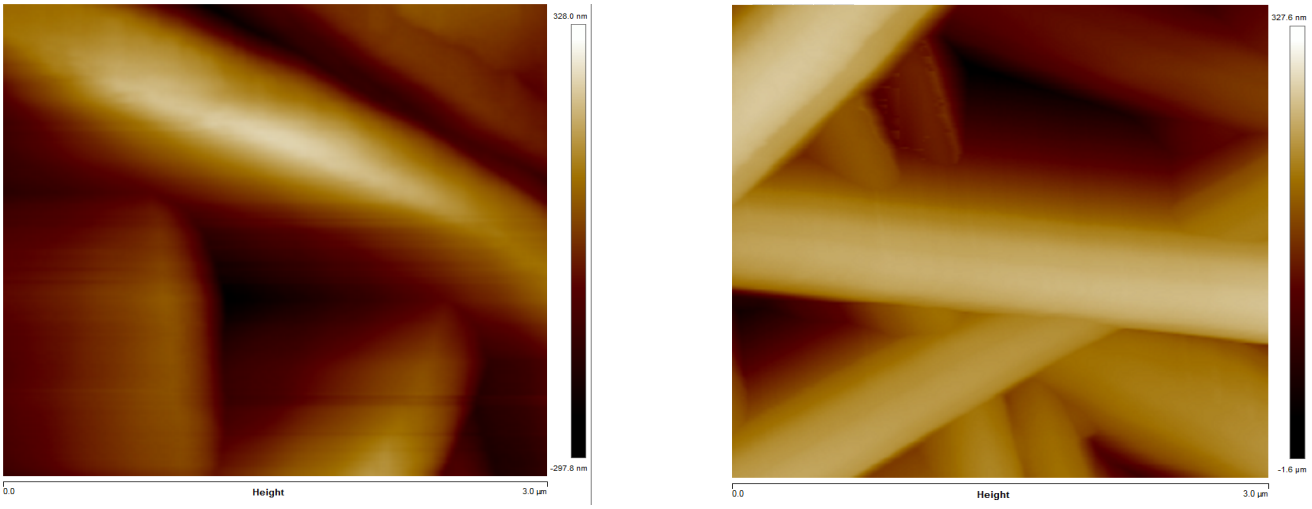

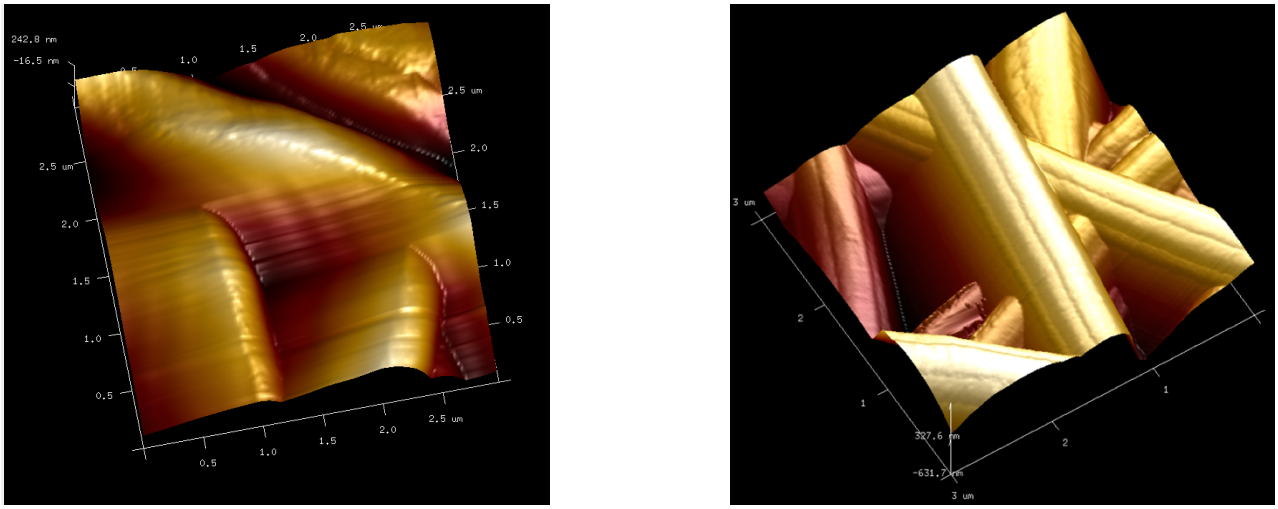

Figure 2.11 – 2D and 3D AFM imaging of sample S2. AFM analysis was performed at environmental temperatures and pressures.

In order to evaluate if the amount of FP present in sample S2 was causing the discrepancies found in the average fiber diameter when measured by AFM, or if the melting behavior of samples S2 and S3 found upon performing SEM was due to FP surrounding PEO fibers, samples S2 and S3 were analyzed by X-Ray Photoelectron Spectroscopy (XPS) in order to have a correct assessment of the superficial composition of the electrospun fibers.

2.6.3 Orodispersible film chemical composition

2.6.3.1 X-Ray Photoelectron Spectroscopy (XPS)

In order to understand if FP had a contribution in fiber production, the elemental compositions of native (i.e., FP, PEO, MET) and hybrid films (i.e. samples S2 and S3) were determined by XPS. Figure 2.12 shows the survey spectra for all the analyzed samples, used as received:

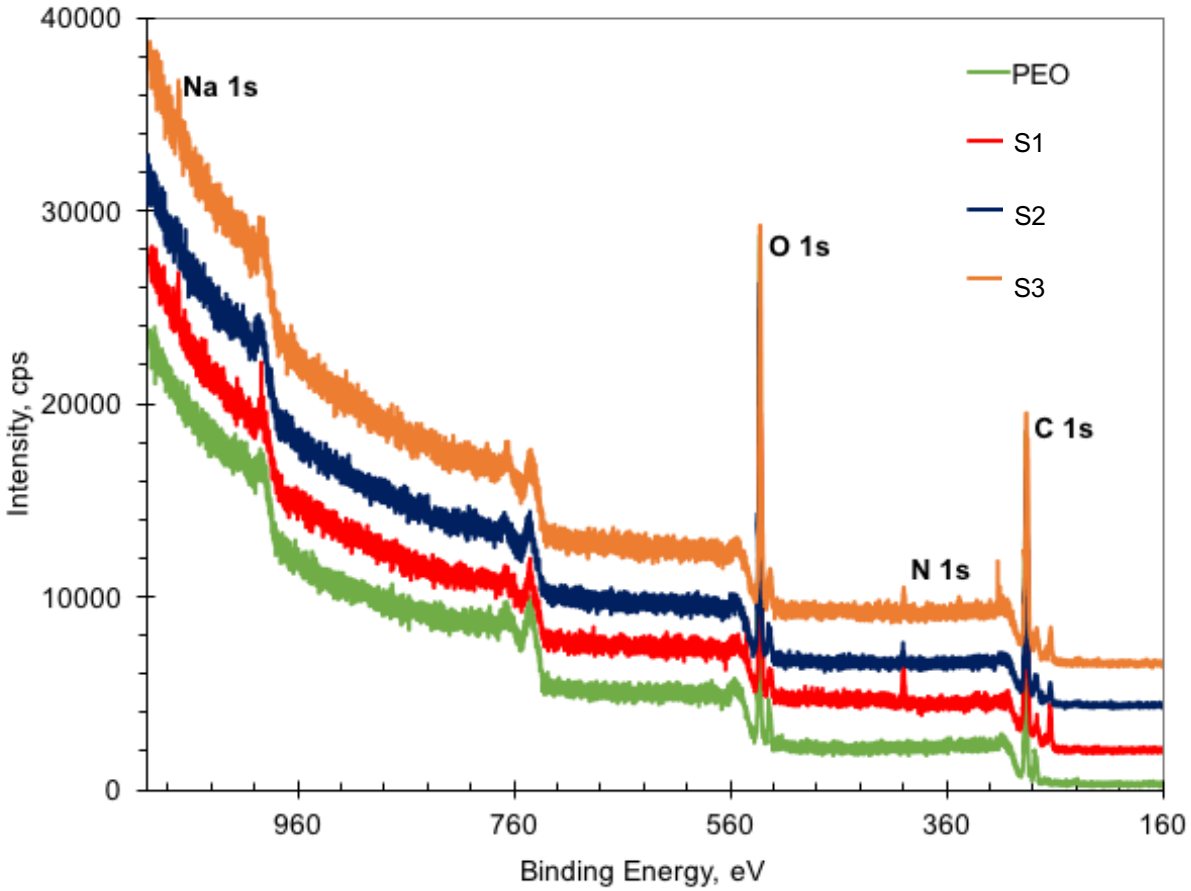

Figure 2.12 - Survey spectra for samples S1, S2 and S3.

The main spectral regions are identified in Figure 2.12 showing that carbon (photoelectrons C 1s) and oxygen (photoelectrons O 1s) are present in all the samples, as expected. However, in sample S1, and in all the samples containing FP, nitrogen (photoelectron N 1s) and sodium (photoelectrons Na 1s) are also present, possibly due to poor purification steps or sample contamination. Spectra for sample S2 and S3 have very similar, therefore, from now on, just the sample S3 will be mentioned. Detailed XPS regions C 1s and O 1s for the samples S1, S2 and S3 are shown in Figure 2.13. The simulated spectra for sample S2 was assessed assuming they were homogeneously physically blended. The difference between the simulation and the real spectra, without prior normalization, is included.

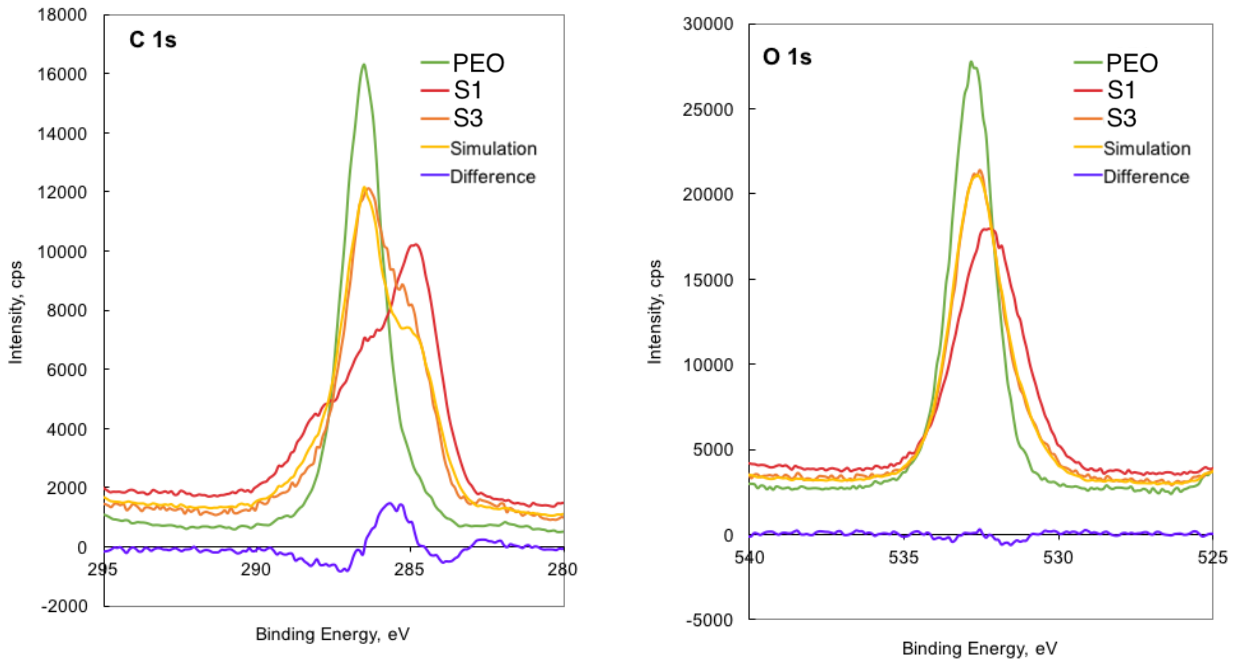

Figure 2.13 - XPS C 1s and O 1s regions of pure PEO (green), sample S1 (red) and S3 (orange). In yellow, simulated spectra with the relative contributions of 0.5 of PEO and 0.5 of FP is included for comparison effects.

When observing the C 1s region, carbon atoms singly bound to oxygen (**C**-O) can be found in all the spectra due to the presence of binding energies (BE) around 286.5 eV. In ODF, a peak at 284.8±0.2 eV appears, possibly assignable to carbonaceous contamination (**C**-**C** and/or -H_2**C**-). In sample S1, a peak was observed at higher binding energy (288.1±0.2 eV) assignable to a carbon double bonded to oxygen (**C**=O and/or O-**C**-O). When analyzing the O 1s region, it is possible to observe that PEO has a component centered at 532.8±0.2 eV assigned to the oxygen singly bound to carbon (**O**-C); a very small component centered at 534.7±0.2 eV is due to water absorption. For samples S1 and S3, besides the peak assignable to **O**-C at, respectively 532.5±0.2 eV and 532.7±0.2 eV, also a component at lower BE (531.3±0.4 eV) is found, being typical of oxygen in carbonyl groups (**O**=C). The "simulated" O 1s and C 1s peaks were obtained, without any prior normalization, assuming that sample S2 is homogeneously distributed and blended in the proportion 1:1(wt.). A perfect match is obtained for O1s region but not for C 1s region, suggesting that there can be some carbon contamination in the sample.

Ideally, FP and PEO should contribute equally to the surface composition of sample S2, since the simulation was obtained by 50% of FP and 50% of PEO. However, simulation for the C 1s region was not a perfect fit using those compositions since FP and PEO were actually blended in the proportion 2:1 (wt.). The data contrarily suggests that a certain PEO is present at the surface of the fibers. Table 2.4 shows the

quantitative results obtained by XPS. Sample S3 presents a lower O/C ratio than the ones found in sample S1 and PEO which may be attributed to the increase of carbon in sample S3 sample related to a carbon contamination.

Nitrogen was also found in XPS N 1s analysis in sample S1 (400.2 eV), element never found before in previous FP analysis (Antunes et al., 2015; Dhadge et al., 2014; Ferreira et al., 2014; Freitas et al., 2010) As a result, it was not possible to pinpoint the atomic percentages corresponding to MET since both compounds have nitrogen in their composition. To assess if the nitrogen in sample S1 arrives from a sample contamination or poor downstream processing, an elemental analysis could be performed in polymer samples from the same batch, before and after purification steps.

Table 2.4 –XPS atomic percentages and ratios

	S1	PEO	S3
C	59.2	61.7	63.2
O	35.3	38.3	34.6
N	5.5	-	1.9
O/C	0.60	0.62	0.55
O-C/C-O	1.39	0.63	0.84
N/C	0.09	-	0.03

2.6.3.2 Fourier Transform Infrared Spectroscopy (FTIR)

FTIR analysis was performed in order to evaluate if all ODF individual components were present in the sample, after electrospinning and solvent casting process. Since the FTIR spectras from both manufacturing techniques were the same, only electrospinning FTIR data from samples S2 and S3 will be presented in Figure 2.14.

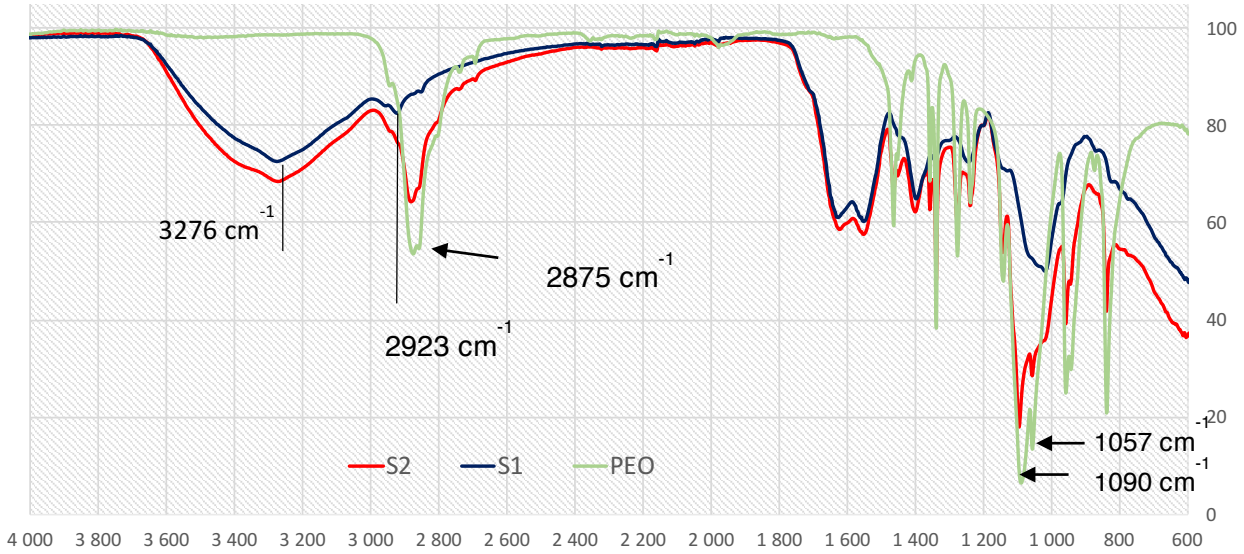

Figure 2.14 – FTIR spectra of sample S2 (dark blue). FP (dark blue) and PEO (green) FTIR spectra were used as controls.

FP spectra is identical to the one reported by Freitas et al., 2010, displaying a broad O-H band around 3276 cm^{-1} that contains the C-H band at 2923 cm^{-1}. The characteristic broadness of the O-H band, present in most exopolysaccharides is due to the great amount of hydroxyl groups present in this type of polymers (Synytsya et al., 2003). FP also presents a possible C-N band between 1000 and 1200 cm^{-1} that can possibly be derived from amount of nitrogen found upon XPS analysis. FP FT-IR spectra presented in Figure 2.14 and FP FT-IR spectra reported by Freitas et al., 2010 come from different batches; yet, the experimental and the reported data share a high similarity, proving that biosynthesis of bacterial polymers has low batch-to-batch variability, being able to obtain consistent and reproducible polymers from batch-to-batch, if fermentation parameters are maintained.

The presence of semi-crystalline PEO is confirmed by bands around 1090 and 1057 cm^{-1} (C-O-C stretching) and 2875 cm^{-1} (C-H stretching) (Gondaliya, 2011). Sample S2 FT-IR spectra appears to result from an overlap of pure FP and pure PEO individual FT-IR spectra, suggesting that the polymers may be physically blended. Furthermore, sample S2 FTIR spectra show the absence of new peaks, which would not occur if chemical bonding was present. As a result, sample S2 spectra results from a widening of the 2916 cm^{-1} band (C-H), deriving from FP and widening of 1090 to 1057 cm^{-1} bands (C-O-C), from PEO.

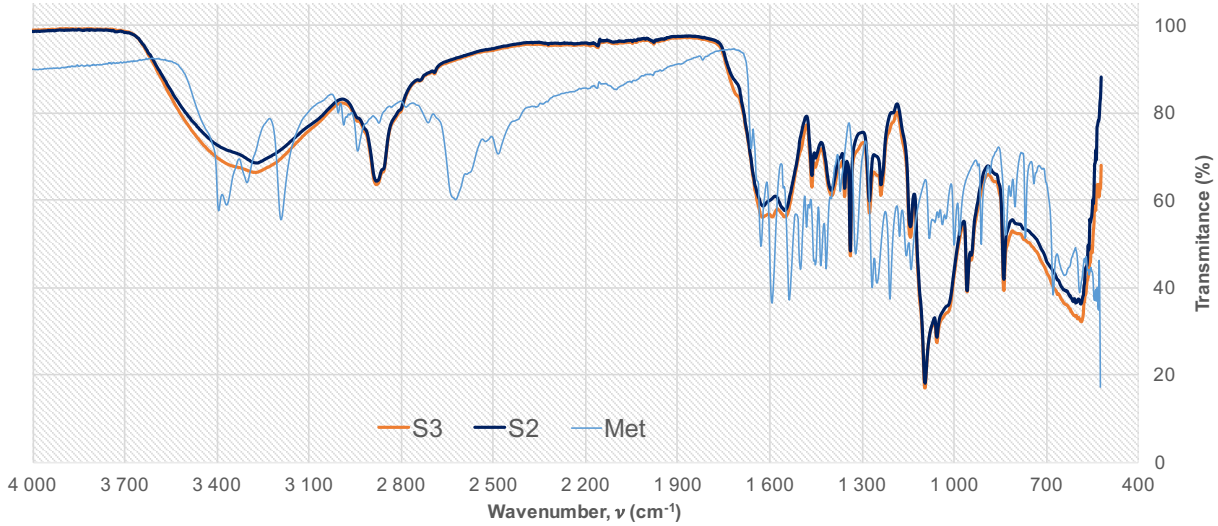

Figure 2.15 - FT-IR spectra of sample S3. The FTIR spectra of sample S2 blend and MET were used as controls.

The presence of MET in the electrospun fibers was also assessed by FT-IR. In Figure 2.15 it is not possible to see the presence of metoclopramide since there is only 5.26 wt.% of the drug in 94 wt.% polymer content. Plus, since by SEM MET seemed to be heterogeneously disperse in sample S3, the portion of sample S3 chosen for FTIR analysis could have had a low drug content, explaining why metoclopramide could not be detected by FTIR. The presence of metoclopramide in the electrospun ODF is supported by SEM analysis due to morphological change in the fibers produced by electrospinning and further in vitro pharmacokinetic studies that will be discussed later in 2.6.4.4.

Physical blending between the used polymers was expected considering all components were physically blended at room temperature and pressure, without pH control. Plus, FP backbone structure remains undisclosed, making it difficult to achieve chemical manipulation or modification of certain intrinsic characteristics. Physical blending will not affect the time required for the ODF to dissolve since both polymers are already hydrophilic. It is also proven that electrospinning is innocuous to the polymeric solution since chemical properties remain unchanged before and after fiber formation, with all the initial components still present in the electrospun fibers.

2.6.4 Orodispersible film characterization

2.6.4.1 Mechanical properties

Orodispersible films require manual handling in order for them to be orally administered. The amount of stress/strain that sample S3 is able to sustain was measured by uniaxial elongation. The results obtained are displayed in Table 2.5.

Table 2.5 – Mechanical properties of sample S3 comprising the Young's modulus (E), stress (σ) and strain (ε); S.D. is the standard deviation. *n=3

ε (%)* (Mean±S.D.)	σ (MPa)* Mean±S.D.)	E (MPa)* (mean±S.D.)
21.05±3.4	2.3±0.9	30.7±10.5

Sample S3 display an elastic modulus (E) within the range of Isoprene (IR) (10 to 40 MPa) or low density rigid polymer foams (23 to 80 MPa) (Gibson et al., 2010). Ferreira et al., 2014 reported that FP had a typical behavior of a ductile film. Sample S3 exhibits a similar behavior with low tensile strength at break (2.3 MPa), high elongation at break (21.05 %) and an elastic modulus (30.7 MPa) within the range of the ones found for electrospinning films (Yao et al., 2014). However, instead of ductile, sample 3 presents what is thought to be the typical behavior of a brittle film, presenting a clean break upon film rupture (Figure 2.16). The mechanical properties of all polymeric matrices are strongly dependent upon the addition of any kind of additive to the native formulation, namely plasticizers and/or cross-linking agents.

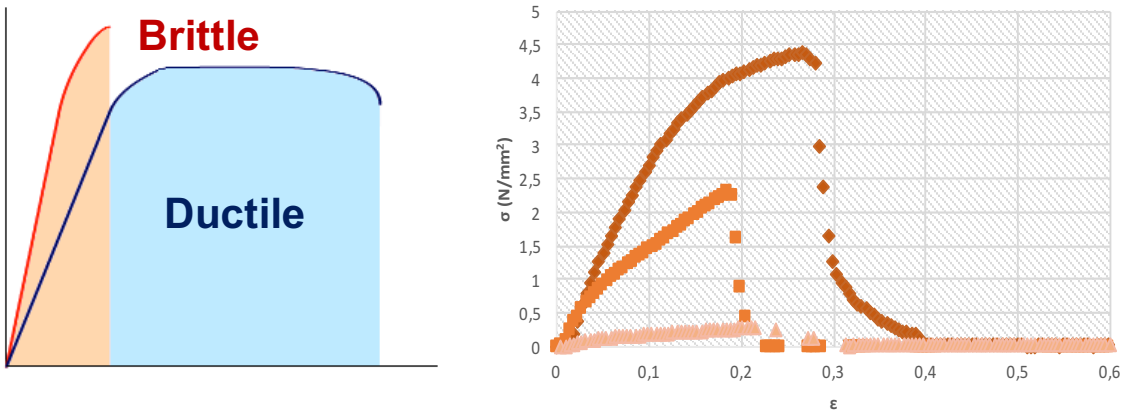

Figure 2.16 – Schematic representation of the difference between ductile and brittle behavior (left); Experimental data retrieved from stress/strain mechanical tests by sample S3 uniaxial elongation (right). Three ODF samples (n=3) were placed between two clamps at a distance of 1 cm and elongated at 2 $mm.min^{-1}$ with a

maximum load of 20N and a maximum displacement of 90 mm. Tests were performed at ambient temperature and pressure.

Ferreira et al., 2014 reports that citric-acid was used as a cross-linking agent in the production of biodegradable films with potential packaging applications. In our formulations, high molecular weight PEO was used as a physical cross-linking agent since it allowed fiber formation upon small amount of PEO addition, maintaining FP as the main component in sample S3. Water content is also an important factor that needs to be considered when analyzing the mechanical properties of hygroscopic polymeric matrices; if the polymer has a high water content, the physical structure of sample S3 can start to degrade before mechanical assessment. For this reason, it is important that prior to mechanical or any type of analysis, ODFs should be stored in vacuum or in an air tight compartment that will avoid the samples' mechanical impairment by environmental conditions, namely humidity.

2.6.4.2 Weight, thickness and surface pH

Fiber deposition in electrospinning tends to follow a Gaussian curve, meaning that the center of the film will have a higher fiber density relatively to the outer edges of the film. As was said in subsection 2.5.2, weight and thickness values were corrected by looping a static collector between known coordinates, allowing the film to display similar thickness throughout its entire area. However, as was previously mentioned in subsection 2.6.2.1, the drug was not homogeneously distributed in sample S3, resulting in film areas that exhibits higher drug loadings. Solid drug deposition can lead to self-assembly phenomenon since the electrical field will be heightened in those areas (Reis et al., 2013). Hence, fibers tend to deposit in areas where the fiber density is higher, leading to discrepancies in weight and thickness. Even so, electrospun sample S3 is according to the requirements for orodispersible platforms (Bala et al., 2013) with average thickness around 104 ± 20 μm and an average weight of 32.600± 0.003 mg for an entire electrospun film. ODF requirements state that sample S3 can have a thickness between 1 and 100 μm, however, when sample S3 exhibited 50 μm, poor manual handling, breaking or rupturing at the slightest touch was observed. As a rule, every system must be evaluated since each polymer or blend behaves differently; for our formulation, the only sample capable of sustaining the number of characterizations performed in this dissertation had to have 100 μm in thickness (i.e. sample S3).

Sample S3 surface pH (Figure 2.17) was around 6.84±0.01, a value within the natural pH of the oral mucosa (Aframian et al., 2006). This indicates that the film has a low potential to irritate the sublingual mucosa, and hence, more acceptable by the patients.

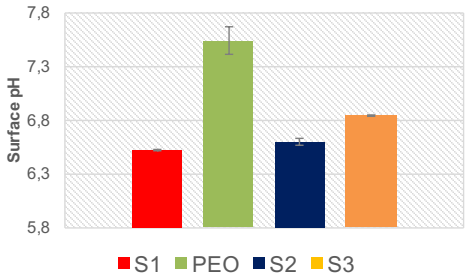

Figure 2.17 – Surface pH of samples S1, S2 and S3. Surface pH is an average result from four consecutive measurements.

2.6.4.3 Disintegration time

Dispersion or disintegration time of orodispersible films is not under rigid protocols by the European Pharmacopoeia (Ph. Eur. 5th, 2000). It can be measured using automatic tablet disintegration tester (DisiTest, Pharmatron) or by Petri dish assay, where an orodispersible film establishes direct contact with a solvent at specific pH and temperature, under possible agitation. Both methods are not suitable for orodispersible film formulation since they require a large amount of fluid that is not encountered within the oral cavity in resting conditions, as mentioned in subsection 1.2. Larger volumes of fluids will naturally decrease the time required for an orodispersible film to disintegrate or dissolve. Vuddanda et al., 2016 used a wet sponge (2 x 6.4 x 0.6 cm) to mimic surface structure and physiology of oral cavity. In this dissertation the same method was used to register the amount of time required for sample S3 to disintegrate, a methodology described in subsection 2.5.6.3. Solvent casting produced ODFs were also assessed for comparison purposes.

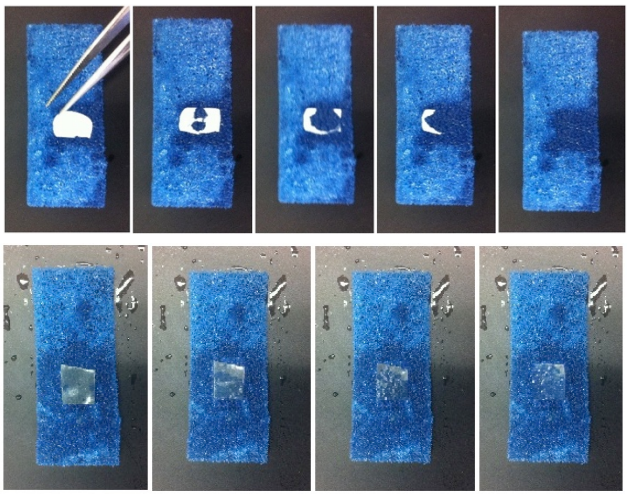

Figure 2.18 – Wetting an disintegration of sample S3 and solvent casting ODFs. The samples were in direct contact with a sponge that was previously hydrated using 250 mL of simulated saliva at pH 6.8. The time required for sample S3 and solvent casting ODFs to dissolve was recorder using a manual chronometer

from a digital watch (Casio). Figure 2.18 show how both formulations behave under the same conditions: sample S3 dissolved in 6 to 10 seconds, while solvent casting ODFs turned to gel and only started to disappear after 3 minutes. In *in vivo* oral conditions, dissolution times are expected to decrease even further for both formulations, since the oral cavity is in dynamic motion due to the movement of the tongue and the stimulation of saliva production. Plus, the fact that electrospun orodispersible films have higher interspace porosity and higher area to volume ratio, makes the amount of connections between the film and the oral mucosa much higher, enabling the adherence of the ODF in a smaller time frame, which leads to faster disintegration times.

2.6.4.4 *In vitro* drug delivery kinetic profile

MET release studies were performed using sample S3 (ES) and solvent casting ODFs (SC) (Figure 2.19). Analyzing plot 1, it is possible to observe the release of 60% of MET into the medium; the results were fitted to Korsmeyer and Peppas equation for slabs (Ritger and Peppas, 1987). The standard deviation for both assays had an average value of 0,012 for electrospinning, and 0,13 for solvent casting. Error bars were omitted from the plots bellow since they were unintelligible.

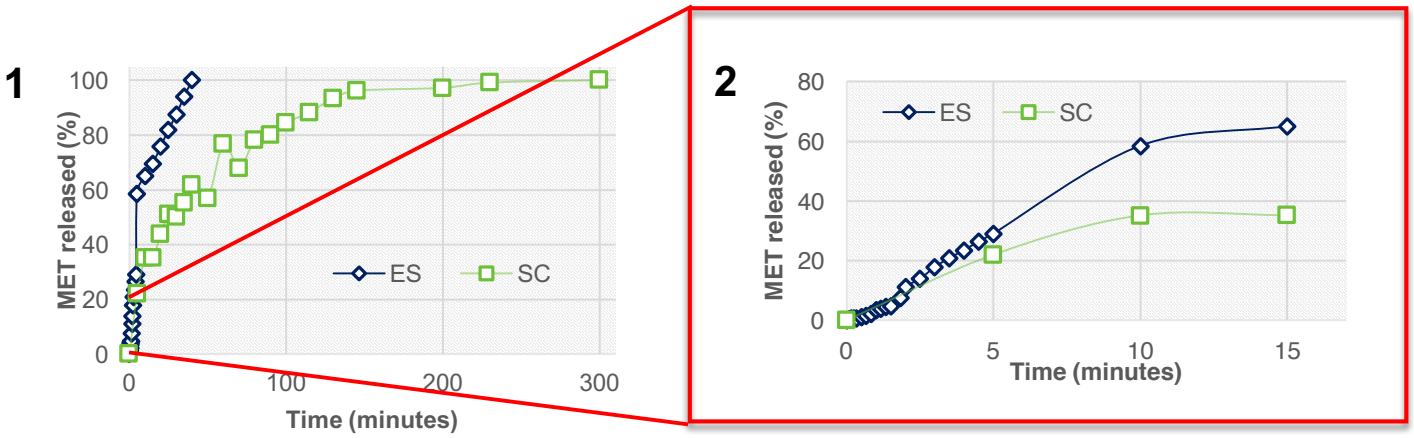

Figure 2.19 – Drug release kinetic profile of MET (1). Drug release from sample S3 (ES) and solvent casting ODFs (SC) is detail (2). MET was quantified by UV/Visible spectrophotometry using a calibration curve available in Annex 4.

Considering that the total amount of MET in the casting solution was 5.26% (subsection 2.5.2), electrospun and solvent casting ODFs were able to entrap approximately 3%, which accounts for 60% of the total amount MET available (Figure 2.19, plot 1). Although sample S3 and solvent casting ODFs have similar MET release profiles, for the same amount of time (plot 2) electrospun ODFs release 60% of its MET content while solvent casting ODFs release only approximately 35% of its MET content (Figure 2.19, plot 2).

The results show that electrospun OFDs have a faster drug release than solvent casting ones, which is a result already expected since electrospun ODFs disintegrate much faster than solvent casting ODFs. It is

also noted that neither ODFs released the 5.26% of MET initially incorporated in the casting solution; the difference in drug loading and entrapment efficiency can be related to the viscosity of the solution. That is, when preparing a solution for electrospinning or solvent casting, it is common to prepare an excess sample volume in order to have more or less 1 mL that is retained in the flask, due to the high viscosity of the sample (e.g. preparing a solution containing 4 mL and be able to retrieve 3 mL). The viscous nature of the sample prevents the total retrieval of the solution and as a consequence, part of the drug is left behind. Additionally, considering that metoclopramide is insoluble in the experimental conditions described in subsection 2.5.2, the drug will not have a homogenous dispersion in the electrospun ODF, possibly leading to the analysis of samples with lower drug content. In order to promote a uniform drug dispersion, acidic solvents can be tested in order to see if an acidic environment is able to dissolve MET, although some cannot homogeneously dissolve FP (Annex 1).

Either way, the goal was to assess the time required for both formulations to release the total amount of drug present in the ODF samples prepared by different methods. The release kinetics from both ODF was modeled according to Korshmeyer and Pappas equation that relates the fractional release of drug at a given time (M_t), to 60% of total drug release over time (M_∞).

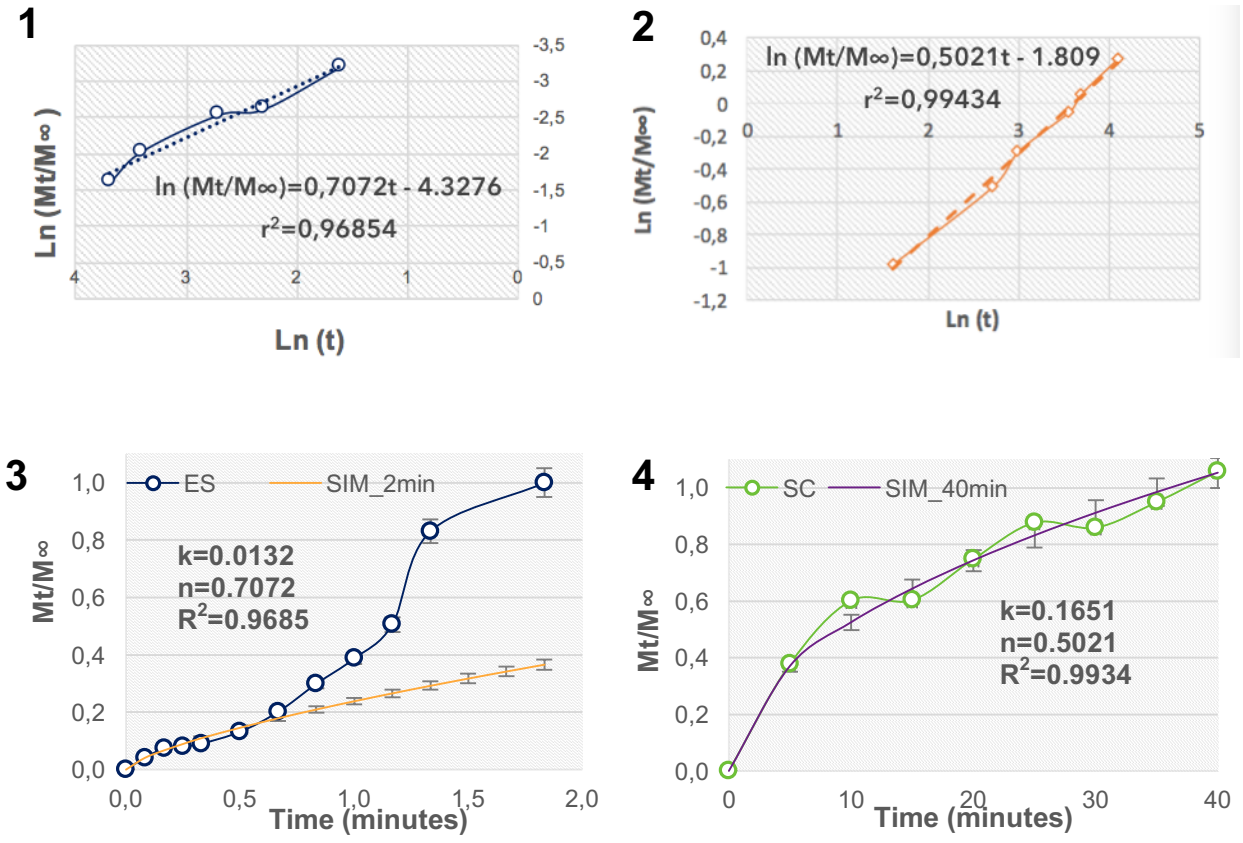

Figure 2.20 – Metoclopramide release studies modeled according to Korsmeyer and Peppas. Drug release modeling of electrospun (ES) and solvent casting (SC) ODFs – plot 1 to 4.

Looking at Figure 2.20, plot 1 it is possible to conclude that the release of MET at pH 6.8 had an anomalous transport (non-Fickian mechanism) in electrospun ODFs, since the diffusional exponent, n>0.5. This means that both mechanisms – water uptake and Fick's diffusion – are responsible for MET release. Since the ODF is extremely thin and hydrophilic, water uptake is difficult to be measured, although it can possibly be the leading cause for ODF disintegration. Also, since the diffusional exponent, n, is further from 0.5, it is thought that drug release is more controlled by water uptake than diffusion. (Cabral, 2013)

The release mechanism of MET for solvent casting ODFs at pH 6.8, (Figure 2.20, plot 2) is still slightly anomalous, although the diffusional exponent is very close to 0.5 implying a greater contribution of the diffusional mechanism than the swelling. (Ritger and Peppas, 1987)

2.6.4.5 Cytotoxicity

As a validation of the previous reported results, eletrospun ODFs effect on cell viability was assessed by resazurin assay. Viable cells are able to metabolize non-fluorescent resazurin to strongly-fluorescent resorufin. The amount of resazurin that is reduced by metabolically active cells is proportional to the amount of viable cells and can be measured by UV analysis at 570 and 600 nm.

Primarily, cell viability was assessed when in contact with a range of concentrations of FP, PEO, MET and ODF, for 24 hours. Afterwards, fresh medium was provided and 24 hours later, resazurin assay was performed. The percentage of relative viable cells is presented in Figure 2.21.

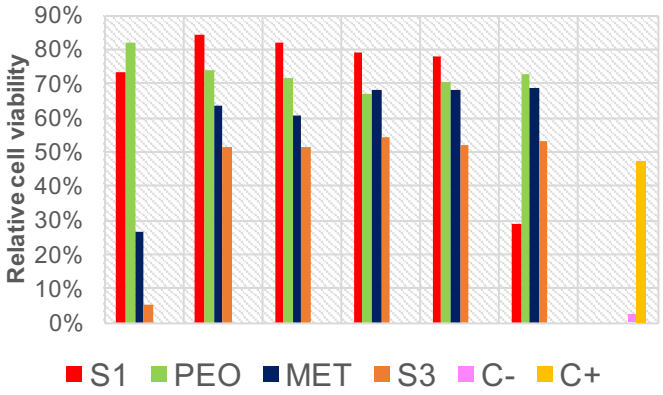

Figure 2.21 – VERO cell viability after exposure to sample S3 and its individual components. Cell viability was assessed 24 hours later to cell exposure by UV/Visible analysis of the metabolized resazurin at 570 and 600 nm. Negative control (C-) contains 10 µL of DMSO; positive control (C+) is composed by the growth of VERO cells in DMEM medium.

Cytotoxic assays revealed that the electrospun ODF is non-toxic to epithelial VERO cells when its drug content is lower than 5 mg/1.2 million cells. The presence of metoclopramide has a cytotoxic effect in all formulations in values higher than 1 mg/well (i.e. 200 µL) which is when MET reaches its solubility threshold. Apart from MET, FP and PEO had no relevant effect in the cells viability.

2.7 Concluding remarks

In this chapter a bacterial expolysaccharide – FucoPol (FP) – was used to produce an orodispersible film (ODF) by electrospinning; solvent casting method was used for comparison purposes. It was not possible to produce fibers from stand-alone FucoPol, and for that reason, high molecular weight poly(ethyle oxide) (PEO) was used as a physical cross-linking agent. The electrospun orodispersible film (ODF) presented fiber diameters around 0.1 to 0.2 micrometers and a mechanical brittle behavior, with dissolution rates from 6 to 10 seconds. ODF release 100% of its drug content in less than 5 minutes by anomalous transport, which means that both swelling and diffusion are responsible for drug release. Metoclopramide dosages above 1mg/mL are toxic to the cells and ODFs surface pH is within the oral cavity usual pH, proving that the obtained ODF formulation is innocuous to the oral flora. Solvent casting films had lower dissolution rates (1 to 3 minutes) and slower release profiles (5 to 10 minutes).

Future work could proceed in order to:

- Perform a drug and solvent screening that dissolve both FucoPol and the chosen drug, creating homogenous fibers with possible higher loading;
- Optimize drug entrapment yields by mixing different amount of drug and quantifying it upon the production electrospun films;
- Optimize drug release protocols in order to have a quantitative and qualitative test that is suited for fast dissolution matrices;
- Perform a screening of cross-linkers and plasticizers in order to use FucoPol in cutaneous and tissue engeneering applications;
- Perform an elemental analysis of same batch EPS in order to assess the presence of nitrogen in the sample;
- Produce microcarriers by electrospray, since FucoPol has no fiber forming abilities.

Production of FucoPol-based 3D constructs by cryotopic gelation

As mentioned in Chapter 1, subsection 1.2.3, the goal of this dissertation is to use the bacterial exopolysaccharide FucoPol, produced by *Enterobacter* A47 in a bioreactor synthesis, in order to produce 3D constructs for oral drug delivery.

In Chapter 2, the fiber forming abilities of FucoPol were assessed in a process known as electrospinning - a fiber forming technique that is able to produce thick controlled films that display a high surface to volume ratio. FucoPol did not show any fiber forming abilities; as a result it was cross-linked with poly (ethylene oxide) in order to produce an orodispersible film (ODF) by electrospinning. The resulting ODF showed faster polymer dissolution rates and increased in vitro drug delivery, when comparing the results to most common ODF production methods.

In Chapter 3, supercritical carbon dioxide will be used in order to aid the production of a FucoPol dry scaffold, previously obtained by cryogelation. The combination of different techniques will allow the production of a porous structure suitable for oral drug delivery. The procedure will be explained along with product characterization will be discussed through the entire chapter, finalizing with the concluding remarks and future perspectives.

3.1 Scaffolds: 3D porous constructs

In tissue engineering, scaffolds are defined as 3D artificial structures capable of promoting cell attachment, migration and delivery, promoting three-dimensional tissue formation while exerting mechanical and biological support *in situ.* (Hollister, 2005) In this dissertation, scaffolds will be defined as 3D polymeric porous structures eligible for drug delivery. The polymers intrinsic chemical characteristics as well as pore size and distribution will dictate the scaffold final application. (Anjum et al., 2016; Knežević and Durand, 2015; Liu et al., 2014)

Although scaffolds are not exclusive to polymeric sources, most of them are made by synthetic polymers due to their wide range of molecular weight, mechanical properties, high purity, reproducibility and known molecular structure (Rodriguez et al., 2014). Despite that fact, natural polymers are gaining relevance due to their low production costs, biocompatibility and biodegradability – desirable characteristics for physiological applications. For example, chitosan – a natural polymer which results from the deacetylation of chitin from the exoskeleton of crustaceans (e.g. shrimp) – has been extensively applied in many sectors due to being nontoxic, biocompatible and biodegradable. It has been used many times as a skin substitute (Kim, 2015) or as base for monolith antibody or adenovirus purification (Barroso et al., 2012*)* (Fernandes et al., 2015). Chitosan was also blended with heparin in order to obtain an artificial macroporous scaffold for tissue engineering applications (Yu et al., 2008) and blended with agarose – a galactose polysaccharide extracted from seaweed – for IgG purification (Sun et al., 2012). Cellulose – a glucose polysaccharide is the main structural component found in the cell wall of plants – has also been used in protein separation through the use of morphology controlled membranes (Barroso et al., 2010) and foams as packaging materials (Svagan et al., 2011)

Bacterial polysaccharides are just now being considered in the world of clinical applications, since their most promising features are already being applied in the food sector as thickening and/or stabilizing agents. The gelling abilities of Kefiran - a water-soluble exopolysaccharide produced by *Lasctobacilus keriranofaciens* from water kefir grain – was assessed by Piermaria et al., 2008 and Zavala et al., 2014 in the production of a cryogel when sucrose and fructose were present. Pullulan and dextran – glucose containing bacterial polysaccharides – hybrid scaffold were also produced by (Autissier et al., 2010) using trisodium trimetaphosphate (SMTP) as a cross-linking agent under alkaline conditions and in the production of small diameter arterial grafts (Chaouat et al., 2006), with pullulan being used as a stand-alone hydrogel for smooth muscle cell culture (Autissier et al., 2007). Sponge-like hydrogels of gellan-gum and curdlan microspheres were also reported by (da Silva et al., 2014) and (Mocanu et al., 2009).

3.2 Production methods for 3D constructs

Multiscale control of the macro and/or micro scale properties of the 3D constructs is possible through the manipulation of the processing parameters involved in each technique, namely temperature and pressure, as well as the choice of solvent and polymer. 3D constructs can be manufactured by numerous techniques (Svec, 2010), (Nichol and Khademhosseini, 2010), (Sears et al., 2016), including the cast of a solution onto a glass plate to produce a 3D scaffold (i.e. solvent-casting); salts are added to the solution in order to produce a porous structure with specific pore diameter (i.e. particulate leaching) (Taherkhani and Moztarzadeh, 2016). Sol-gel (Owens et al., 2016), electrospinning (Zhu et al., 2015), supercritical fluids (García-González et al., 2012), freeze-drying (Sultana et al., 2015) and cryogelation (Oliveira et al., 2015) are other techniques used in the production of #D porous structures.

In this dissertation the focus will be on cryogelation technique associated with solvent extraction by supercritical carbon dioxide, since the coupling of these techniques allows for the production of a macroporous interconnected pore structure suitable for drug delivery (Liang and Kiick, 2014), separation and/or downstream processing applications (Fernandes et al., 2015)

3.2.1 Cryogelation

As mentioned in subsection 1.2.2, some polysaccharides possess gelling or film forming abilities when mixed with water. Since the grand majority is only soluble in aqueous solvents, they can produce hydrogels, jellified structures with temperature as crosslinker (e.g. gelatin). Some can also display foaming abilities, producing supercritical dried aerogels, polymeric structures that result from solvent extraction by supercritical fluids, creating light, foam-like structures with controlled porosity upon system depressurization. Cryogels are highly porous structures produced by freezing a solution, suspension or gel at subzero temperatures. The interconnected porous structure is formed by nucleation process, followed by ice crystal growth due to solvent crystallization. Lower temperatures have faster freezing times (e.g. -80 ºC), inducing smaller crystal formation, that in return produces smaller pore sizes. Higher subzero temperatures (e.g. -20 ºC) promote slower freezing times, allowing ice crystals to grow heterogeneously, inducing the formation of bigger pores. By tuning the freezing temperature at which a given solution is frozen, macro (>50 nm), mesoporous (2 to 50 nm) or nanoporous (< 2 nm) structures are feasible to be obtained.(Xu, 2013)

Figure 3.1 shows a schematic representation of the production of scaffolds through cryogelation. After pore formation by freezing step, cryogels can have their solvent removed by sublimation (i.e. lyophilization), a common method that can hinder the internal cryogel structure by promoting pore collapse, inducing polymer shrinkage (e.g. xerogels) or cracked structures, upon solvent evaporation. Combining cryogelation with supercritical fluid extraction allows for the internal structure of the cryogel

to be maintained, since the scaffold structure is filled with liquid-like gas that will hold the structure together, avoiding pore collapse.

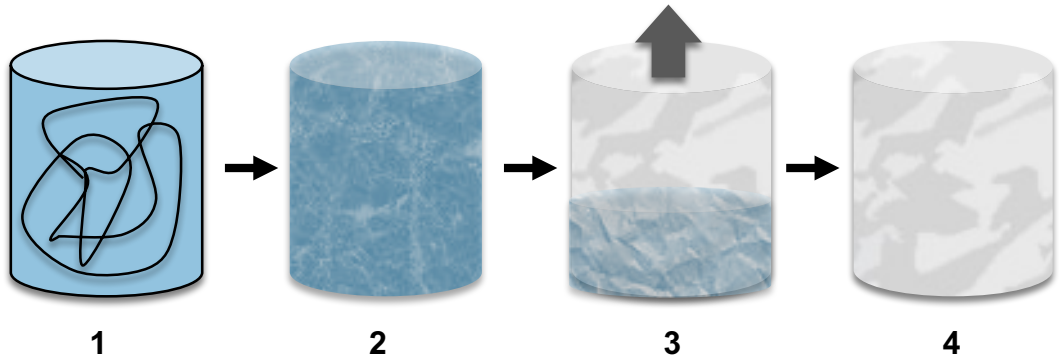

Figure 3.1 – Schematic representation of cryogelation process. A homogeneous casting solution (1) is frozen at subzero temperatures where pore formation begins due to ice crystal growth (2); solvent extraction process (3) is required in order to obtain a dried cryogel with interconnected pores (4). Adapted from LANG et al

3.3 Supercritical Fluid Technology

Supercritical is what is said of a fluid that has surpassed its critical temperature and pressure, i.e., a fluid is supercritical when the difference between the liquid and vapor phases disappears. In this region, the fluid exhibits both liquid and gas attributes, displaying density that of a liquid and the diffusivity of a gas (Table 3.1) .

Table 3.1 – Typical properties of gases, supercritical fluids (SCF) and liquids. (Foster et al., 2010)

Property	Gas	SCF	Liquid
Density (g.com^{-3})	10^{-3}	0.3	1
Viscosity (Pa.s)	10^{-5}	10^{-4}	10^{-3}
Diffusivity (cm^2.s)	10^{-2}	10^{-3}	10^{-6}

Carbon dioxide (CO_2) is the most used SF, displaying a low critical point (7.37 MPa; 304.13 K) (Figure 3.2) and a GRAS (Generally Recognized as Safe) status, being easily separable from solvents and polymeric mixtures or residues due to its gaseous form in standard conditions of temperature and pressure (Table 3.1). A small change in temperature and/or pressure can increase de CO_2 solvation power close to the critical point since there is an enhancement in the heat capacity of the fluid in that region. Plus, CO_2 is nontoxic, nonflammable and cheap, since it can be reused. (Kiran et al., 2012)

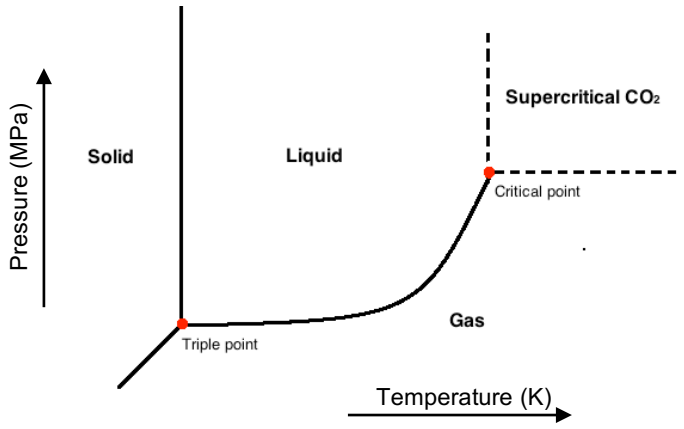

Figure 3.2 – CO_2 phase diagram.

Supercritical CO_2 has many different applications, being used as as a solvent in polymer synthesis (Restani et al., 2012) or as an anti-solvent in spray assisted particle formation (PGSS) (Gonçalves et al., 2015), in extraction processes (SFE), in membrane production by drying (RESS) (Morgado et al., 2014) or as a porogenic agent (Craveiro et al., 2014). CO_2 can also be used for analytical purposes in supercritical fluid chromatography (SFC) in protein or virus purification (Fernandes et al., 2015). Barroso et al., 2012 combined cryogelation process with a supercritical carbon dioxide extraction process, in order to obtain functional monolithic platforms for antibody purification.

3.3.1 Supercritical carbon dioxide ($scCO_2$)-assisted drying

Supercritical carbon dioxide ($scCO_2$)-assisted drying is a green technology that can form solvent-free ready-to-use 3D constructs with high controlled morphology, by manipulating process parameters, namely temperature, pressure and depressurization rate. This procedure has cost-effective benefits since it reduces the solvent recovery process. Additionally, CO_2 can be reused and scaffold production is less time consuming than other common processes, like lyophilizaton.

In order to extract the solvent, it must have affinity with CO_2.When drying polysaccharide-based cryogel structures, as most polysaccharide are water soluble, very often the solvent is water since water is the greenest solvent that can be used for pharmaceutical or biological applications. Aqueous solutions have low affinity with CO_2, increasing CO_2 consumption and the time required to obtain dried scaffolds. To increase the affinity between water and CO_2 (i) a co-solvent is used (e.g. ethanol) or (ii) water can be entirely removed by a water-replacement step known as phase inversion. Phase inversion involves a solvent exchange process in which a cryogel is directly submerged in a new

solvent which has to precipitate the gel structure, be miscible in water, have high affinity for $scCO_2$, be innocuous when present in pharmaceutical formulations. The new solvent freezing point is also relevant, since the solvent cannot solidify in order for phase inversion to occur (García-González et al., 2011, 2012).

3.4 Xerostomia

Xerostomia a symptom frequently associated with salivary gland hypofunction, characterized by the reduction or absence in saliva production. Xerostomia is a side effect caused by several factors; the most prevalent is related to polymedication, affecting 20% of elderly patients, the most polymedicated group of people present in modern society. Head and neck radiation can cause changes in the secretory cells resulting in thicker as well as lower saliva flow. Autoimmune diseases, like the Sjögren's syndrome affect many post-menopausal women due to lymphocytic infliltration of salivary glands and diabetes mellitus, among others. Patients who suffer from xerostomia commonly describe it as having a ''dry mouth'' sensation, which can lead to hoarseness, difficulty in speaking and swallowing. Plus, since the antimicrobial activity of the saliva is absent, xerostomia when left untreated can increase the occurrence of oral plaque and dental cavities and in worst cases, halitosis, oral ulcers, cracked tongue and oral candidiasis.

In order to manage xerostomia, saliva substitutes and xerostomia therapies are a growing market since 2006, predicted to be worth $270 million by 2019 (Global Data, 2012). There are a number of over-the-counter products that act a saliva substitutes in order to release xerostomia symptoms (Table 3.2). Recent studies report the use of bacterial exopolysaccharides as a saliva substitute, taking advantage of their thickening properties (e.g. xantham gum).

Many oral formulations use citric or ascorbic acid to stimulate saliva production, although oral recurrent acidic exposure will decrease the natural pH of the oral cavity, promoting enamel abrasion, demineralization and leading to oral cavity increase. The use of xylitol as a saliva stimulant is a great alternative, since oral bacteria, including *streptococcus mutans*, cannot metabolize xylitol,. (Haghgoo et al., 2015)

Table 3.2 – Over the counter products for xerostomia releave.

	Commercial name	Active ingredient	Type of drug	Oral dosage form	Manufacturer
Dry mouth	Decadron	Dexamethasone	Corticosteroid	Tablet	Merk & Co., Inc.
	Ativan	Lorazepam	Benzodiazepine	Tablet	Mylan
	Salagen	Pilocarpine hydrochloride	Cholinergic agonist	Tablet	Eisai Pharmaceuticals
	Evoxac	Cevimeline hydrochloride	Muscarinic agonist	Capsule	SnowBrand Pharmaceuticals
	Aquoral	Oxidized glycerol triesters	Lipids	Spray	Mission Pharmacal
	Caphosol®	High concentrations of calcium and phosphate ions		Mouth rinse	EUSA Pharma
	NeutraSal	Supersaturated calcium phosphate		Dissolving powder	NeutraSal
	Moi-Stir®	Mixture of calcium, sodium, magnesium and potassium		Spray	Pendopharm
	Glandosane®	n.a.		Spray	Fresenius Kabi

3.4.1 Xylitol

Xylitol (Figure 3.3) is a low calorie crystalline carbohydrate occurring naturally in some fruits and xylan-rich plants. It is many times associated with oral dosage forms since a number of clinical trials proved that xylitol acts as an enamel remineralization agent while playing an active role in cavity reduction.

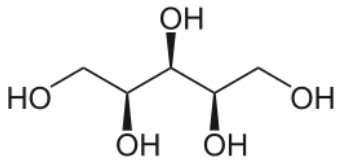

Figure 3.3 – Xylitol molecular structure.

Patients that suffer from hyposalivation have a greater probability of suffering from periodontal disease since they do not possess the necessary saliva flow to have an antiseptic and healthy oral cavity. Their exposure to bacterial oral disease increases. Xylitol is frequently administered as a sugar-free gum in order to induce a stimulus in saliva production while fighting against cavities. There are a number of marketed products that already incorporate xylitol in their formulations, namely sugar-free chewing gums, mints and candies (Ly et al., n.d.).

Most xerostomia relieving formulations demonstrate a peak in saliva production over a short period of time, not being able to sustain drug release. Plus, many symptom relieving excipients come in the form of medicated chewing gums that can cause stress and induce fatigue in mouth. Hydrogels are a good alternative since as they slowly dissolve in the mouth they can also capture some part of the produced saliva, retaining it in the oral cavity and increasing the time the mouth is exposed to the drug.

Combining FucoPol thicknening abilities with xylitol, a salivary stimulant, xerostomia symptoms can be relieved while promoting good oral health in patients experiencing hyposalivation. **The objective is to produce a FucoPol-based cryogel with a specific xylitol loading, using supercritical carbon dioxide extraction process in order to dry the FucoPol scaffold.**

3.5 Experimental Section

3.5.1 FucoPol downstream processing

FucoPol used in this chapter was extracted and purified following the same procedure described in 2.5.1: FucoPol downstream processing.

3.5.2 Scaffold production

In order to produce scaffolds, two samples were prepared, containing approximately 1.4 g and 2.1 g of FucoPol and 0.7 g of xylitol (Sigma-Aldrich) and added to 14 and 18 mL of deionized water, resulting in 10% and 11.67wt.% of FucoPol and 5% and 3,89wt.% of xylitol in the casting solution. In total, the resulting scaffold will contain 66.65% and 75 wt. % of FucoPol, and 33.34% and 25 wt.% of xylitol, respectively (Table 3.3).

Table 3.3 – Sample formulations used in the production of scaffolds by cryogelation coupled with supercritical carbon dioxide ($scCO_2$)-assisted drying: Sample FPX1 - 10 wt.% of FucoPol (FP) **(**bacterial exopolysaccharide produced and provided by Pure Cultures Group from UCIBIO-REQUIMTE/FCT/UNL, Mw ~10^6) and 5wt.% of Xylitol (Sigma-Aldrich) in 14 mL of deionized water; Sample FPX2 – 11.67 wt. % of FucoPol and 3.89wt.% of xylitol in 18 mL of deionized water. *Apparent viscosity was measured at 25 ºC and 45 ºC (Annex 5).

		FucoPol (FP) (g)	Xylitol (g)
Samples	**FPX1**	1.40	0.70
	FPX2*	2.10	0.70

Solvent: Deionized water

3.5.2.1 Cryogelation and water-replacement

Cryogel production parameters were based on Barroso et al., 2014. 18 mL of samples FPX1 and FPX2 were transferred into 2 mL stainless-steel molds. Cryogelation process occurred for a minimum of 24 hours at -20 ºC (VWR Signature Refrigerated/Heating Circulating Bath), subsequently followed by water-replacement.

A small amount of FucoPol and xylitol was immersed in a small amount of water miscible solvents (Phenomenex, 2011). The solvent where both samples did not dissolve was chosen for water-replacement step. Cryogels were removed from the stainless-steel molds and submersed freely in an given amount of solvent. Water-replacement occurred for 48 hours, at -20 ºC (VWR Signature

Refrigerated/Heating Circulating Bath). The structures formed after samples FPX1 and FPX2 were frozen for 48 hours at -20 ºC are designated as SCA1 and SCA2.

3.5.2.2 Supercritical carbon dioxide ($scCO_2$)-assisted drying

Supercritical carbon dioxide ($scCO_2$)-assisted drying was used to remove the solvent from the polymeric matrix using the experimental apparatus described below (Figure 3.4).

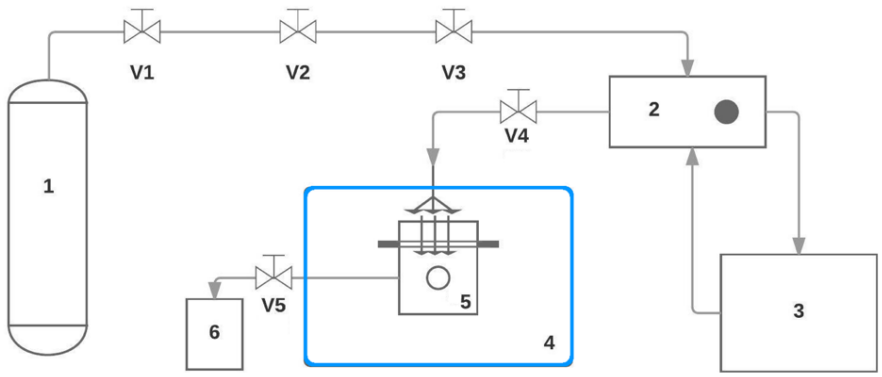

Figure 3.4 – Schematic representation of the supercritical apparatus used to produce scaffolds; (1) CO2 tank (Air Liquid), Gilson HPLC pump (2), Frigomix S cryostat, Braun (3), thermostatic water bath (Hart Scientific, Model 2200) (4), stainless-steel high pressure cell (Temtem et al., 2008) (5), Jasco BP-2080 Plus Automatic Back Pressure Regulator (6). Manual valves (V1 to V5); CO_2 entry valve (V4); CO_2 exit valve (V5).

Water-free cryogels (e.g. samples SCA1 and SCA2) were re-inserted into the stainless-steel molds and transferred inside a 33 mL high-pressure cell, that homogenously disperses CO_2 inside the cell (Temtem et al., 2008) (5). The cell was closed with a teflon o-ring, 8 stainless-steel screws and a sapphire window, to prevent pressure oscilations, and immersed in a thermostated water bath (Hart Scientific, Model 2200)(4) at 40±0.01 ºC. An inlet valve for CO_2 admission (V4) is connected to the high pressure cell were CO_2 (Air Liquid), previously cooled at -15 ºC (Frigomix S, Braun cryostat) (3) is loaded into the stainless-steel cell by a HPLC (Gilson) pump (2) at a rate of 10 mL/minute. The pressure inside the cell is monitored by a pressure transducer (Setra Systems Inc., Model 204) with a precision of ±100 Pa and a back pressure regulator (Jasco BP-2080 Plus Automatic Back Pressure Regulator) (6) to a maximum of 150 bar, for 8h. In the end, the system was depressurized along 10 to 20 minutes.

3.5.3 Analysis of supercritical process parameters

The behaviour of FucoPol, an amourphous polymer (Lourenço, 2015), in the presence of xylitol, was assessed by Differential Scanning calorimetry (DSC), previously described in 2.5.3.2 Differential Scanning Calorimetry (DSC). Calorimetric experiences were carried out by DSC Q2000 (Tzero™

DSC technology, TA Instruments Inc.) under anhydrous high purity nitrogen at a flow rate of 50 $mL.min^{-1}$ and temperatures that ranged from -90 to +180°C, at a rate of 5°C.min^{-1} Sample SCA2 was sealed in aluminium hermetic pans (TA Tzero Pan and lid), punctured for water evaporation.

3.5.4 Scaffold morphological analysis

Average pore diameter throughout sample SCA2 was performed using Scanning Electron Microscopy (SEM), previously described in 2.5.4.1 Scanning Electron Microscopy (SEM). A Hitachi S-2400 microscope was used, with an accelerating voltage of 15kV and a magnification of 5 and 10K. SCA2 was frozen, fractured in liquid nitrogen for cross-section analysis, attached to an aluminum stub and gold coated previously to SEM analysis.

3.5.5 Scaffold chemical composition

The presence of xylitol and FucoPol in sample SCA2 was attained by Fourier Transform Infrared Spectroscopy (FT-IR), previously described in 2.5.5.2 Fourier Transform Infrared Spectroscopy (FTIR). Attenuated Total Reflectance (ATR) sampling accessory (Smart iTR) was used on a Thermo Nicolet 6700 Spectrometer. Spectra acquisition was obtained with a 45° incident angle in 4000–525 cm^{-1}, with a 4 cm^{-1} resolution.

3.5.6 Scaffold characterization

In order to assess the process reproducibility, 5 samples of SCA2 (n=5) were assessed in terms of weight, thickness and surface pH, as previously described in 2.5.6.1.

3.5.6.1 Water uptake[1]

Water difusion and absorption plays an important role in the performance and disintegration of hydrophilic polymeric sctructures like FucoPol-based cryogel. Swelling can be observed upon water absorption by hydrophilic structures, but that is not always the case (e.g. kitchen sponges absorb water but do not swell; their size remains the same). Since the SCA2 sample will be applied orally, the amount of synthetic simulated saliva that could be absorbed, previous to mass-loss, was measured at 1, 3, 5, 7, 10 15, 30, 60, 90 and 120 minutes. 2 samples of SCA2 (n=2) were transferred to thermostatic bath (Concenssus S.A.R.L.) containing two glass flasks filled with 10 mL of simulated

[1] Simulated saliva was prepared according to Marques et al., 2011, by weighting 8 g/L^{-1} of sodium chloride (Panreac), 2.38 g/L^{-1} of sodium phosphate dibasic (Sigma-Aldrich), 0.19 g/L^{-1} of potassium phosphate monobasic (Sigma-Aldrich) and 0.05 mg/ L^{-1} of Lysozyme (Sigma-Aldrich). Phosphoric acid (Sigma-Aldrich) was used to adjust pH 6.8.

saliva (Marques et al., 2011) at pH 6.8, 37 ºC under stirring. The samples were trapped in a porous stainless-steel mesh in order to prevent excessive mass scattering to the aqueous environment. Samples were weighted before and after water uptake; the difference in weight in consecutive measures, before sample SCA2 starts to lose mass, translates into the samples' ability to absorb water.

3.5.6.2 *In vitro* disintegration time[1]

The time required for scaffold disintegration was performed over the course of 5, 15, 30, 60, 90 and 120 minutes. 3 samples of SCA2 (n=3) were transferred to glass flasks containing 10 mL of simulated saliva (Marques et al., 2011) at pH 6.8, 37 ºC and 100 rpm (Orbital shaker Rotaterm, JP Selecta), Samples were trapped in a porous stainless-steel mesh in order to prevent excessive mass scattering to the aqueous environment. Samples were weighted before and after water evaporation by lyophilization (Lyo Quest-55, Telstar).

3.5.6.3 *In vitro* release studies[1]

Chromatography is an analytical technique that involves the separation, identification and quantification of different components on the basis of differences encountered between the mobile and the stationary phase. There are a number of chromatographic procedures that can be applied according to the properties of a given sample. High performance liquid chromatography (HPLC) is a liquid chromatograph technique that is distinguishable from other liquid chromatography techniques due to the pressures provided to the system in order to separate a complex mixture (50 to 350 bar). The apparatus usually includes a sampler, a pump and a detector that generates a signal proportional to the amount of sample in the complex mixture. Although optical detectors account for almost 71% of HPLC detectors, electrochemical detectors (EC) possess higher sensitivities and selectivity of detection without the need for secondary reactions. Plus, they are useful for compounds that do not possess chromophore of fluorophore groups (e.g. xylitol) making them unsuitable for UV and fluorescence detection.

A preliminary study of the qualitative release of xylitol from 3 SCA2 samples (n=3) was obtained. The samples were transferred to glass flasks containing 10 mL of simulated saliva (Marques et al., 2011) at pH 6.8, 37 ºC and 100 rpm (Orbital shaker Rotaterm, JP Selecta). Several aliquots were retrieved after 10, 20 and 30 minutes, over the course of approximately 4 hours. Samples were trapped in a porous stainless-steel mesh in order to prevent excessive mass scattering to the aqueous environment. Xylitol was quantified by High Performance Liquid Chromatography (HPLC), using DIONEX, Model ICS3000 equipped with an electrochemical detector. Sample separation was conducted on an Aminotrap and Carbopac PA10 4x250mm column (Thermo DIONEX) at a flow rate of 1 mL/minute of NaOH 18 mM mobile phase; column temperature was 30 ºC. Total run time per

sample was 20 minutes, with injection volumes of 25 µL.

The total mass of xylitol released from samples SCA2 is the sum of all aliquots retrieved throughout the 4 hours. Transport mechanism that induces drug release from samples SCA2 was determined by alternative solution for short-time behavior of the Korsmeyer-Peppas equation for cylinders, assuming perfect sink and boundary conditions (Equation 3.1)

$$\frac{M_t}{M_\infty} = 4\sqrt[2]{\frac{D}{\pi a^2}}\, t^n \qquad \textbf{Equation 3.1}$$

Here, *k*, a constant, is difined by $4\sqrt[2]{\frac{D}{\pi a^2}}$, with *D* being the constant drug diffusion coefficient, *a* is the cylinder radius, *n* is the diffusional exponent, indicative of the transport mechanism and *t* is the time. Fickian diffusion is defined by n=0.45 and non-Fickian diffusion by n>045, for cylinders.

3.5.6.4 Cytotoxicity

Cytotoxic assays were performed according to the method described in 2.5.6.6 Cytotoxicity, using 1% (w/v) FucoPol, 5 % (w/v) of xylitol and 1% (w/v) of a scaffold sample was performed using a 96-well plate, described in **Figure 3.5**.

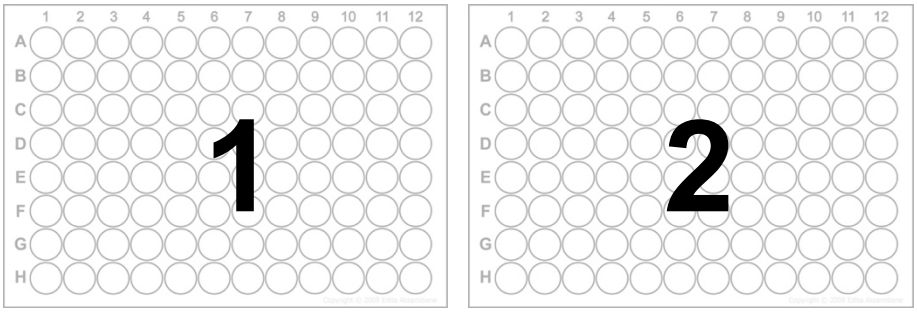

Figure 3.5 - Schematic representation of the two 96-well plates used to test the substracts' cytotoxicity used to produce sample SCA2: Plate (1) - FucoPol (1 to 5); Xylitol (6 to 10);positive control (C+): Dulbecco's Modified Eagle Medium (DMEM) with 10 µl of dimethylsulfoxide (DMSO) (11); negative control (C-): cells grown in DMEM (12); Plate (2) – SCA 2 (1 to 5); positive control (C+): DMEM with 10 µl of DMSO (Merk) (11); negative control (C-): cells grown in DMEM media (12). Successive dilutions of each component were performed in each plate: ½, ¼, 1/8, 1/8, 1/16, 1/32 (w/v) from A to F, with respective media control H (1 to 4). Adapted from http://www.cellsignet.com, assessed in 1st March 2016.

3.6 Results and Discussion

As was mentioned in 1.3, FucoPol was used to create two oral drug delivery platforms. With that in mind, in Chapter 3 the goal was to assess the interaction between FucoPol and supercritical carbon dioxide ($scCO_2$). A small amount of FucoPol, in its solid form, was inserted in a 33 mL stainless-steel high pressure cell at 200 bar and 40 ºC. FucoPol did not "melt" or dissolved in $scCO_2$, hence, FucoPol did not possess the ability to form foams. (Bhamidipati et al., 2013)

FucoPol was used in scaffold production using $scCO_2$-assisted drying. In order to lower the time required for solvent extraction and structure formation, and considering that FucoPol is water-soluble, scaffold production by cryogelation was performed. However, water has low affinity for CO_2. Hence, a water-replacement step is required for excess water removal from the cryogel structure.

3.6.1 Scaffold production

In order to obtain a ready-to-use, dry scaffold, the choice of solvent in water-replacement step must be carefully evaluated, in the sense that the solvent chosen must not dilute the sample, i.e., must not dissolve FucoPol or xylitol. A number of water miscible solvents were tested in order to assess which demonstrated a better anti-solvent effect upon the individual components of the cryogel (Table 3.4).

Table 3.4 – Water miscible solvents tested as anti-solvents to FucoPol and xylitol. The solvents were classified as partially soluble (PS), non soluble (NS) or soluble (S) according to their ability to dissolve each component. Xylitol solubility was assessed first and later, FucoPol solubility was tested in the solvents that did not solubilize xylitol.

	Xylitol	FP	Water
Acetic acid (Panreac)	PS	PS	Miscible
Acetone (LabChem)	NS	NS	Miscible
Acetonitrile (Sigma-Aldrich)	NS	PS	Miscible
Dimethylformamide RS (Carlo Erba)	S	-	Miscible
Dimethylsulfoxide RPE (Carlo Erba)	S	-	Miscible
1,4-Dioxane (Scharlau)	PS	-	Miscible
Ethanol 96º (Carlo Erba)	S	NS	Miscible
Methanol RS (Carlo Erba)	PS	NS	Miscible
2-Propanol (LabChem)	NS	NS	Miscible
Tetrahydrofuran (Sigma-Aldrich)	NS	PS	Miscible

Acetone and 2-propanol were the only two solvents that did not dissolve both FucoPol and xylitol. Since they both have a good affinity to CO_2 (Table 3.5) both solvents were used in the water-replacement step.

Table 3.5 – Solubility and boiling temperature parameters of the solvents involved in water-replacement (Hansen, 2007)

	δ (MPa)	$T_{boiling}$ (ºC)
Acetone	19.9	56.1
2-propanol	23.6	82.6
Water	47.8	100

Considering the previous information, and the work of Barroso et al., 2014, a preliminary 3D structure was produced (i.e. SCA1), using sample FPX1, in the course of 24 hours at -20 ºC. Afterwards, the cryogel was directly immersed in acetone in order to avoid any possible diffusivity barriers and acetone-water replacement occurred for 48 hours at -20 ºC. SCA1 was dried for 3 hours, using $scCO_2$ at 45 ºC, 150 bar and 10 mL/minute of CO_2. Depressurization occurred for 10 minutes. The results are shown in Figure 3.6.

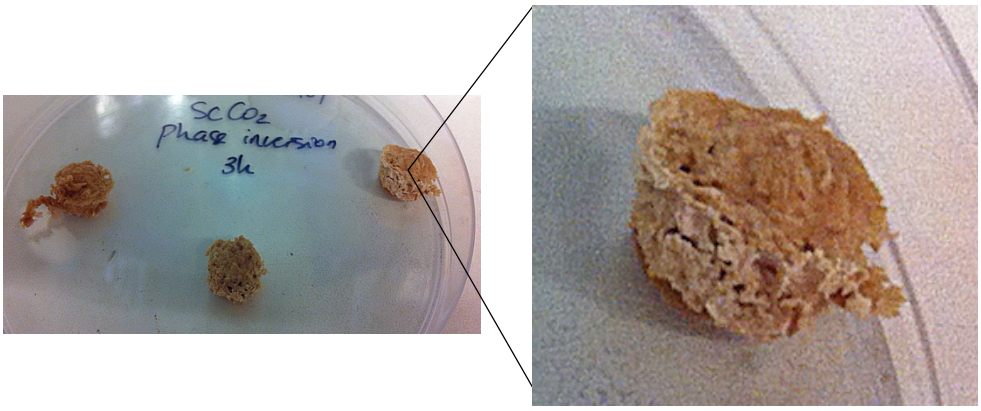

Figure 3.6 – Scaffolds prepared by cryogelation at -20 ºC (24h) using water-acetone replacement (- 20 ºC, 48h hours) prior to $scCO_2$-assisted drying at 150 bar, 45º C, 10 mL.min^{-1} (3 hours).

Analyzing Figure 3.6, it is possible to infer that water-acetone replacement was successful due to the production of rigid, dry and shrunken scaffold (i.e. SCA1) (García-González et al., 2012). However, scaffolds were extremely porous, presenting heterogeneously distributed macroporous that disrupted the pore interconnectivity, resulting in the formation of holes within the polymeric matrix. Extreme pore enlargement associated with polymer shrinkage may have a higher manifestation in low concentrated polymer solutions, due to a higher water content that will induce the formation of ice crystals with increased dimensions. Furthermore, at -20 ºC the crystals experience slower freezing times, having time to fully grow and expand during cryogelation process.

Since low polymer concentration could be the contributing factor to pore collapse in SCA1 (Figure 3.6), a second attempt to produce a scaffold was performed, using solution sample FPX2 (Table 3.3) in order to produce scaffold SCA2. The solvent chosen for the water-replacement step was also changed from acetone to 2-propanol. From this moment on, the results showed are related to the characterization of SCA2, produced by cryogelation coupled with supercritical carbon dioxide assisted drying, using the formulations displayed in Table 3.3 of subsection 3.5.2.

In order to simplify data presentation and the discussion of the obtained results, FPX2 will represent the experimental formulation used to prepare scaffold SCA2, while all the compounds present in those formulations will be mentioned as FP (i.e. FucoPol) and Xylitol, from this moment on until the end of subsection 3.6.5.4.

3.6.2 Analysis of supercritical process parameters

3.6.2.1 Differential Scanning Calorimetry (DSC)

As mentioned in 2.6.1.2, Differential scanning calorimetry was performed in order to evaluate if SCA2 had any phase transformations, as melting (transition from crystal to liquid) or crystallization (transition from melt to a crystalline solid), occurring at temperatures T_m and T_c. Glass transition temperature is defined, T_g. when a material avoids crystallization and is supercooled, increasing the viscosity and vitrifying the material in a disordered solid (amorphous material). (Shawe et al., 2000)

Differential scanning calorimetry was performed in order to determine if the scaffolds can undergo any kind of induced thermal degradation above 40 ºC. These were the temperatures used to dry the scaffolds in supercritical conditions. As reported in 2.6.1.2, FP is known to be amourphous form previous work (Cândido, 2015), presenting a degradation temperature around 268 ºC. SCA2 results from a blend of FP and xylitol; Figure 3.7 provides the DSC data from analyzed scaffold.

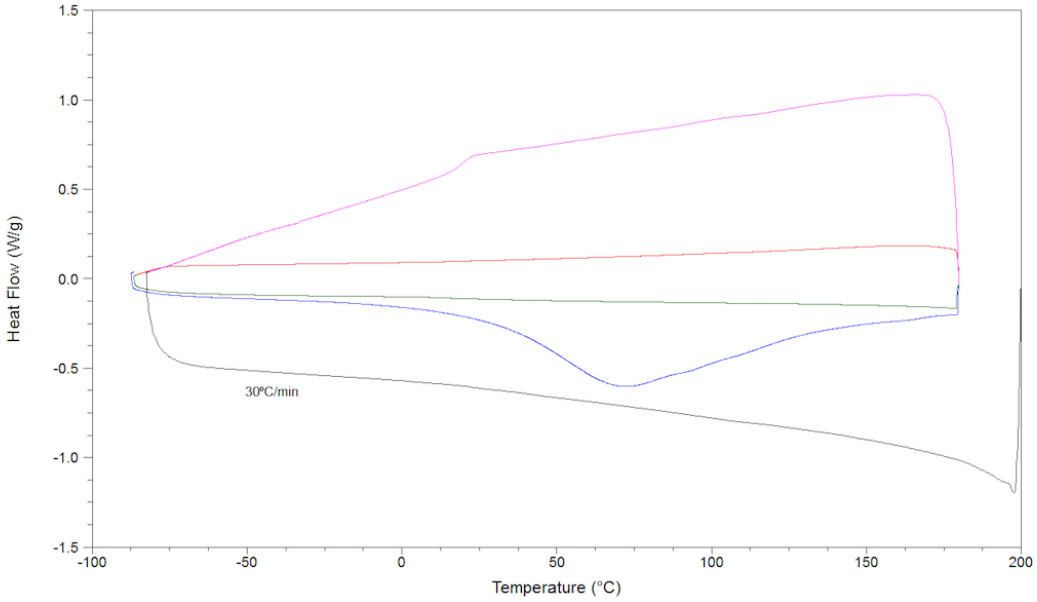

Figure 3.7 – Thermal analysis (DSC) of scaffolds produced by 66.66% of FucoPol and 33% of xylitol, at a temperature range of -90 ºC to 180 ºC at 5 ºC.min^{-1}. SCA2 sample was inserted into an aluminum hermetic pan in order to allow water evaporation. DSC analysis lasted over 4 hours, using three heating cycles to induce sample melting (blue, green, brown) and two cooling cycles for sample recrystallization (red, pink). Water evaporation was registered in the first heating cycle (blue). The last heating cycle (brown line) was performed at 30 ºC.min^{-1}.

DSC analysis show that the scaffold lacks melting or crystallization events, so SCA2 should be completely amorphous. This is a characteristic behavior found in pure FucoPol solutions (Lourenço et al). Since xylitol acts as a solvent for FucoPol, increasing the solubilization power of water, its influence on the thermal behavior of FP is apparently null, unlike the behavior found in 2.6.1.2, where FP was physically cross-linked with poly (ethylene oxide).

The combination of FP and xylitol does not alter the amorphous state of FP. The blend remains complety amourphous, so it is safe to say that working supercritical temperatures (above 40 ºC) will not promote or induce melting of the sugar content present in both FP and xylitol, since there are no registered phase transitions.

3.6.3 Scaffold morphological analysis

Visual representation of the scaffolds produced by cryogelation, using 75% of FP and 25% of xylitol and 2-propanol for the water-replacement step. Scaffolds were dried using supercritical carbon dioxide ($scCO_2$)-assisted-drying. The results are displayed in Figure 3.8.

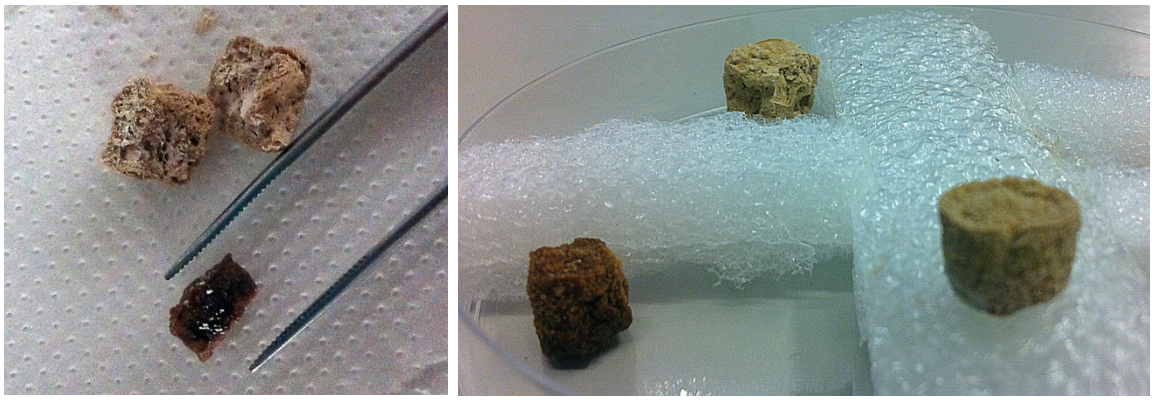

Figure 3.8 – Visual representation of the scaffolds obtained by cryogelation at -20 ºC (24h) using 2-propanol-water replacement (- 20 ºC, 48h hours) prior to $scCO_2$-assisted drying (150 bar, 40º C, 10 $mL.min^{-1}$, 8 hours).

Analyzing Figure 3.8, it is possible to infer that 2-propanol-water replacement was successful, since a rigid, dry scaffold was obtained. The increase in FP concentration led to a uniform scaffold morphology, both external and internal, not found in the scaffolds containing 66.66 wt.% of FP and 33.33 wt.% of xylitol, produced using acetone for water-replacement step (Figure 3.6). When acetone was replaced by 2-propanol, the time required for scCO2-assisted phase inversion increased from 3 to 8 hours since scaffold production below 8 hours produced scaffolds with a residual amount of moisture. When comparing the two solvents (Table 3.5), 2-propanol exhibits a higher boiling point that acetone, which can lead to lower vapor pressure, resulting in slower solvent extraction upon $scCO_2$-assisted drying.

Combining acetone-water replacement with higher FP concentrations in sample FPX2 was the next step since through this combination the time required for scCO2-assisted phase inversion is reduced and the scaffolds obtained will possibly have uniform morphology; however, given the time and the amount of FP available, further process optimization was not viable. The remaining scaffold replicates were produced under the same conditions as the scaffolds displayed in Figure 3.8, in order to obtain comparable results.

3.6.3.1 Scanning Electron Microscopy (SEM)

Morphological imaging of SCA2 polymeric scaffolds was assessed by SEM; results are shown in Figure 3.9. Through SCA2 cross-section is possible to notice the presence of asymmetrical layers in outer layers of the scaffolds (red arrows); the dense outer layer provides resistance, integrity and rigidity to the scaffolds' morphology. The production of asymmetrical membranes upon $sccO_2$-drying was also reported by Morgado et al., 2014 in the production of PVA/chitosan wound dressings.

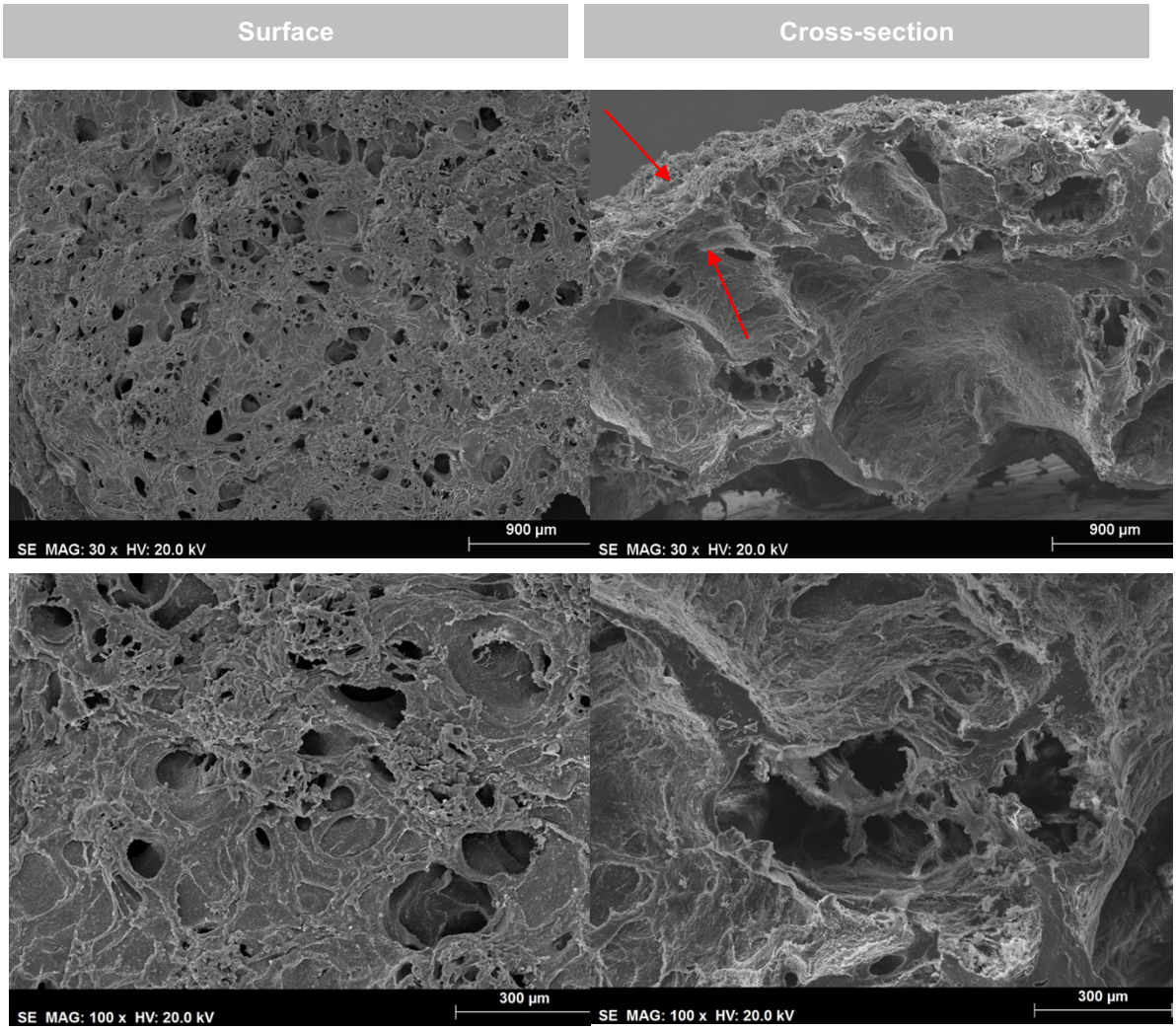

Figure 3.9 – SEM imaging of superficial and cross-section SCA2 scaffolds containing 075 wt.% of FP and 25 wt.% of xylitol, under 30k (upper row) and 100k (lower row) amplifications. Cryogelation occurred for 24h at -20 ºC with subsequent 2-propanol-water replacement for 48 hours at -20 ºC and supercritical carbon dioxide ($scCO_2$)-assisted drying for solvent extraction for 8 hours at 40ºC, 150 bar, 10 mL/minute of CO_2 and depressurization rates around 10-20 minutes.

The average pore diameter found in the surface of the scaffold, measured by ImageJ software, presented an average size of 126.26 µm, indicating the presence of macroporous (>50 nm). However, when observing the SCA2 cross-section it is possible to perceive the heterogeneous distribution of the pores within the polymeric scaffold, due to the presence of holes and pockets. Average pore diameter ranged from 105.4 µm to 1.94 mm, values that can be narrowed by decreasing cryoglation temperature. Lower subzero temperatures (e.g. -80 ºC) promote faster freezing times that induce smaller ice crystal formation, which in turn produce a higher number of pore with smaller diameters.

Additionally, slower $scCO_2$-assisted dryingdepressurization rates can prevent further pore enlargement.

By SEM imaging, it is possible to conclude that for our formulation and purpose, cryogelation is a suitable technique that is able to create a macroporous scaffold. Although the SCA2 presents heterogeneous pore distribution, xylitol should be released and absorbed by the oral mucosa since xylitol presents a low molecular weight, suitable to be released from the porous structure. A controlled release of xylitol, over time, can possibly require lower pore diameter and/or the presence of dendrimers.

3.6.4 Scaffold chemical composition

3.6.4.1 Fourier Transformed Infrared Spectroscopy (FTIR)

FTIR analysis was performed in order to evaluate if all the individual componentes of the scaffolds - FucoPol and xylitol - were present in the sample, after cryogelation and $scCO_2$-assisted drying. FT-IR spectra of SCA2 is presented in Figure 3.10.

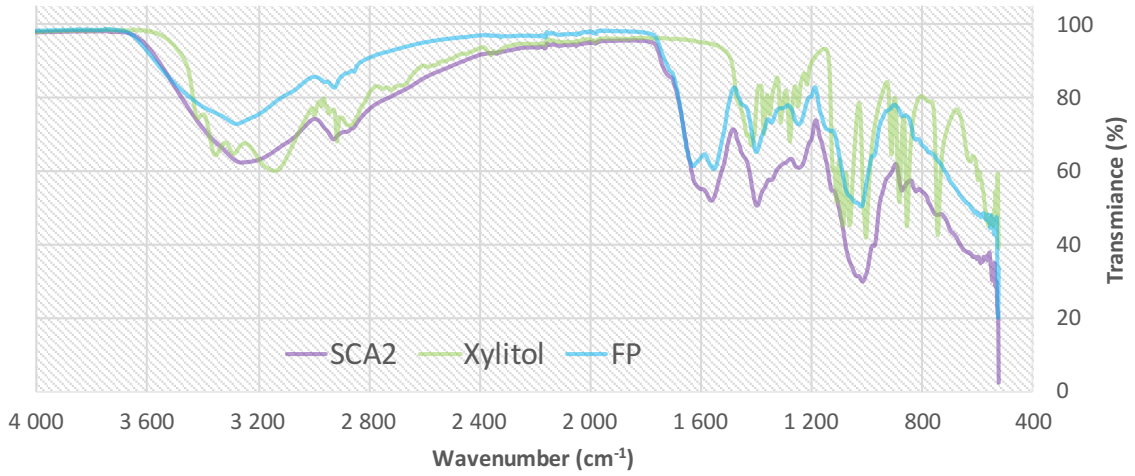

Figure 3.10 – FT-IR spectra of SCA2. The individual FTIR spectra of FP and xylitol were used as controls.

FP spectra, previously reported in 2.5.5.2, remains identical to the one reported by Freitas et al., 2010, displaying a broad O-H band around 3276 cm^{-1}, a C-H band at 2923 and 1400 cm^{-1} and C-O or possible C-N band between 1000 and 1200 cm^{-1} that can possibly be derived from amount of nitrogen found upon XPS analysis.

Xylitol and FP have somewhat similar TIR spectra, sharing bands around 3296 to ~3400 cm^{-1} (O-H stretching), 2866 to 2994 cm^{-1} (C-H stretching) and 1007-1312 cm^{-1} (C-O stretching) Similar to the ODF spectra found in 2.5.5.2, SCA2 FT-IR spectra also appears to derive from an overlap between pure FP and pure xylitol individual FT-IR spectra, suggesting that the latter may be physically blended.

As a result, ODF spectra results from a widening of the 3276 cm^{-1} band (O-H) due to the contribution of the 3296 cm^{-1} band from xylitol, and a widening of 1450 to 1470 cm^{-1} bands (C-H), due to the contribution of both FP and xylitol. SCA2 FTIR spectra is closely related to the profile of FP FTIR spectra, since FP acounts for 75 wt. % of the SCA2.

3.6.5 Scaffold characterization

3.6.5.1 Weight, thickness and surface pH

In order to assess the scaffolds reproducibility, weight and thickness measures were mesured. Scaffolds that arise from cryogelation (i.e. cryotopic scaffolds) present an average thickness around 700 µm and an average weight of (13.2±6.3) x 10 mg. The surface pH (Figure 3.11) of SCA2 scaffolds was within the normal pH range found for the oral mucosa (Aframian et al., 2006). Pharmaceutical excipients should have a neutral behavior in order to be innocuous to the oral cavity. Scaffold presents a slightly alkaline surface pH of 7.73, as a result of hydroxyl group increase due to xylitol content.

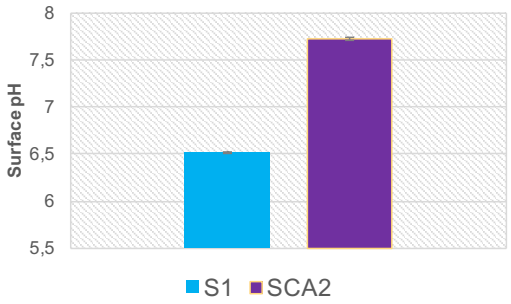

Figure 3.11 – Surface pH of SCA2 samples. Surface pH is an average result from six consecutive measurements applied to FP, and SCA2 samples.

3.6.5.2 Water uptake and *in vitro* disintegration studies

Since SCA2 scaffolds are mainly made of FP – a hydrophilic polymer – when the cryogels directly contact the oral cavity, saliva absorption will occur, simultaneously to continuous disintegration and xylitol release from the porous scaffold. In order to determine the amount of water uptake before mass loss, in vitro disintegration and water uptake studies were perfomes. The results are shown in Figure 3.12.

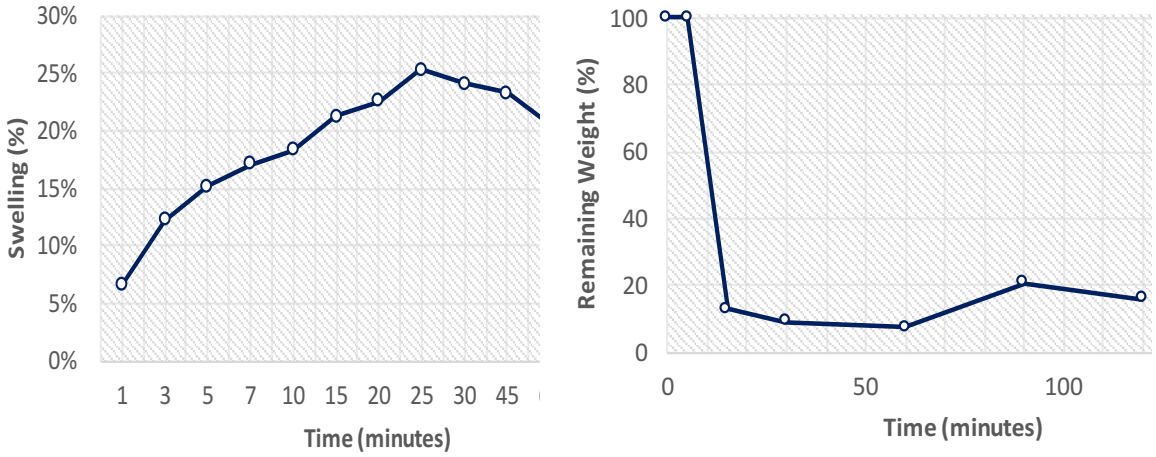

Figure 3.12 – Water uptake ability (left) and *in vitro* disintegration time (right) of SCA2 samples (n=3) using 10 mL of simulated saliva at pH 6.8, 37 ºC . Disintegration studies were also performed at 100 rpm.

SCA2 samples were able to absorb 30% of water before experiencing mass loss. When combining the data regarding water uptake and *in vitro* disintegration studies, it is possible to observe that scaffold degradation occurs between 5 to 15 minutes while swelling phenomena is observed up to 25 minutes. One possible explanation could rely on the vigorous agitation encountered in *in vitro* degradation studies, that can have increased scaffold disintegration, causing a discrepant behavior found when combining both tests. Another assay should be performed in order to fully comprehend the scaffold degradation coupled with its water uptake ability. The use of same process parameters is proposed in both assays: smaller degradation times and milder agitation speeds at 37 ºC and pH 6.8.

3.6.5.3 *In vitro* drug delivery kinetic profile

Preliminary qualitative studies regarding the release of xylitol at pH 6.8, from SCA2 scaffold samples were performed. The results are showed in Figure 3.13.

Pharmacokinetic studies were performed in the presence of negative controls (n=3) that did not possess xylitol or the same amount of FP present in the scaffold samples of SCA2. This was due to the fact that the amount of FP available was insufficient to produce both negative controls and drug loaded scaffold. Plus, the time required for FP production, purification and extraction combined with cryogel preparation, scCO2-assisted drying and product characterization, exceeded the time available to complete this dissertation. Hence, qualitative studies of the release of FP were obttained. In these studies, it is not possible to have an accurate measure for the amount of xylitol released or entrapped, since the analytical values can be masked by some part of FP that is released upon scaffold degradation. Nevertheless, the amount of FP that can be considered as a contamination agent to xylitol release should be constant throughout the time, and should not affect the release

profile of xylitol from the SCA2 samples. With that in mind, xylitol release seems to follow Fick's diffusion law; a closer look to the possible mechanism of transport is provided by the Korsmeyer-Peppas equation (Equation 3.1), applied for cylinders. This model only accounts for the first 20% release of the drug. Since the diffusion exponent, *n,* is higher than 0.45, xylitol release can be possibly associated with anomalous transport, meaning that both Fickian and non-Fickian mechanisms could be involved in the release of xylitol (e.g. diffusion and swelling).

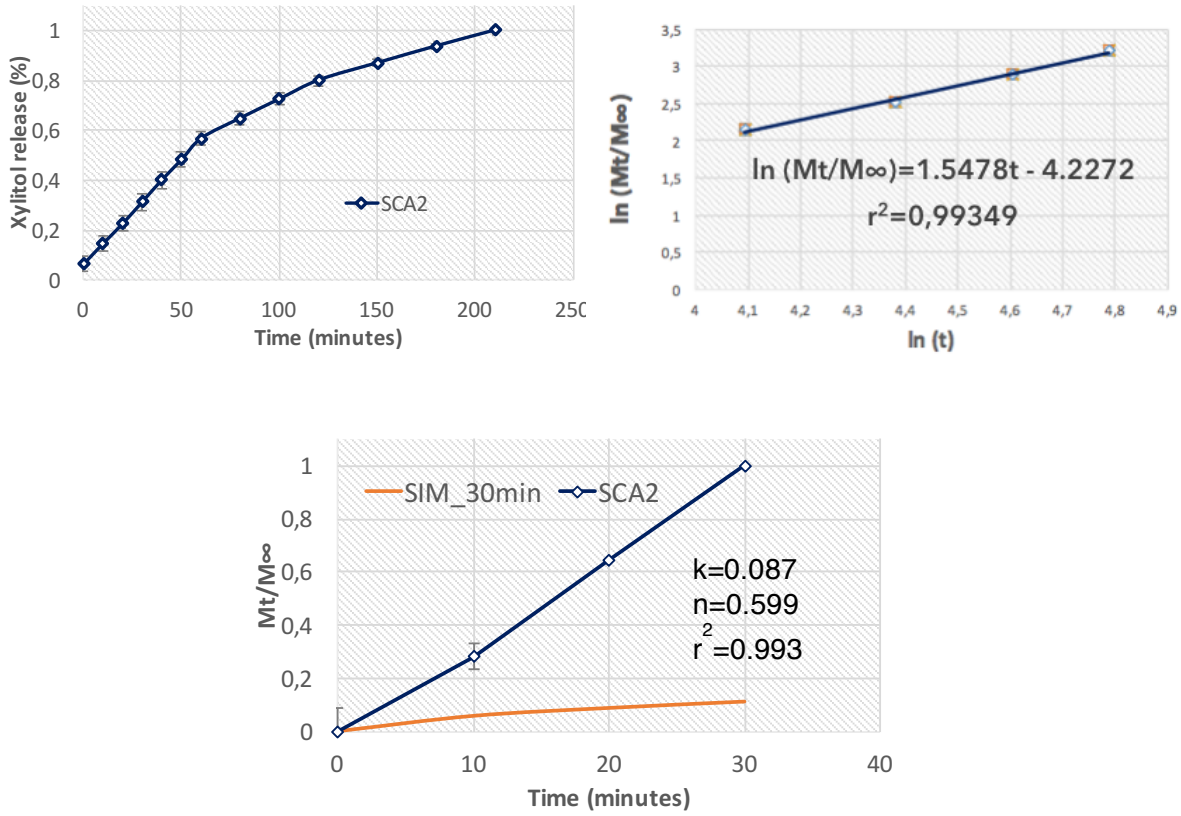

Figure 3.13 – Xylitol qualitative release studies from SCA2 samples. The presence of xylitol in SCA2 samples was assessed by HPLC using an electrochemical detector, a flow rate of 1 mL/minute of NaOH 18 mM mobile phase, a column temperature of 30 ºC and an injection volume of 25 µL.

In order to accurately perform pharmacokinetic studies that provide reliable, quantitative analytical information regarding xylitol release from SCA2 porous scaffolds, triplicates of a negative control need to be performed (75 wt.% of FP) in the same conditions as the SCA2 scaffolds were performed (3.5.2). That way, the contribution of FP to the acquired data can be subtracted, leaving only xylitol to be quantified over time.

3.6.5.4 Cytotoxicity

In order to confirm the scaffolds lack of cytotoxicity, the effect of SCA2 cryogels, and all its individual components on epithelial cells, was assessed. As in 2.6.4.5, all the elements were in direct contact

with cell media for 24 hours. Afterwards, fresh DMEM media was provided and 24 hours later, a resazurin test was performed. The percentage of viable cell is displayed in Figure 3.14.

Citotoxic assays revealed that SCA2 scaffold samples did not present any significant changes in cell viability; in fact, the presence of xylitol and FP presence seem to increase cell density, when compared to the positive control, a behavior that can be related to the sugar content present in both FP and xylitol.

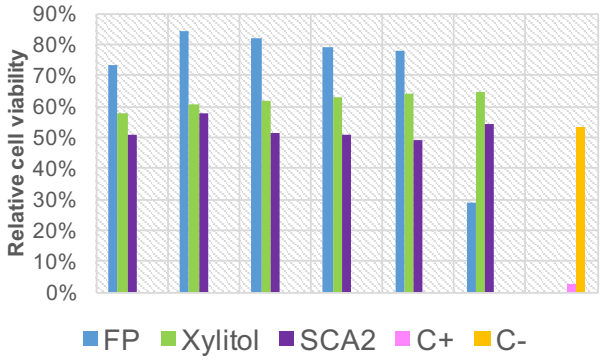

Figure 3.14 - VERO cell viability after exposure to SCA2 samples and its individual components, FP and xylitol. Cell viability was assessed 24 hours after to cell exposure to the provided material. Cell viability was determined by UV/Visible analysis in order to quantify the metabolized resazurin at 570 and 600 nm. Negative control (C-) contained 10 µL of DMSO; positive control (C+) consisted in DMEM media.

3.7 Concluding remarks

In this chapter a bacterial expolysaccharide – FucoPol (FP) – was used to produce a cryogel at subzero temperatures. Supercritical fluid-assisted drying was used in order to extract the solvent from the polymeric matrix, resulting in dry, ready-to-use porous scaffolds. Pore size and distribution upon cryogelation is intimately related with the freezing temperatures to which the solution is exposed to, and the time required for cryogelation to occur. As mentioned before, the work in chapter 3 is based on the work of Barroso *et al.* 2014 who prepared macroporous monolithic platform that allowed antibody purification. In this chapter, a FucoPol-based macroporous scaffold was produced by cryogelation at -20 ºC, for 24 hours. Since the scaffold revealed a heterogeneous pore size distribution, decreasing the cryogelation temperature can possibly lead to smaller pores that are homogeneously distributed throughout the scaffold. Another way that can be used to tune pore size distribution is through the screening of different organic solvents required for the water-replacement step (Temtem *et al.*, 2006).

Solvent screening can also aid supercritical carbon dioxide ($scCO_2$)-assisted drying, in the sense that it can decrease the time required to produce a polymeric structure. The use of a co-solvent or the increase of pressure near the critical point of carbon dioxide can increase the solvation power of CO_2, which in turn lead to a faster solvent extraction and less consumed CO_2. Nevertheless, a scaffold

made from a mixture of 75 wt.% of FucoPol and 25 wt.% of xylitol was obtained, revealing 30% of water uptake, disintegrating in approximately 15 minutes. The scaffold was validated by exposure to epithelial cells for 24 h, revealing to be non-toxic. The pH at the scaffold surface is within the oral cavity's own pH, proving that the obtained formulation is innocuous.

Future work should address the following studies:

- Temperature screening and its effect on pore size and distribution in cryogelation and water-replacement steps;
- Polymer concentration screening in order to assess the optimal polymer concentration required for cryogel production, while avoiding polymer shrinkage;
- Pressure optimization: the process should be performed using high pressures in order to try to decrease the production time;
- Temperature optimization: tuning the temperature can increase the solvation behavior of CO_2 which will decrease the time required to produce the scaffolds.

Concluding remarks and future work

4.1 Contributions

In this dissertation, the main goal was to use a sugar-rich bacterial exopolysaccharide in the production of 3D drug delivery platforms - an orodispersible film and a scaffold.

An orodispersible film was produced by electrospinning, a fiber forming technique that allows the production of thin controlled films that possess unique properties. In this dissertation, the assessment of FucoPols' fiber forming abilities and its ability to expand was determined by electrospinning and supercritical exposure of the polymer. The main contributions are stated bellow:

- **FucoPol did not display the ability to form fibers on its own** when exposed to electrospinning conditions that involved the use of voltages that ranged from 0 to 20 kV, rates of 0.1 to 1.5 $mL.h^{-1}$, relative humidity of 20 to 40 %, temperatures of 20-27 ºC, and collector/needle distances of 10 to 25 cm. Polymer concentration ranged from 0.25 wt.% to 5 wt.%. FucoPol did, however, display the ability to produce micro to nanobeads by electrospray, an ability that was previously explored by Lourenço, 2015 using spray-drying technique.
- **An orodispersible film containing a physical blend of 66 wt.% of FucoPol with 33 wt.% of poly (ethylene oxide) was attained by electrospinning**, with experimental conditions involving 13.5 kV voltage, 0.5 $mL.h^{-1}$ rate, relative humidity of 20 to 30 %, average temperatures of 25 ºC and collector/needle distances of 23 cm.
- **FucoPol did not display the ability to form foams under supercritical conditions** that went

from 0 to 200 bar at 40 ºC; carbon dioxide (CO_2) was the chosen supercritical fluid. In order for foaming to happen, a supersaturation of $scCO_2$ state must occur, with following phase separation, nucleation and porew growth either by an increase of temperature or a decrease in pressure. Phase separation and nucleation did not occur. FucoPol remain unaltered, concluding that there was a potential application of FucoPol in the production of porous polymeric matrices that could be dried using continuous supercritical conditions (e.g. supercritical carbon dioxide drying).

- **A 3D macroporous scaffold was attained by cryogelation at -20 ºC, using a physical blend between 75 wt.% of FucoPol and 25 wt.% of xylitol.** Supercritical carbon dioxide ($scCO_2$)-assisted drying was used to extract the solvent from the cryogel and prevent internal pore collapse. Solvent extraction lasted for 8 hours, with a carbon dioxide (CO_2) rate of 10 mL/minute at 40 ºC and 150 bar.

4.2 Future work

ODFs is still in need of optimization regarding its initial formulation; its notorious hygroscopic behavior needs to be evaluated and controlled since the films were mechanically affected in the presence of any residual water, which can hamper manual handling. Overall, our work can be improved in the future by:

- proper ***in vitro*** **pharmacokinetic release studies** that are able to decrease the inaccuracy associated with the measurements, by creating a more suited testing method;
- the **incorporation of hydrophilic drugs** that can be easily blended in the casting solution, producing a homogenous dispersion upon electrospinning film production;
- **drug entrapment assays** performed in order to perceive the minimal amount of drug required to achieve drug loadings that match the ones recommended by the patient information leaflets.

Addittionally, a FucoPol-based scaffold was produced by cryotropic gelation, a technique that allows the formation of porous structures by ice crystal growth control through the manipulation of subzero temperatures. Similar to electrospinning, this process is a low footprint, environmentally friendly technique that allows the formation of macroporous structures. Supercritical assisted solvent extraction from the previously obtained cryogels was performed in order to prevent internal scaffold collapse, many times encountered in sublimation methods. In this preliminary study, 3D scaffolds were obtained, although the process requires some extensive degree of optimization. Firstly, since FucoPol naturally exhibits poor mechanical strength, **lower freezing temperatures** are better suited, in this case, since smaller pores will be obtained due to rapid freezing times that do not allow ice crystal growth. Second, **solvent adjustment** in water-replacement step needs to be performed since acetone can lower supercritical drying process production times, producing dry scaffolds in 3 hours, instead of 8 hours. Even then, **solvent exchange** time in water-replacement step must be carefully evaluated since it can vary from polymer to polymer, increasing or decreasing with the complexity of the casting solution. Furthermore, **manipulation of process**

parameters in supercritical extraction is also a feasible alternative that can lead to the production of dry scaffolds in smaller time frames, since an increase in pressure and/or temperature improves the solvation power of the CO_2, which leads to the removal of higher amounts of solvent, lowering the costs associated to higher running times.

FucoPol microparticle production should be explored by electrospray or supercritical spray assisted atomization should be a promising alternative since FucoPol is not soluble in CO_2, does not have foaming abilities and already displays the ability to produce microparticles by electrospray. Furthermore, hydrogel production by sol-gel approach should be a practical alternative for FucoPol-based scaffolds due to its thickening abilities. Additionally, unless FucoPol is cross-linked with polymers that display a more hydrophobic character, striving to have pore controlled FucoPol-based structures seems irrelevant, since they will eventually collapse due to the polymers' faster degradation rates, that are a result of its hydrophilic nature.

References

Aframian, D.J., Davidowitz, T., Benoliel, R., 2006. The distribution of oral mucosal pH values in healthy saliva secretors. Oral Dis. 12, 420–423.

Agarwal, P., Chakraborty, H., 2015. Production of Pullulan Polysaccharide from Aureobasidium pullulan and to Study its Properties. LS Int. J. Life Sci. 4, 62–66.

Alipour, S., Akbari, S., Ahmadi, F., 2015. Development and in vitro evaluation of fast-dissolving oral films of ondansetron hydrochloride. Trends Pharm. Sci. 1, 25–30.

Allen, T.M., Cullis, P.R., 2004. Drug delivery systems: entering the mainstream. Science (80-.). 303, 1818–1822.

Anjum, F., Lienemann, P.S., Metzger, S., Biernaskie, J., Kallos, M.S., Ehrbar, M., 2016. Enzyme responsive GAG-based natural-synthetic hybrid hydrogel for tunable growth factor delivery and stem cell differentiation. Biomaterials 87, 104–117.

Antunes, S., Freitas, F., Alves, V.D., Grandfils, C., Reis, M.A.M., 2015. Conversion of cheese whey into a fucose- and glucuronic acid-rich extracellular polysaccharide by Enterobacter A47. J. Biotechnol. 210, 1–7.

Autissier, A., Le Visage, C., Pouzet, C., Chaubet, F., Letourneur, D., 2010. Fabrication of porous polysaccharide-based scaffolds using a combined freeze-drying/cross-linking process. Acta Biomater. 6, 3640–8.

Autissier, A., Letourneur, D., Le Visage, C., 2007. Pullulan-based hydrogel for smooth muscle cell culture. J. Biomed. Mater. Res. Part A 82, 336–342.

Bala, R., Pawar, P., Khanna, S., Arora, S., 2013. Orally dissolving strips: A new approach to oral drug delivery system. Int. J. Pharm. Investig. 3, 67.

Barroso, T., Aguiar-Ricardo, A., Roque, C., 2014. Functional monolithic platforms for antibody purification (PhD dissertation). Faculdade de Ciências e Tecnologia, Universidade NOVA Lisboa.

Barroso, T., Roque, A.C.A., Aguiar-Ricardo, A., 2012. Bioinspired and sustainable chitosan-based monoliths for antibody capture and release. RSC Adv. 2, 11285–11294.

Barroso, T., Temtem, M., Hussain, A., Aguiar-Ricardo, A., Roque, A.C.A., 2010. Preparation and characterization of a cellulose affinity membrane for human immunoglobulin G (IgG) purification. J. Memb. Sci. 348, 224–230.

Benny, I.S., Gunasekar, V., Ponnusami, V., 2014. Review on Application of Xanthan Gum in Drug Delivery. Int J PharmTech Res 6, 1322–1326.

Bhamidipati, M., Scurto, A.M., Detamore, M.S., 2013. The future of carbon dioxide for polymer processing in tissue engineering. Tissue Eng. Part B. Rev. 19, 221–32.

Borges, A.F., Silva, C., Coelho, J.F.J., Simões, S., 2015. Oral films: Current status and future perspectives. J. Control. Release 206, 1–19.

Cabral, R.M.P., 2013. Development of chitosan-based microparticles for pulmonary drug delivery (MSc dissertation). Faculdade de Ciências e Tecnologia, Universidade NOVA Lisboa.

Cândido, S.R., 2015. Design and Characterization of Novel Biopolymeric Structures using Biocompatible Ionic Liquids (MSc dissertation). Faculdade de Ciências e Tecnologia, Universidade NOVA de Lisboa.

Canejo, J.P., Borges, J.P., Godinho, M.H., Brogueira, P., Teixeira, P.I.C., Terentjev, E.M., 2008. Helical twisting of electrospun liquid crystalline cellulose micro- and nanofibers. Adv. Mater. 20, 4821–4825.

Casettari, L., Bonacucina, G., Morris, G.A., Perinelli, D.R., Lucaioli, P., Cespi, M., Palmieri, G.F., 2015. Dextran and its potential use as tablet excipient. Powder Technol. 273, 125–132.

Casper, C.L., Stephens, J.S., Tassi, N.G., Chase, D.B., Rabolt, J.F., 2004. Controlling surface morphology of electrospun polystyrene fibers: Effect of humidity and molecular weight in the electrospinning process. Macromolecules 37, 573–578.

Chaouat, M., Le Visage, C., Autissier, A., Chaubet, F., Letourneur, D., 2006. The evaluation of a small-diameter polysaccharide-based arterial graft in rats. Biomaterials 27, 5546–53.

Chiu, T.-W., Chen, Y.-T., 2015. Preparation of CuCrO2 nanowires by electrospinning. Ceram. Int. 41, S407–S413. ceramint.2015.03.224

Cooley, J.F., 1900. GB Patent No. 6385, Southhampton Buildings, London: Haseltine, Lake & Co.

Costa, L.M.M., 2010. Effect of Solution Concentration on the Electrospray/Electrospinning Transition and on the Crystalline Phase of PVDF. Mater. Sci. Appl. 01, 246–251.

Craveiro, R., Martins, M., Santos, G.B., Correia, N., Dionisio, M., Barreiros, S., Duarte, A.R.C., Reis, R.L., Paiva, A., 2014. Starch-based polymer–IL composites formed by compression moulding and supercritical fluid foaming for self-supported conductive materials. RSC Adv. 4, 17161–17170.

Cruz, M., Freitas, F., Torres, C. a V, Reis, M. a M., Alves, V.D., 2011. Influence of temperature on the rheological behavior of a new fucose-containing bacterial exopolysaccharide. Int. J. Biol. Macromol. 48, 695–699.

da Silva, J.A.L., Rao, M.A., 2007. Rheological behavior of food gels. Rheol. Fluid Semisolid Foods Springer US, 339–401.

da Silva, L.P., Cerqueira, M.T., Sousa, R.A., Reis, R.L., Correlo, V.M., Marques, A.P., 2014. Engineering cell-adhesive gellan gum spongy-like hydrogels for regenerative medicine purposes. Acta Biomater. 10, 4787–97.

de Mônaco Lopes, B., Lessa, V.L., Silva, B.M., de Silva Carvalho, M.A., Schnitzler, E., Lacerda, L.G., 2015. Xanthan gum: properties, production conditions, quality and economic perspective. J. Food Nutr. Res. 54.

Deitzel, J.., Kleinmeyer, J., Harris, D., Beck Tan, N.., 2001. The effect of processing variables on the morphology of electrospun nanofibers and textiles. Polymer (Guildf). 42, 261–272.

Dhadge, V.L., Morgado, P.I., Freitas, F., Reis, M.A., Azevedo, A., Aires-Barros, R., Roque, A.C.A., 2014. An extracellular polymer at the interface of magnetic bioseparations. J. R. Soc. Interface 11, 163–170.

Dodds, M., Roland, S., Edgar, M., Thornhill, M., 2015. Saliva A review of its role in maintaining oral health

and preventing dental disease. BDJ Team 2, 15123.

Dodds, M.W.J., Johnson, D.A., Yeh, C.-K., 2005. Health benefits of saliva: a review. J. Dent. 33, 223–233.

Doshi, J., Reneker, D.H., 1995. Electrospinning Process and Applications of Electrospun Fibers. J. Electrostat. 35, 151–160.

Epstein, J.B., Thariat, J., Bensadoun, R., Barasch, A., Murphy, B.A., Kolnick, L., Popplewell, L., Maghami, E., 2012. Oral complications of cancer and cancer therapy. CA. Cancer J. Clin. 62, 400–422.

Fernandes, C.S.M., Gonçalves, B., Sousa, M., Martins, D.L., Barroso, T., Pina, A.S., Peixoto, C., Aguiar-Ricardo, A., Roque, A.C.A., 2015. Biobased monoliths for adenovirus purification. ACS Appl. Mater. Interfaces 7, 6605–6612.

Ferreira, A.R. V, Torres, C.A. V, Freitas, F., Reis, M.A.M., Alves, V.D., Coelhoso, I.M., 2014. Biodegradable films produced from the bacterial polysaccharide FucoPol. Int. J. Biol. Macromol. 71, 111–116.

Foster, N.R., Lucien, F.P., Mammucari, R., 2010. Basic Physical Properties, Phase Behavior and Solubility, in: Handbook of Green Chemistry, Volume 4: Green Solvents. pp. 77–100.

Freitas, F., Alves, V.D., Gouveia, A.R., Pinheiro, C., Torres, C.A. V, Grandfils, C., Reis, M.A.M., 2014. Controlled production of exopolysaccharides from enterobacter A47 as a function of carbon source with demonstration of their film and emulsifying abilities. Appl. Biochem. Biotechnol. 172, 641–657.

Freitas, F., Alves, V.D., Pais, J., Costa, N., Oliveira, C., Mafra, L., Hilliou, L., Oliveira, R., Reis, M. a M., 2009. Characterization of an extracellular polysaccharide produced by a Pseudomonas strain grown on glycerol. Bioresour. Technol. 100, 859–865.

Freitas, F., Alves, V.D., Reis, M. a M., 2011. Advances in bacterial exopolysaccharides: From production to biotechnological applications. Trends Biotechnol. 29, 388–398.

Freitas, F., Alves, V.D., Torres, C. a V, Cruz, M., Sousa, I., Melo, M.J., Ramos, A.M., Reis, M. a M., 2010. Fucose-containing exopolysaccharide produced by the newly isolated Enterobacter strain A47 DSM 23139. Carbohydr. Polym. 83, 159–165.

Ganesh, V.A., Nair, A.S., Raut, H.K., Walsh, T.M., Ramakrishna, S., 2012. Photocatalytic superhydrophilic TiO2 coating on glass by electrospinning. RSC Adv. 2, 2067–2072.

García-González, C. a., Alnaief, M., Smirnova, I., 2011. Polysaccharide-based aerogels - Promising biodegradable carriers for drug delivery systems. Carbohydr. Polym. 86, 1425–1438.

García-González, C.A., Camino-Rey, M.C., Alnaief, M., Zetzl, C., Smirnova, I., 2012. Supercritical drying of aerogels using CO2: Effect of extraction time on the end material textural properties. J. Supercrit. Fluids 66, 297–306.

Garg, T., Goyal, A.K., 2014. Medicated Chewing Gum : Patient Compliance Oral Drug Delivery System. Drug Deliv. Lett. 4, 72–78.

Gibson, L.J., Ashby, M.F., Harley, B.A., 2010. Cellular Materials in Nature and Medicine, Cellular Materials in Nature and Medicine. Cambridge University,

Global Data, H. and M., 2012. Xerostomia therapeutics - Pipeline assessment and Market Forecasts.

Global Industry Analysts, H. and M., 2011. Biotech Cancer Therapies Yet to Overcome Teething Issues -

Market Research. Global.

Goki Eda, S.S., 2007. Bead-to-Fiber Transition in Electrospun Polystyrene. Wiley Intersci. 21, 449–456.

Goldstein, J., Newbury, D.E., Echlin, P., Joy, D.C., Romig Jr, A.D., Lyman, C.E., Fiori, C., Lifshin, E., 2012. Scanning electron microscopy and X-ray microanalysis: a text for biologists, materials scientists, and geologists. Springer Science & Business Media.

Gonçalves, V.S.S., Matias, A.A., Rodríguez-Rojo, S., Nogueira, I.D., Duarte, C.M.M., 2015. Supercritical fluid precipitation of ketoprofen in novel structured lipid carriers for enhanced mucosal delivery--a comparison with solid lipid particles. Int. J. Pharm. 495, 302–11.

Gondaliya, N., 2011. Structural and Conductivity Studies of Poly(Ethylene Oxide) – Silver Triflate Polymer Electrolyte System. Mater. Sci. Appl. 02, 1639–1643.

Haghgoo, R., Afshari, E., Ghanaat, T., Aghazadeh, S., 2015. Comparing the efficacy of xylitol-containing and conventional chewing gums in reducing salivary counts of Streptococcus mutans: An in vivo study. J. Int. Soc. Prev. Community Dent. 5, S112–7.

Hansen, C.M., 2007. Hansen Solubility Parameters: A User's Handbook, Second Edition. CRC Press.

Hearnden, V., Sankar, V., Hull, K., Juras, D.V., Greenberg, M., Kerr, A.R., Lockhart, P.B., Patton, L.L., Porter, S., Thornhill, M.H., 2012. New developments and opportunities in oral mucosal drug delivery for local and systemic disease. Adv. Drug Deliv. Rev. 64, 16–28.

Hernández-Navarro, N., González-González, V., Moreno-Cortez, I.E., Garza-Navarro, M.A., 2016. Electrospun polyvinylidene fluoride nanofibers by bubble electrospinning technique. Mater. Lett. 167, 34–37.

Hoffmann, E.M., Breitenbach, A., Breitkreutz, J., 2011. Advances in orodispersible films for drug delivery. Expert Opin. Drug Deliv. 8, 299–316.

Höhne, G., Hemminger, W.F., Flammersheim, H.-J., 2013. Differential scanning calorimetry. Springer Science & Business Media.

Hollister, S.J., 2005. Porous scaffold design for tissue engineering. Nat Mater 4, 518–524.

Illangakoon, U.E., Gill, H., Shearman, G.C., Parhizkar, M., Mahalingam, S., Chatterton, N.P., Williams, G.R., 2014. Fast dissolving paracetamol/caffeine nanofibers prepared by electrospinning. Int. J. Pharm. 477, 369–379.

Jalili, R., Shepherd, R.L., 2013. Wet-spinning of multifunctional graphene fibers using graphene oxide liquid crystals 248–249.

Jiang, H., Fang, D., Hsiao, B., Chu, B., Chen, W., 2004. Preparation and characterization of ibuprofen-loaded poly(lactide-co-glycolide)/poly(ethylene glycol)-g-chitosan electrospun membranes. J. Biomater. Sci. Polym. Ed. 15, 279–296. d

Kadajji, V.G., Betageri, G. V., 2011. Water soluble polymers for pharmaceutical applications. Polymers (Basel). 3, 1972–2009.

Kailash, A., Kumar, A.K., Yadav, H.K.S., 2014. FAST DISSOLVING TABLETS – A REVIEW 3, 678–701.

Kasim, N. a, Whitehouse, M., Ramachandran, C., Bermejo, M., Lennernäs, H., Hussain, A.S., Junginger,

H.E., Stavchansky, S. a, Midha, K.K., Shah, V.P., Amidon, G.L., 2004. Molecular Properties of WHO Essential Drugs and Provisional Biopharmaceutical Classification. Mol. Pharm. 1, 85–96.

Kim, S.K., 2015. Functional Marine Biomaterials: Properties and Applications, Woodhead Publishing Series in Biomaterials. Elsevier Science.

Kiran, E., Debenedetti, P.G., Peters, C.J., 2012. Supercritical Fluids: Fundamentals and Applications, Nato Science Series E: Springer Netherlands.

Knežević, N.Ž., Durand, J.-O., 2015. Large pore mesoporous silica nanomaterials for application in delivery of biomolecules. Nanoscale 7, 2199–209.

Kojima, H., Yoshihara, K., Sawada, T., Kondo, H., Sako, K., 2008. Extended release of a large amount of highly water-soluble diltiazem hydrochloride by utilizing counter polymer in polyethylene oxides (PEO)/polyethylene glycol (PEG) matrix tablets. Eur. J. Pharm. Biopharm. 70, 556–562.

Kolakovic, R., Viitala, T., Ihalainen, P., Genina, N., Peltonen, J., Sandler, N., 2013. Printing technologies in fabrication of drug delivery systems. Expert Opin. Drug Deliv. 10, 1711–23.

Leuner, C., Dressman, J., 2000. Improving drug solubility for oral delivery using solid dispersions. Eur. J. Pharm. Biopharm. 50, 47–60.

Li, Z., Wang, C., 2013. Effects of Working Parameters on Electrospinning. One-Dimensional nanostructures 15–29.

Liang, D., Hsiao, B.S., Chu, B., 2007. Functional electrospun nanofibrous scaffolds for biomedical applications. Adv. Drug Deliv. Rev. 59, 1392–1412. d

Liang, Y., Kiick, K.L., 2014. Heparin-functionalized polymeric biomaterials in tissue engineering and drug delivery applications. Acta Biomater. 10, 1588–600.

Liu, J., Wang, X., Wang, T., Li, D., Xi, F., Wang, J., Wang, E., 2014. Functionalization of monolithic and porous three-dimensional graphene by one-step chitosan electrodeposition for enzymatic biosensor. ACS Appl. Mater. Interfaces 6, 19997–20002.

Loo, J.A., 1997. Studying noncovalent protein complexes by electrospray ionization mass spectrometry. Mass spectrometry Reviews 16, 1-23.

Lopes, M., 2012. Projecto e Implementação de um Sistema para Electrofiação Controlado por Computador (MSc dissertation). Faculdade de Ciências e Tecnologia, Universidade NOVA Lisboa.

Lourenço, A.S., 2015. FucoPol as encapsulating matrix of bioactive compounds (MSc dissertation). Instituto Superior de Agronomia, Universidade de Lisboa.

Ly, K.A., Milgrom, P., Rothen, M., 2006. Xylitol, Sweeteners, and Dental Caries.Pediatric Dentistry 28, 154-163.

Mahdi, M.H., Conway, B.R., Smith, A.M., 2015. Development of mucoadhesive sprayable gellan gum fluid gels. Int. J. Pharm. 488, 12–19.

Marieb, E.N., Hoehn, K., 2007. Human anatomy & physiology. Pearson Education.

Marques, M.R.C., Loebenberg, R., Almukainzi, M., 2011. Simulated biological fluids with possible application in dissolution testing. Dissolution Technol. 18, 15–28.

McLaughlin, R., Banbury, S., Crowley, K., 2009. Orally Disintegrating Tablets - The Effect of Recent FDA Guidance on ODT Technologies and Applications. Pharm. Technol. September, 6.

Meireles, I.T., Brazinha, C., Crespo, J.G., Coelhoso, I.M., 2013. A new microbial polysaccharide membrane for ethanol dehydration by pervaporation. J. Memb. Sci. 425-426, 227–234.

Meurant, G., 1987. Profiles of Drug Substances, Excipients and Related Methodology, Analytical Profiles of Drug Substances. Elsevier Science.

Mit-uppatham, C., Nithitanakul, M., Supaphol, P., 2004. Ultrafine Electrospun Polyamide-6 Fibers: Effect of Solution Conditions on Morphology and Average Fiber Diameter. Macromol. Chem. Phys. 205, 2327–2338.

Mocanu, G., Mihai, D., Moscovici, M., Picton, L., LeCerf, D., 2009. Curdlan microspheres. Synthesis, characterization and interaction with proteins (enzymes, vaccines). Int. J. Biol. Macromol. 44, 215–21.

Morgado, P.I., Lisboa, P.F., Ribeiro, M.P., Miguel, S.P., Simões, P.C., Correia, I.J., Aguiar-Ricardo, A., 2014. Poly(vinyl alcohol)/chitosan asymmetrical membranes: Highly controlled morphology toward the ideal wound dressing. J. Memb. Sci. 469, 262–271.

Morton, W.J., 1902. Method of dispersing fluids. U.S. Patent No. 705,691.

Nagy, Z.K., Balogh, A., Démuth, B., Pataki, H., Vigh, T., Szabó, B., Molnár, K., Schmidt, B.T., Horák, P., Marosi, G., Verreck, G., Van Assche, I., Brewster, M.E., 2015. High speed electrospinning for scaled-up production of amorphous solid dispersion of itraconazole. Int. J. Pharm. 480, 137–142.

Nagy, Z.K., Balogh, A., Drávavölgyi, G., Ferguson, J., Pataki, H., Vajna, B., Marosi, G., 2013. Solvent-Free Melt Electrospinning for Preparation of Fast Dissolving Drug Delivery System and Comparison with Solvent-Based Electrospun and Melt Extruded Systems. J. Pharm. Sci. 102, 508–517.

Neves, N.M., Campos, R., Pedro, A., Cunha, J., Macedo, F., Reis, R.L., 2007. Patterning of polymer nanofiber meshes by electrospinning for biomedical applications. Int. J. Nanomedicine 2, 433–438.

Nichol, J.W., Khademhosseini, A., 2010. Modular tissue engineering: Engineering biological tissues from the bottom up. Soft Matters 5, 1312–1319.

Niederhuber, J.E., Armitage, J.O., Doroshow, J.H., Kastan, M.B., Tepper, J.E., 2013. Abeloff's Clinical Oncology Review. Elsevier Health Sciences.

Norton, C.L., 1936. Method of and apparatus for producing fibrious or filamentary material. U.S. Patent No. 2,048,651.

Oliveira, S.M., Reis, R.L., Mano, J.F., 2015. Towards the design of 3D multiscale instructive tissue engineering constructs: Current approaches and trends. Biotechnol. Adv. 33, 842–55.

Owens, G., Singh, R.K., Foroutan, F., Alqaysi, M., Han, C.-M., Mahapatra, C., Kim, H.-W., Knowles, J.C., 2016. Sol-gel Based Materials for Biomedical Applications. Prog. Mater. Sci. 77, 1–79.

Panda, P.K., Ramakrishna, S., 2007. Electrospinning of alumina nanofibers using different precursors. J. Mater. Sci. 42, 2189–2193.

Ph. Eur. 5th, 2000. European Pharmacopoeia 5.0, 5th Edition, i-3086

Ph. Eur. 8th Edition, 2015. European Pharmacopoeia 8.6 index. 8th Edition

Pham, Q.P., Sharma, U., Mikos, A.G., 2006. Electrospinning of polymeric nanofibers for tissue engineering applications: a review. Tissue Eng. 12, 1197–1211.

Phenomenex, 2011. Solvent miscibility table. Phenomenex Cat. 18–19.

Piermaria, J.A., Mariano, L., Abraham, A.G., 2008. Gelling properties of kefiran, a food-grade polysaccharide obtained from kefir grain. Food Hydrocoll. 22, 1520–1527.

Prausnitz, M.R., Langer, R., 2008. Transdermal drug delivery. Nat Biotech 26, 1261–1268.

Preis, M., Knop, K., Breitkreutz, J., 2014. Mechanical strength test for orodispersible and buccal films. Int. J. Pharm. 461, 22–29.

Qiu, X., Hu, S., 2013. "Smart" materials based on cellulose: A review of the preparations, properties, and applications. Materials (Basel). 6, 738–781.

Rathbone, M.J., Hadgraft, J., Roberts, M.S., 2008. Modified Release Drug Delivery Technology 2.

Reis, M.A.M., Oliveira, R., Freitas, F., Alves, V.D., 2016. Fucose-containing bacterial biopolymer. Int. Appl. Status Rep. WO2011/073874.

Reis, T.C., Correia, I.J., Aguiar-Ricardo, A., 2013. Electrodynamic tailoring of self-assembled three-dimensional electrospun constructs. Nanoscale 5, 7528–36.

Restani, R.B., Morgado, P.I., Ribeiro, M.P., Correia, I.J., Aguiar-Ricardo, A., Bonifácio, V.D.B., 2012. Biocompatible polyurea dendrimers with pH-dependent fluorescence. Angew. Chemie - Int. Ed. 51, 5162–5165.

Rigort, A., Bäuerlein, F.J.B., Villa, E., Eibauer, M., Laugks, T., Baumeister, W., Plitzko, J.M., 2012. Focused ion beam micromachining of eukaryotic cells for cryoelectron tomography 109.

Ritger, P.L., Peppas, N.A., 1987. A simple equation for description of solute release II 5, 23–36.

Rodriguez, F., Cohen, C., Ober, C.K., Archer, L., 2014. Principles of Polymer Systems, Sixth Edition. CRC Press.

RömLing, U., Galperin, M.Y., 2015. Bacterial cellulose biosynthesis: diversity of operons, subunits, products, and functions. Trends Microbiol. 23, 545–557.

Rowland, M., 1972. Influence of Route of Administration on Drug Availability. J. Pharm. Sci. 61, 70–74.

Saigal, N., Baboota, S., Ahuja, A., Ali, J., 2008. Fast-dissolving intra-oral drug 769–782.

Schramm, G., 1994. A Practical Approach to Rheology and Rheometry. Rheology 291.

Sears, N.A., Dhavalikar, P.S., Seshadri, D., Cosgriff-Hernandez, E., 2016. A Review of 3D Printing of Tissue Engineering Constructs. Tissue Eng. Part B. Rev.

Shamma, R., Elkasabgy, N., 2014. Design of freeze-dried Soluplus/polyvinyl alcohol-based film for the oral delivery of an insoluble drug for the pediatric use. Drug Deliv. 7544, 1–11.

Shawe, J., Riesen, R., Widmann, J., Schubnell, M., 2000. Interpreting DSC curves. Mettler Toledo GmbH Anal.

Shen, B. De, Shen, C.Y., Yuan, X.D., Bai, J.X., Lv, Q.Y., Xu, H., Dai, L., Yu, C., Han, J., Yuan, H.L., 2013. Development and characterization of an orodispersible film containing drug nanoparticles. Eur. J.

Pharm. Biopharm. 85, 1348–1356.

Slavkova, M., Breitkreutz, J., 2015. Orodispersible drug formulations for children and elderly. Eur. J. Pharm. Sci. 75, 2–9.

Smith, B.C., 2011. Fundamentals of Fourier Transform Infrared Spectroscopy, Second Edition, 2nd Editio. ed. Taylor & Francis.

Soares Nunes, L.A., Mussavira, S., Bindhu, O., 2015. Clinical and diagnostic utility of saliva as a non-invasive diagnostic fluid – a Systematic Review. Biochem. Medica 25, 177–92.

Srikanth, R., Reddy, C.H.S.S.S., Siddartha, G., Ramaiah, M.J., Uppuluri, K.B., 2015. Review on production, characterization and applications of microbial levan. Carbohydr. Polym. 120, 102–114.

Stephen, A.M., Phillips, G.O., Williams, P.A., 2006. Food polysaccharides and their applications.

Stijnman, A.C., Bodnar, I., Tromp, R.H., 2011. Food Hydrocolloids Electrospinning of food-grade polysaccharides. Food Hydrocoll. 25, 1393–1398.

Stosik, A.G., Junginger, H.E., Kopp, S., Midha, K.K., Shah, V.P., Stavchansky, S., Dressman, J.B., Barends, D.M., 2008. Biowaiver monographs for immediate release solid oral dosage forms: Metoclopramide hydrochloride. J. Pharm. Sci. 97, 3700–3708.

Strober, W., 2001. Trypan blue exclusion test of cell viability. Curr. Protoc. Immunol. A3–B.

Sultana, N., Hassan, M.I., Lim, M.M., 2015. Composite Synthetic Scaffolds for Tissue Engineering and Regenerative Medicine. Springer International Publishing, Cham, pp. 45–60.

Sun, S., Tang, Y., Fu, Q., Liu, X., Guo, L., Zhao, Y., Chang, C., 2012. Monolithic cryogels made of agarose–chitosan composite and loaded with agarose beads for purification of immunoglobulin G. Int. J. Biol. Macromol. 50, 1002–1007.

Svagan, A.J., Berglund, L.A., Jensen, P., 2011. Cellulose Nanocomposite Biopolymer Foam Hierarchical Structure Effects on Energy Absorption. ACS Appl. Mater. Interfaces 3, 1411–1417.

Svec, F., 2010. Porous polymer monoliths: amazingly wide variety of techniques enabling their preparation. J. Chromatogr. A 1217, 902–24.

Synytsya, A., Čopíková, J., Matějka, P., Machovič, V., 2003. Fourier transform Raman and infrared spectroscopy of pectins. Carbohydr. Polym. 54, 97–106.

Taherkhani, S., Moztarzadeh, F., 2016. Fabrication of a poly (ε-caprolactone)/starch nanocomposite scaffold with a solvent-casting/salt-leaching technique for bone tissue engineering applications. J. Appl. Polym. Sci.

Takeuchi, H., Yamakawa, R., Nishimatsu, T., Takeuchi, Y., Hayakawa, K., Maruyama, N., 2013. Design of rapidly disintegrating drug delivery films for oral doses with hydoxypropyl methylcellulose. J. Drug Deliv. Sci. Technol. 23, 471–475.

Tasselli, F., Mirmohseni, A., Dorraji, M.S.S., Figoli, A., 2013. Reactive & Functional Polymers Mechanical , swelling and adsorptive properties of dry – wet spun chitosan hollow fibers crosslinked with glutaraldehyde. React. Funct. Polym. 73, 218–223.

Taylor, G., 1964. Disintegration of Water Drops in an Electric Field, in: Proceedings of the Royal Society of

London. Series A, Mathematical and Physical Sciences. pp. 383–397.

Temtem, M., Casimiro, T., Mano, J.F., Aguiar-Ricardo, A., 2008. Preparation of membranes with polysulfone/polycaprolactone blends using a high pressure cell specially designed for a CO2-assisted phase inversion. J. Supercrit. Fluids 43, 542–548.

Thieme, M., Agarwal, S., Wendorff, J.H., Greiner, A., 2009. Electrospinning and cutting of ultrafine bioerodible poly(lactide-co-ethylene oxide) tri- and multiblock copolymer fibers for inhalation applications. Polym. Adv. Technol.

Tkatch, V.I., Limanovskii, A.I., Denisenko, S.N., Rassolov, S.G., 2002. The effect of the melt-spinning processing parameters on the rate of cooling 323, 91–96.

Torres, C.A.V., 2012. Engineering of bacterial exopolysaccharides: from synthesis to properties.

Torres, C.A.V., Ferreira, A.R.V., Freitas, F., Reis, M.A.M., Coelhoso, I., Sousa, I., Alves, V.D., 2015. Rheological studies of the fucose-rich exopolysaccharide FucoPol. Int. J. Biol. Macromol. 79, 611–

U.S. Food and Drug Administration, F., 2009. Dosage Form Monograph, Data Standards Manual. Dev. Approv. Process.

van der Heide, P., 2011. X-ray Photoelectron Spectroscopy: An introduction to Principles and Practices. Wiley.

Venugopal, V., 2011. Marine Polysaccharides: Food Applications. CRC Press.

Vuddanda, P.R., Mathew, A.P., Velaga, S., 2016. Electrospun nanofiber mats for ultrafast release of ondansetron. React. Funct. Polym. 99, 65–72. doi:10.1016/j.

Wang, J., Schipper, H.M., Velly, A.M., Mohit, S., Gornitsky, M., 2015. Salivary biomarkers of oxidative stress: A critical review. Free Radic. Biol. Med. 85, 95–104.

Xu, Q., 2013. Nanoporous Materials: Synthesis and Applications. Taylor & Francis.

Yang, F., Hanna, M.A., Sun, R., 2012. Value-added uses for crude glycerol--a byproduct of biodiesel production. Biotechnol. Biofuels 5, 1–10.

Yang, Q., Zhenyu, L.I., Hong, Y., Zhao, Y., Qiu, S., Wang, C.E., Wei, Y., 2004. Influence of solvents on the formation of ultrathin uniform poly(vinyl pyrrolidone) nanofibers with electrospinning. J. Polym. Sci. Part B Polym. Phys. 42, 3721–3726.

Yao, J., Bastiaansen, C., Peijs, T., 2014. High Strength and High Modulus Electrospun Nanofibers. Fibers 2, 158–186.

Yazgan, G., Popa, A.M., Rossi, R.M., Maniura-Weber, K., Puigmart??-Luis, J., Crespy, D., Fortunato, G., 2015. Tunable release of hydrophilic compounds from hydrophobic nanostructured fibers prepared by emulsion electrospinning. Polym. (United Kingdom) 66, 268–276.

Ye, L., Cao, J., Chen, L., Geng, X., Zhang, A.Y., Guo, L.R., Gu, Y.Q., Feng, Z.G., 2015. The fabrication of double layer tubular vascular tissue engineering scaffold via coaxial electrospinning and its 3D cell coculture. J. Biomed. Mater. Res. - Part A 103, 3863–3871.

Yu, S., Wu, Y., Mi, F., Shyu, S., 2008. Polysaccharide-based artificial extracellular matrix: Preparation and characterization of three-dimensional, macroporous chitosan, and heparin composite scaffold. J. Appl.

Polym. Sci. 109, 3639–3644.

Zavala, L., Roberti, P., Piermaria, J.A., Abraham, A.G., 2014. Gelling ability of kefiran in the presence of sucrose and fructose and physicochemical characterization of the resulting cryogels. J. Food Sci. Technol. 52, 5039–5047.

Zhang, M., Ogale, A.A., 2013. Letter to the Editor Carbon fibers from dry-spinning of acetylated softwood kraft lignin. Carbon N. Y. 69, 626–629.

Zhou, H., Green, T.B., Joo, Y.L., 2006. The thermal effects on electrospinning of polylactic acid melts. Polymer (Guildf). 47, 7497–7505.

Zhu, W., Masood, F., O'Brien, J., Zhang, L.G., 2015. Highly aligned nanocomposite scaffolds by electrospinning and electrospraying for neural tissue regeneration. Nanomedicine 11, 693–704.

Zuheir, A., Samein, L.H., Aiash, N., 2013. Preparation and in vitro evaluation of Metoclopramide HCL hollow-type suppository. Int. J. Pharm. Pharm. Sci. 5, 660–666.

Supplementary Information

6.1 Annex 1

Electrospinning solutions for of stand-alone FucoPol

- **Solvents and polymer concentration**

Table 6.1 – Solvent screening for FucoPol electrospun solutions (A1 to A8). *Acetic acid (Sigma Aldrich). **Formic acid (Sigma Aldrich).

		FucoPol wt.%							
		A1	**A2**	**A3**	**A4**	**A5**	**A6**	**A7**	**A8**
Solvents	Water	-	1%	1.5%	2%	-	-	-	-
	Acidic water 1%	0.5%	1%	1.5%	-	2.5%	3%	3.5%	-
	Acidic water 60%	-	-	-	-	2.5%	-	-	-
	AA*(40%)/FA**(60%)	0.5%	1%	1.5%	2%	-	3%	-	5%

Several solutions (i.e. A1 to A8) were prepared with FucoPol concentrations ranging from 0.5% to 5% (w/v). A number of solvents were tested as showed in Table 6.1; acetone and ethanol were not accounted for since related work shows that FucoPol is insoluble in both reagents.

- **Electrospinning process**

Electrospinning was performed in the host's lab at 30% to 40% of relative humidity. The polymeric solution was pumped through a 21-gauge needle (12.04 mm internal diameter) by means of a digital pump, at a rate ranging from 0.01 to 0.5 $mL.h^{-1}$. The solution was ejected, with a voltage 6.5 to 20 kV and fibers were collected in a static parchment paper plate located 10 to 15 cm from the tip of the needle.

6.2 Annex 2

- **Electrospinning solutions for FucoPol and crosslinking agents**

Table 6.2 – Cross-linkers tested in order to allow electrospinning production of an orodispersible film containing FucoPol. [1]Hydroxilpropil cellulose; [2]Poly(ethylene oxide); [3]Poly(vynil alcohol); [4]Polyvynilpirrolidone.

FucoPol 2% (w/v)	Dextran	Glycerol	HPC[1]	PEO[2]	PVA[3]	PVP[4]	Sorbitol
Electrospinning	15%	0.2%	5%	0.25%	-	0.5%	0.2%
	50%	0.37%	7%	0.5%		0.75%	0.5%
	-	0.4%	15%	-		1%	1%
	-	1%	-	-		-	1.5%
	-	2%	-	-		-	2%
Solvent casting	-	1%	-	0.5%	0.5%	0.25%	2%
		-		1%	-	0.5%	-
		-		-	-	-	-

Solvent: Deionized water

The minimal amount of crosslinking agent required for fiber production was tested. The samples present in Table 6.2 were additionally performed by solvent casting method, for comparison purposes.

- **Electrospinning process**

Electrospinning assays were performed at 25% to 46% of relative humidity. The polymeric solution was pumped through a 21-gauge needle (12.04 mm internal diameter) by means of a digital pump, at a rate ranging from 0.3 to 0.8 $mL.h^{-1}$. The solution was ejected, with a voltage 12 to 25 kV and fibers were collected in a static aluminum paper plate located 15 to 25 cm from the tip of the needle.

6.3 Annex 3

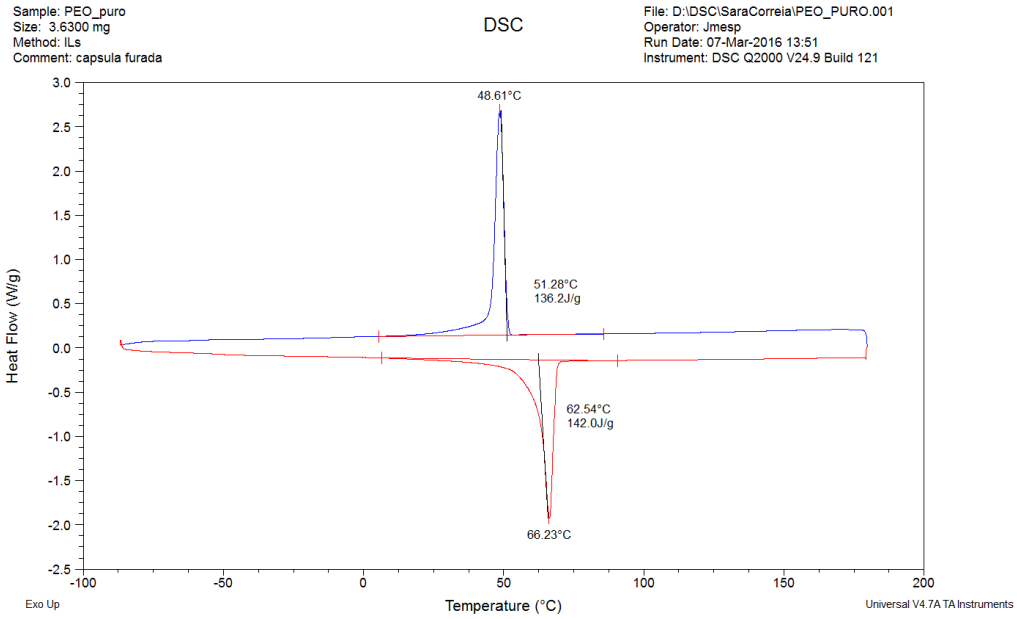

Figure 6.1 – DSC data from pure poly (ethylene oxide) showing Tg and Tc temperatures.

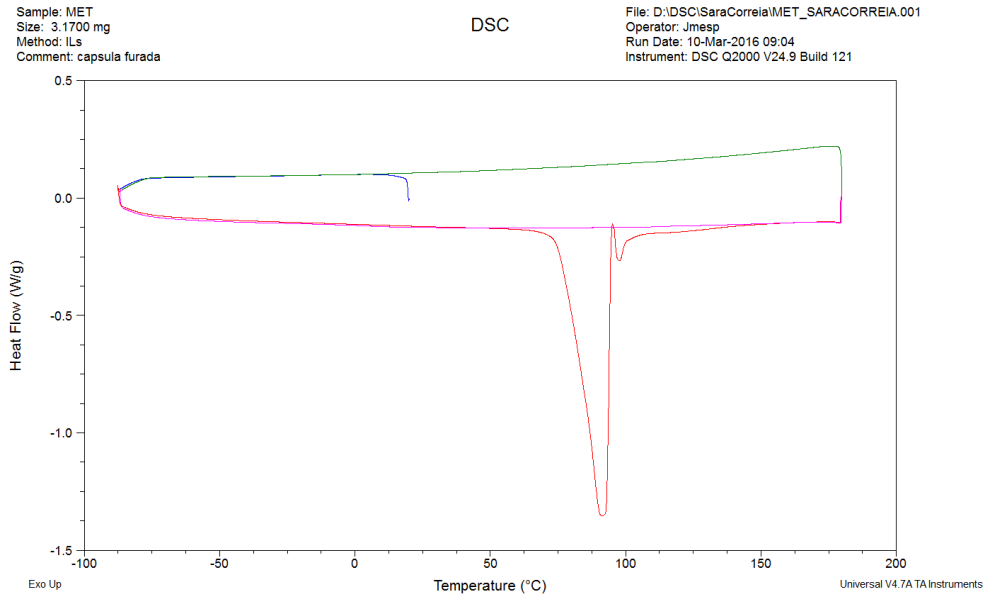

Figure 6.2 – DSC data from pure metoclopramide showing Tg temperature.

6.4 Annex 4

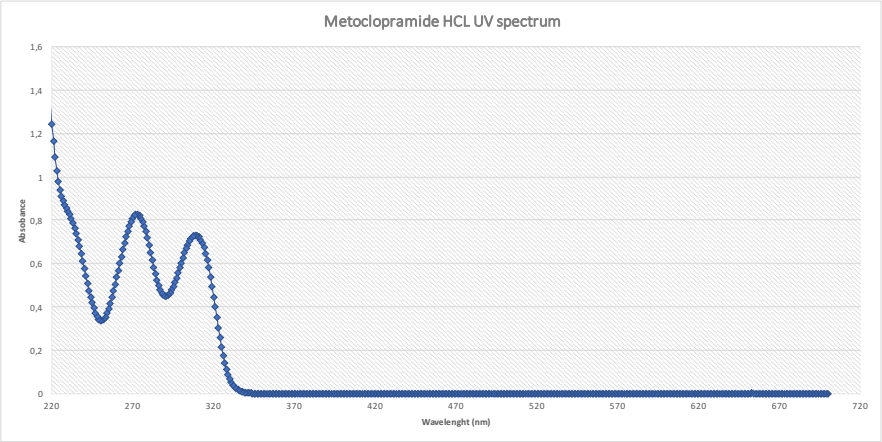

Figure 6.3 - Metoclopramide UV profile from 200 to 700 nm (UV/Vis Perkin Lambda).

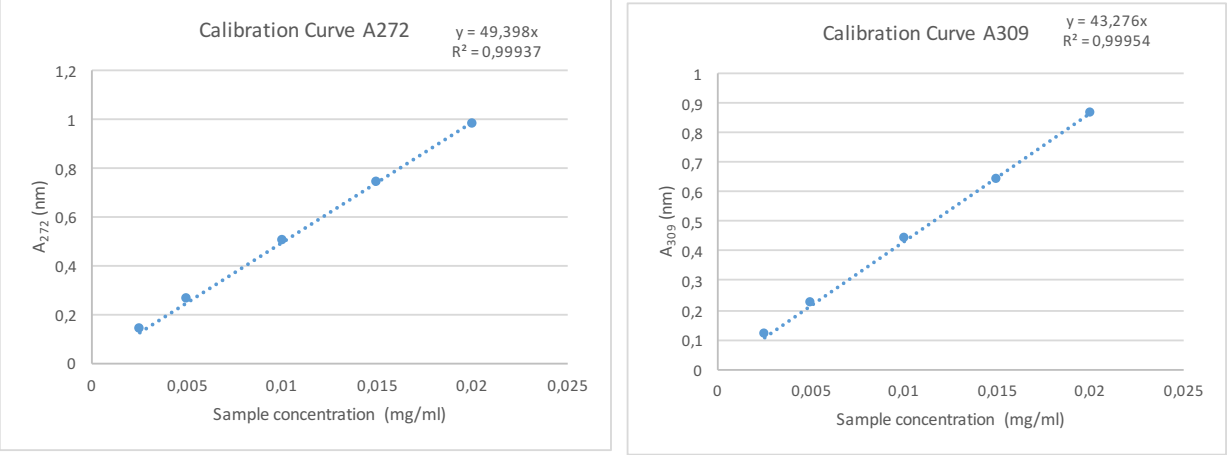

Figure 6.4 – Calibration curve used to quantify the amount of metoclopramide released upon in vitro pharmacokinetic studies.

6.5 Annex 5

- **Apparent viscosity**

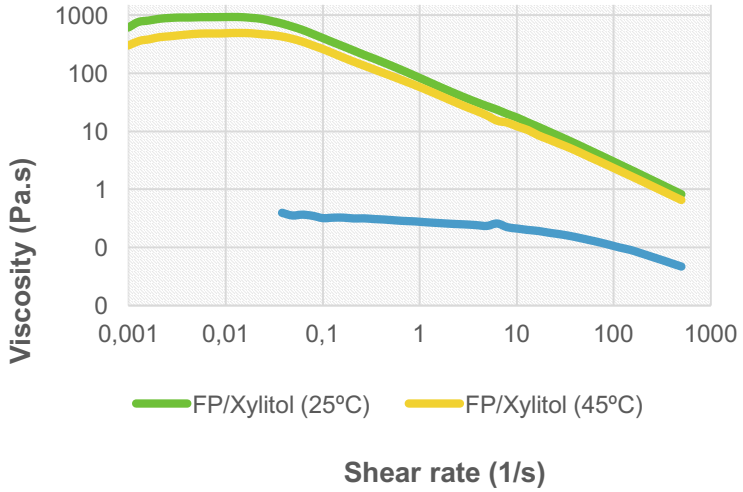

Figure 6.5 – Apparent viscosity of a scaffold sample at 25 ºC and 45 ºC

In order for the internal structure of the matrix not to collapse upon solvent exchange and scCO2 drying step, an appropriate polymer concentration must be achieved. Since the amount of polymer content is intimately connected an increase in the solutions viscosity, rheology measures at 25 and 45 ºC were accesses in order to see if the temperature had any influence in the scaffold. Scaffold has a very similar behavior displayed in subsection 2.6.1.1 but at higher viscosity values. Scaffold presents a Newtonian plateau around 0.011 Pa.s followed by shear-thinning behavior characteristic of disrupting the internal structure.